POSTFLIGHT ATTITUDE DETERMINATION
TALOS-TERRIER-BRANT-NIHKA 52.002 LESSARD
(LESSARD, NORWAY)

Prepared for

National Aeronautics and Space Administration
Goddard Space Flight Center
Wallops Flight Facility

Wallops Island, Virginia 23337

By

NSROC II

Prepared by:
Christopher Smith

_____
Christopher Smith
Engineer
Flight Performance

Reviewed by:
Michael Disbrow

_____
Michael Disbrow
Engineer
Flight Performance

Approved by:
D. Brent Edwards

_____
D. Brent Edwards
Lead Engineer
Flight Performance

TABLE OF CONTENTS

LIST OF FIGURES

1. INTRODUCTION

Mission: Talos-Terrier-Brant-Nihka 52.002 UE Lessard

Principal Scientific Investigation: Dr. Marc Lessard, University of New Hampshire

Mission Manager: Mr. Jay Scott

Launched: December 13, 2015, 07:34:00 GMT

Attitude Solution T0: 07:34:00 GMT

Launch Site: ASC, Norway

Launcher: Athena: Latitude: 69.29422°, Longitude: 16.01925° (WGS-84)

Launcher Settings (Actual): 80.28° QE, 12.08° AZ

ACS: NSROC Inertial Attitude Control System (NIACS)

Attitude Sensors:

Main Payload: GLNMAC / NIACS, Honeywell HMR magnetometer, Cornell magnetometer.
Sub Payload: Horizon Crossing Indicator (HCI), WAASP Slit Solar Sensors, WAASP magnetometer, Cornell magnetometer

Payload Weight: 766.3 lbs.

Apogee: 447.8 km at T+ 408.55 sec (GPS)

Purpose of Mission: RENU 2 will investigate neutral upwelling in the magnetic cusp region.

1.1 Mission Requirements

1. Three axis attitude solution will be provided for the Main and Sub-payload bodies.
2. Burnout roll rate will be trimmed to 4 $\pm$ 0.5 Hz.
3. Rates will be damped for sub payload skirt deployment.
4. Align to T+500 –B field for sub-payload deployment.
5. Coning half angle < 3 degrees at sub payload ejection.
6. 1.0 $\pm$ 0.1 Hz spin rate for 1st forward boom deployment.
7. 0.5 $\pm$ 0.05 Hz final spin rate.
8. Final main payload alignment to T+500 –B field.

Data Acquisition: The GLNMAC is part of the NIACS. The GLNMAC will provide quaternions that can be converted into DCMs and a 3-2-1 (roll-pitch-yaw, standard Aerospace sequence) Euler sequence for an attitude solution. The GLNMAC also provides an onboard discrete pulse which will be used with the GLNMAC 1pps time event module to synchronize the onboard clock with the ground based telemetry clock.

Solar sensors and HCI data will be sent from the sub payload in the form of TM counts where spikes in the data will give the specific times needed to determine when the sun and earth horizon were seen.

Honeywell and Cornell magnetometer data will be sent through a serial stream in the TM and converted with calibration data.

Multiple TM sources were combined for the best quality TM data for the final attitude solutions.

Data Delivery:

Final attitude knowledge is provided in a comma delimited text file e-mailed to the experiment team, ACS Engineer, and mission manager. Any updates to the solution will be sent to the ACS Engineer and PI.

Mission Success Criteria:

None related to attitude, however attitude is a part of the requirements matrix.

Accuracy Requested/Expected: ± 1° accuracy is expected with the GLNMAC solution.
± 3° accuracy is expected with the Sol-Mag solution.
±10° accuracy is expected with the HCI-Mag solution.

52.002 Lessard Sensor Map

10/12/2015 Rev C

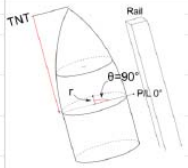

Sensor							Location				Orientation (Positive)			Notes	Verified By:
Name	TM Channel(s)	Model #	S/N	Owner	Measure	Type	TNT	Angular	Radius	Section	x-Axis	y-Axis	z-Axis		
Main P/L:															
WAASP Accelerometers	A88,A89,A90	WAASP	91605	Electrical	Accelerometer	3-axis	119.99	N/A	N/A	Main P/L TM	0	90	AFT	Main P/L TM	B. Banks
Digital Magnetometer	R2	Honeywell HMR2300	315,787	Electrical	Magnetometer	3-axis	51.65	315	6.25	Main P/L Exp	225	315	FWD	Fwd Structure	E. Bowden
Main P/L TX Thermistor	A158	Fenwal 15K	-	Electrical	Temperature	Scalar	98.79	N/A	N/A	TM				Main P/L TM	B. Banks
Main P/L PCM Thermistor	A159	Fenwal 15K	-	Electrical	Temperature	Scalar	96.12	N/A	N/A	TM				Main P/L TM	B. Banks
Skin Thermistor	A160	Fenwal 15K	-	Electrical	Temperature	Scalar	109.68	102	8.51	TM				Main P/L TM	B. Banks
WAASP Temperature	A91	WAASP	91605	Electrical	Temperature	Scalar	119.99	N/A	N/A	TM				Main P/L TM	B. Banks
GLNMAC Accelerometers	A107,A106,A105	-	-	GNC	Accelerometer	3-axis	129.74	N/A	N/A	ACS	90	0	AFT	X&Y changes	E. Bowden
GLNMAC Gyro	A110,A109,A108	-	-	GNC	Gyro	3-axis	129.74	N/A	N/A	ACS	90	0	AFT	X&Y changes	E. Bowden
UNH Racetrack Mag	S21	-	-	Experimenter	Magnetometer	3-axis	90.71	180	32.48	Main P/L Exp	180	270	FWD	Main P/L Exp - Deployed	B. Banks
Cornell Mag	S1	-	-	Experimenter	Magnetometer	3-axis	90.71	0	29.60	Main P/L Exp	FWD	0	90	Main P/L Exp - Deployed	B. Banks
SUB P/L:															
Motor Pressure(3rd Stage) BBV	A33	Taber P/N A2911C252AAXASR7	-	Flt Perf	Pressure	Scalar	301.60	-	-	BBV					J. Polidan
Motor Pressure(4th Stage) Nihka	A34	Taber P/N A2911C252AAXASR7	-	Flt Perf	Pressure	Scalar	212.70	-	-	Nihka					J. Polidan
WAASP Accelerometers	A6,A7,A8	WAASP	92915	Electrical	Accelerometer	3-axis	185.78	N/A	N/A	SUB P/L TM	0	270	FWD	SUB P/L TM	B. Banks
WAASP Magnetometer	A9,A10,A11	WAASP	92915	Electrical	Magnetometer	3-axis	185.78	N/A	N/A	SUB P/L TM	0	90	FWD	SUB P/L TM	B. Banks
WAASP Temperature	A12	WAASP	92915	Electrical	Temperature	Scalar	185.78	N/A	N/A	SUB P/L TM				SUB P/L TM	B. Banks
WAASP Solar Sensors	A5	WAASP	92915	Electrical	Sun Sensor	Other	176.22	0,90,180,270	8.63	SUB P/L TM				SUB P/L TM	B. Banks
SUB P/L TX Thermistor	A28	Fenwal 15K	-	Electrical	Temperature	Scalar	184.45	N/A	N/A	SUB P/L TM				SUB P/L TM	B. Banks
SUB P/L PCM Thermistor	A29	Fenwal 15K	-	Electrical	Temperature	Scalar	185.28	N/A	N/A	SUB P/L TM				SUB P/L TM	B. Banks
Horizon Crossing Indicator(HCI)	A30,T2	HCI	5127	Flt Perf	Temperature	Scalar	185.78	80	7.09	SUB P/L TM	20 Aft	N/A	N/A	SUB P/L TM	B. Banks
Cornell Magnetometer	S1	Cornell Mag	-	Experimenter	Magnetometer	3-axis	176.67	180	5.46	SUB P/L Exp	FWD	270	0	SUB P/L Exp	B. Banks

1.2 Sensor Map

Figure 1. Sensor Map

2. ATTITUDE SENSORS

2.1 Sensor Configurations

This section will describe in detail, how the attitude sensors are configured for this mission.

2.1.1 Main Payload: GLNMAC (Gimbal-mounted LN-200 with Sandia Miniature Airborne Computer)

The GLNMAC is a roll-stabilized inertial measurement unit that provides attitude knowledge in all three axes within one degree of certainty. The GLNMAC contains a strap-down fiber optic gyro and silicon accelerometers. Roll-isolation is provided by having the LN-200 mounted on a gimbal, thereby making it inertially stable from the spinning vehicle. Ideally, GLNMACS are mounted such that the vehicle's spin axis is parallel to the gimbal's rotational axis. For this mission, no significant offsets were seen with the mounting of the GLNMAC.

A full 3-axis attitude solution with an accuracy of $\pm$ 1° is provided by a GLNMAC. The GLNMAC provides the attitude solution (at a sample rate of 50 samples per second) in the form of DCMs (or quaternions) which are referenced to the body frame.

2.1.2 Main Payload: NIACS

The payload contained a NIACS (NSROC Inertial Attitude Control System), which used a predictive magnetic field algorithm to align the payload to the calculated –B field at T+500 prior to the sub payload separation. NIACS contains a GLNMAC which provides 3-axis attitude knowledge within +/- 1° of accuracy. The attitude solution is provided in the form of Direction

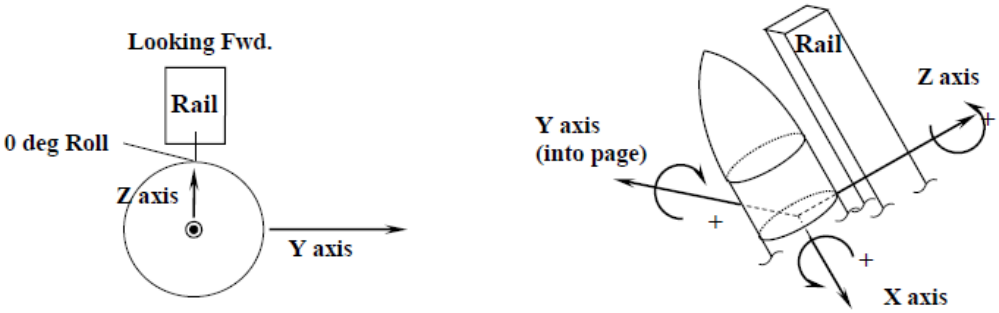

Figure 3: NIACS Payload Axes

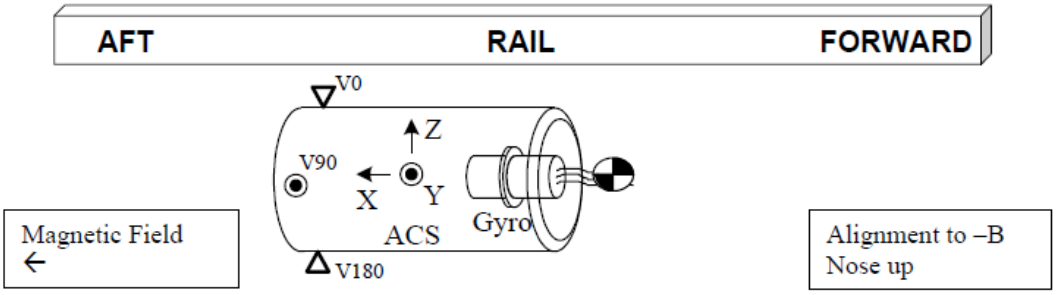

Cosine Matrices relative to the GAN0 (T0 launcher) frame. Orientation of the GLNMAC gyro is shown in Figure 2.

Figure 2. NIACS Polarity Map

2.1.3 Main Payload: Honeywell Magnetometer

Digital ACS Mag: Honeywell HMR2300

The following is a list of the specifications of the magnetometer:

1. Three axis magnetometer
2. Range of ± 120 uT.
3. Sample rate of 154 samples per second (50 Hz through ACS data stream).

During the magnetic calibration, the magnetometer was verified to be oriented in the following way relative to the payload: x axis = payload 225°, y axis = payload 315°, z axis = forward.

The DCM to rotate the Honeywell magnetometer into the FP frame is:

$$Direction\ Cosine\ Matrix\ (dcm) = \begin{bmatrix} 0 & -0.7071 & 0.7071 \\ 1 & -0.7071 & -0.7071 \\ 1 & 0 & 0 \end{bmatrix}$$

2.1.4 Main Payload: Cornell Magnetometer

Digital Science Mag

The following is a list of the specifications of the magnetometer:

1. Three axis magnetometer
2. Range of ± 60 uT.
3. Sample rate of 1000 samples per second.

During the magnetic calibration, the magnetometer was verified to be oriented in the following way relative to the payload when deployed: x axis = payload forward, y axis = payload 0°, z axis = payload 90°.

The DCM to rotate the Cornell magnetometer into the FP frame is:

$$Direction\ Cosine\ Matrix\ (dcm) = \begin{bmatrix} 1 & 0 & 0 \\ 0 & 0 & -1 \\ 0 & 1 & 0 \end{bmatrix}$$

2.1.5 Sub Payload: WAASP Magnetometer

WAASP Magnetometer

The following is a list of the specifications of the magnetometer:

1. Three axis magnetometer
2. Range of ± 60 uT.
3. Sample rate of 500 samples per second in TM.

During the magnetic calibration the magnetometer was verified to be oriented in the following way relative to the payload: x axis = payload 0°, y axis = payload 90°, z axis = forward.

The DCM to rotate the WAASP magnetometer into the FP frame is:

$$Direction\ Cosine\ Matrix\ (dcm) = \begin{bmatrix} 0 & 0 & -1 \\ 0 & 1 & 0 \\ 1 & 0 & 0 \end{bmatrix}$$

2.1.6 Sub Payload: Cornell Magnetometer

Digital Science Mag

The following is a list of the specifications of the magnetometer:

1. Three axis magnetometer
2. Range of $\pm$ 60 uT.
3. Sample rate of 1000 samples per second.

During the magnetic calibration, the magnetometer was verified to be oriented in the following way relative to the payload: x axis = forward, y axis = payload 270°, z axis = payload 0°.

The DCM to rotate the Honeywell magnetometer into the FP frame is:

$$Direction\ Cosine\ Matrix\ (dcm) = \begin{bmatrix} 1 & 0 & 0 \\ 0 & -1 & 0 \\ 0 & 0 & -1 \end{bmatrix}$$

2.1.7 Sub Payload: Solar Sensors (ARL SLITS)

The following is a list of the specifications of the solar sensors:

1. Four solar sensors mounted at payload 0° (straight), payload 90° (15° tilt), payload 180° (straight), and payload 270° (15° tilt).
2. 5°x150° field of view.
3. Sample rate of 4000 samples per second (all four sensors are muxed into one channel).

2.1.8 Sub Payload: Horizon Crossing Indicator (HCI)

The following is a list of the specifications of the HCI:

1. Analog and Digital signals
2. -10° tilt relative to the payload y-z plane.
3. Sample rate of 1000 samples per second for the analog signals and 250 samples per second for each digital signal (2 bytes).

2.2 Results of Integration, Testing, and Calibration

Magnetic calibration was performed on October 5, 2015 for the main payload Honeywell and Cornell mags. The sub payload Cornell and WAASP mags were also calibrated on October 5, 2015. The main and sub payloads were calibrated with the booms deployed and stowed. The Cornell and Honeywell mags are digital, while the WAASP is analog (the y-cable could not be attached to the sub payload WAASP due to its location). To collect data for the calibration, TM data was recorded and analyzed. A 50 vector thin shell vector test was ran for the sub and main payloads. Since science data was taken with the booms deployed, results from the booms deployed tests will be shown.

The results presented below show that the magnetometers functioned nominally during integration and testing. A nominal magnetometer is considered to be one that can measure the magnetic field's aspect angle to within 3º and the magnetic field strength to within 1 uT.

2.2.1 Main Payload HMR: Booms Deployed Calibration Results

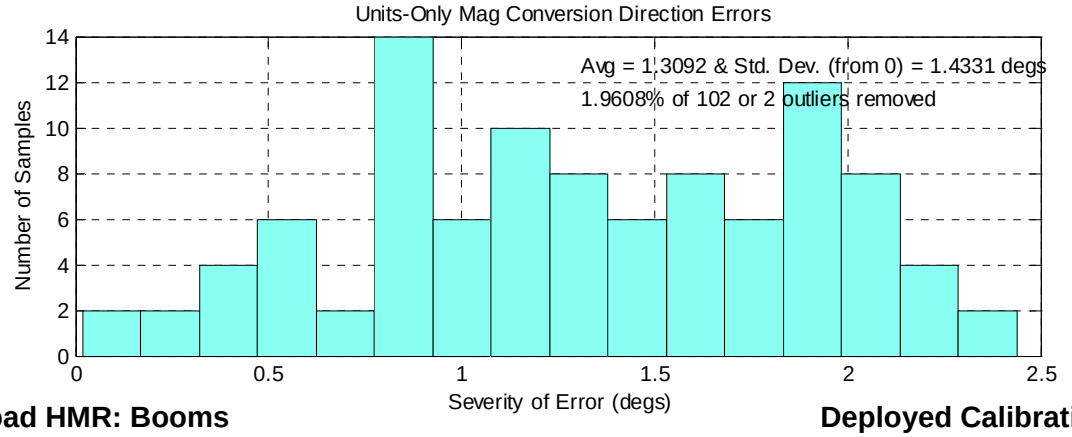

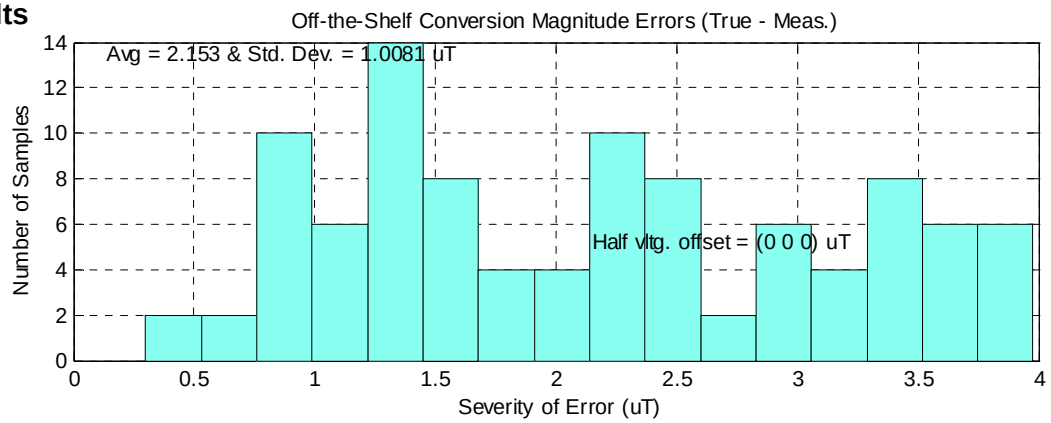

Figure 3. Main Payload HMR: Uncalibrated Magnetometer (Booms Deployed)

Figure 3 shows that without the calibration coefficients the average directional error is ~1.3° with a standard deviation of 1.4°. Error in the measurement of the magnitude of the magnetic field has an average of 2.2 uT with a standard deviation of 1.0 uT. The errors seen prior to the calibration are within the expected accuracy of the Honeywell magnetometer.

The calibration resulted in the following equation that was used to convert the raw magnetometer output to the measure of the Earth's magnetic field.

$$\mathbf{C} = \begin{bmatrix} 104.2641 & -0.8269 & -1.6490 \\ -0.8319 & 104.1876 & -0.8860 \\ -0.2001 & -2.7198 & 102.8743 \end{bmatrix} \cdot \underbrace{\left(\begin{bmatrix} Mx \\ My \\ Mz \end{bmatrix} - \begin{bmatrix} 1.0617 \\ 0.1065 \\ -0.8353 \end{bmatrix} \right)}_{\text{zero-bias adjustment}} volts$$

Once the calibration coefficients have been applied to the magnetometer data the errors have decreased and are shown in Figure 4.

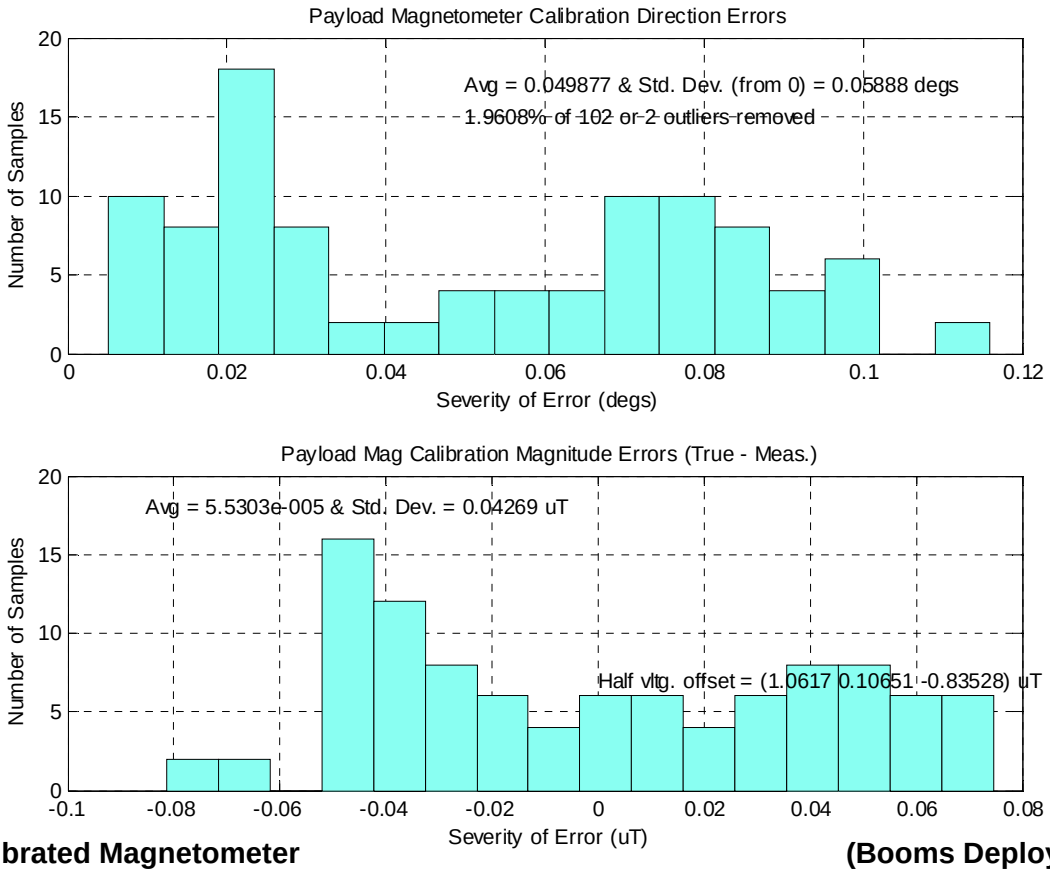

4. Figure Main Payload HMR: Calibrated Magnetometer (Booms Deployed)

Figure 4 shows that with the calibration coefficients, the average directional error is ~0.05° with a standard deviation of 0.06°. Error in the measurement of the magnitude of the magnetic field has an average of 0.00006 uT with a standard deviation of 0.04 uT. Results show that the calibration coefficients provide an improvement to the raw magnetic data.

The magnetic calibration verified that the magnetometer chosen will not experience clipping at Andoya Space Center, Norway.

2.2.3 Main Payload Science: Booms Deployed Calibration Results

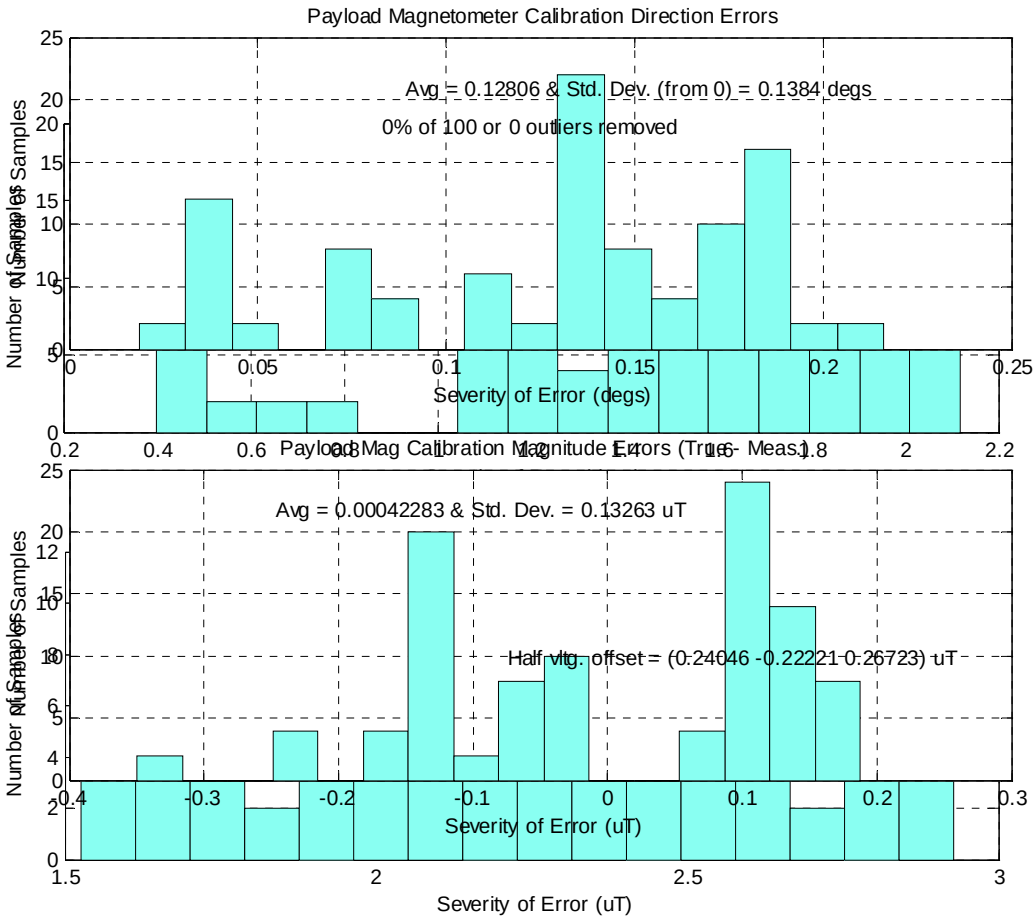

Figure 5. Main Payload Science: Uncalibrated Magnetometer (Booms Deployed)

Figure 5 shows that without the calibration coefficients the average directional error is ~1.5° with a standard deviation of 1.5°. Error in the measurement of the magnitude of the magnetic field has an average of 2.3 uT with a standard deviation of 0.4 uT. The errors seen prior to the calibration are within the expected accuracy of the Honeywell magnetometer. The exact cause is unknown but some contributors could be, internal electronics and the position of the mag in the calibration facility relative to the center of the theoretical magnetic sphere used for calibration.

The calibration resulted in the following equation that was used to convert the raw magnetometer output to the measure of the Earth's magnetic field.

$$\mathbf{C} = \begin{bmatrix} 103.4610 & -2.1279 & -0.6164 \\ 2.2273 & 104.2215 & -2.6024 \\ 0.1603 & 2.3237 & 104.0756 \end{bmatrix} \cdot \underbrace{\left(\begin{bmatrix} Mx \\ My \\ Mz \end{bmatrix} - \begin{bmatrix} 0.2405 \\ -0.2222 \\ 0.2672 \end{bmatrix} \right)}_{\text{zero-bias adjustment}} volts$$

Once the calibration coefficients have been applied to the magnetometer data the errors have decreased and are shown in Figure 6.

Figure 6. Main Payload Science: Calibrated Magnetometer (Booms Deployed)

Figure 6 shows that with the calibration coefficients, the average directional error is ~0.13° with a standard deviation of 0.14°. Error in the measurement of the magnitude of the magnetic field has an average of 0.0004 uT with a standard deviation of 0.13 uT. Results show that the calibration coefficients provide an improvement to the raw magnetic data.

The magnetic calibration verified that the magnetometer chosen will not experience clipping at Andoya Space Center, Norway.

2.2.3 Sub Payload WAASP: Booms Deployed Calibration Results

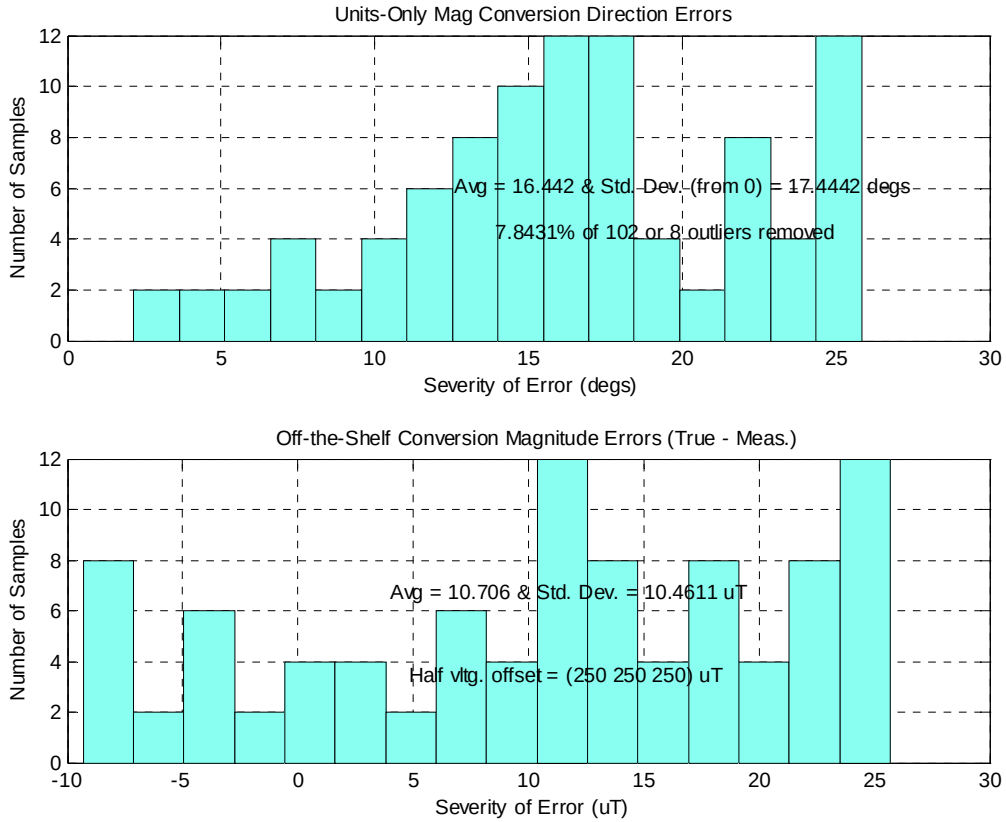

Figure 7. Sub Payload WAASP: Uncalibrated Magnetometer (Booms Deployed)

Figure 7 shows that without the calibration coefficients the average directional error is ~16.4° with a standard deviation of 17.4°. Error in the measurement of the magnitude of the magnetic field has an average of 10.7 uT with a standard deviation of 10.5 uT. The initial errors seen in the WAASP magnetometer are abnormally high. The exact cause of the errors is unknown, but some possible factors are: the magnetometer being mounted in the TM thus creating a magnetically unclean environment, not having the sub payload directly in the middle of the 6 foot theoretical magnetic field sphere for calibration, or a large internal bias due to the electronics in the sub payload.

The calibration resulted in the following equation that was used to convert the raw magnetometer output to the measure of the Earth's magnetic field.

$$\mathbf{C} = \begin{bmatrix} 133.6754 & -1.5100 & 4.0288 \\ -13.9908 & 144.7925 & 2.1981 \\ 4.6755 & 4.8605 & 105.5070 \end{bmatrix} \cdot \underbrace{\left(\begin{bmatrix} Mx \\ My \\ Mz \end{bmatrix} - \begin{bmatrix} 13.5643 \\ 4.7236 \\ -12.4903 \end{bmatrix} \right)}_{\text{zero-bias adjustment}} volts$$

Once the calibration coefficients have been applied to the magnetometer data the errors have decreased and are shown in Figure 8.

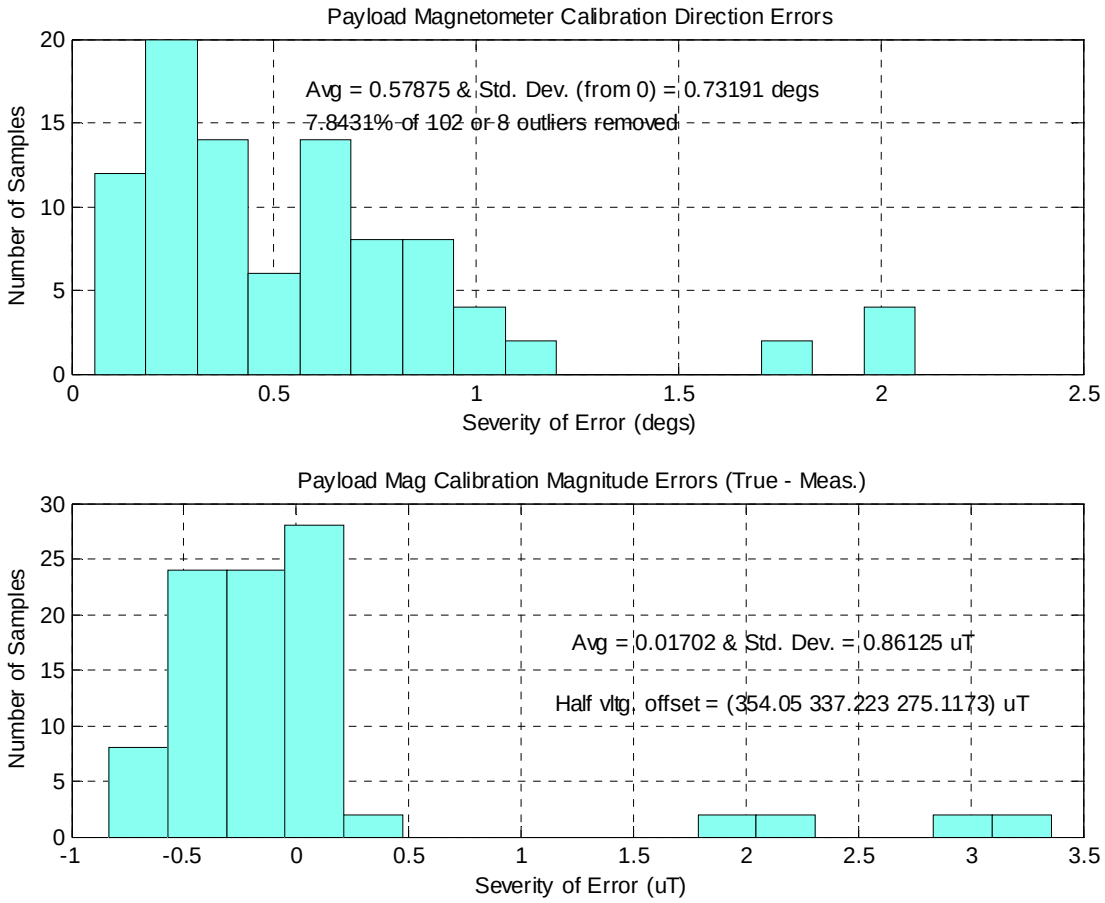

Figure 8. Sub Payload WAASP: Calibrated Magnetometer (Booms Deployed)

Figure 4 shows that with the calibration coefficients, the average directional error is ~0.58° with a standard deviation of 0.73°. Error in the measurement of the magnitude of the magnetic field has an average of 0.02 uT with a standard deviation of 0.86 uT. Due to the large errors prior to the calibration, this magnetometer will not be used for the final attitude solution.

The magnetic calibration verified that the magnetometer chosen will not experience clipping at Andoya Space Center, Norway.

2.2.4 Sub Payload Science: Booms Deployed Calibration Results

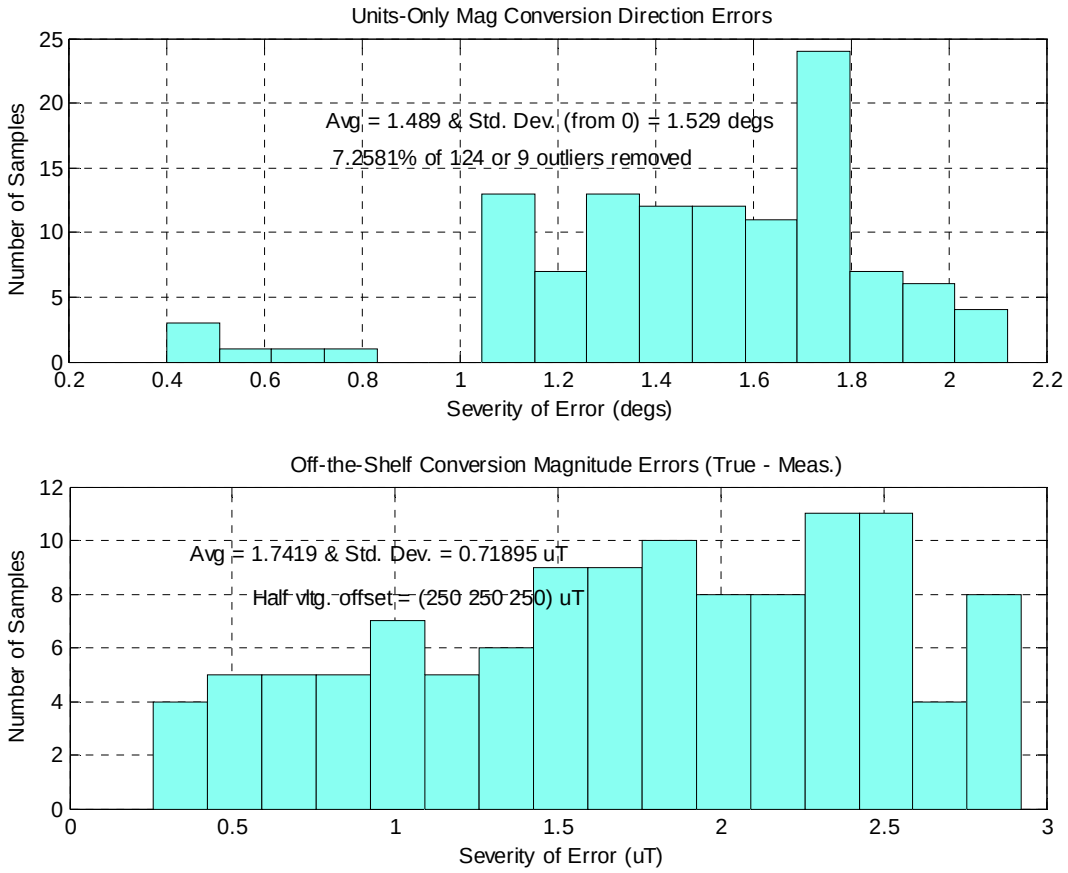

Figure 9. Uncalibrated Magnetometer (Booms Deployed)

Figure 9 shows that without the calibration coefficients the average directional error is ~1.49° with a standard deviation of 1.53°. Error in the measurement of the magnitude of the magnetic field has an average of 1.74 uT with a standard deviation of 0.72 uT. The errors seen prior to the calibration are within the expected accuracy of the Honeywell magnetometer. The exact cause is unknown but some contributors could be, internal electronics and the position of the mag in the calibration facility relative to the center of the theoretical magnetic sphere used for calibration.

The calibration resulted in the following equation that was used to convert the raw magnetometer output to the measure of the Earth's magnetic field.

$$\mathbf{C} = \begin{bmatrix} 103.4599 & -2.1140 & -0.6155 \\ 2.2251 & 104.2291 & -2.5995 \\ 0.1608 & 2.3275 & 104.0555 \end{bmatrix} \cdot \underbrace{\left(\begin{bmatrix} Mx \\ My \\ Mz \end{bmatrix} - \begin{bmatrix} 0.1978 \\ -0.1660 \\ 0.2189 \end{bmatrix} \right)}_{\text{zero-bias adjustment}} volts$$

Once the calibration coefficients have been applied to the magnetometer data the errors have decreased and are shown in Figure 10.

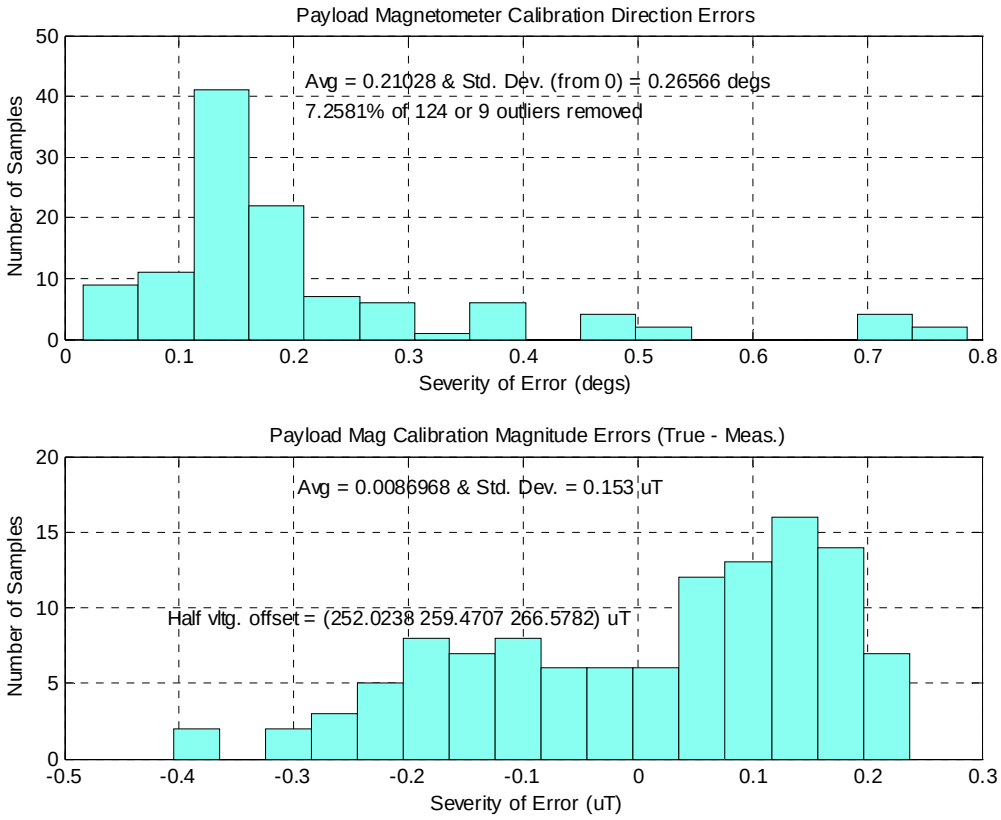

Figure 10. Calibrated Magnetometer (Booms Deployed)

Figure 10 shows that with the calibration coefficients, the average directional error is ~0.21° with a standard deviation of 0.27°. Error in the measurement of the magnitude of the magnetic field has an average of 0.01 uT with a standard deviation of 0.15 uT. Results show that the calibration coefficients provide an improvement to the raw magnetic data.

The magnetic calibration verified that the magnetometer chosen will not experience clipping at Andoya Space Center, Norway.

2.2.5 Sub Payload Solar Sensors Calibration Results

Calibration of the solar sensors was performed on August 28th, 2015. The purpose of the calibration is to determine how well the solar sensors can measure the solar aspect angle. To determine the accuracy, the sub payload skin with the solar sensors is placed on a rate table and spun at different elevations with a mirror shining light on the payload. Data is collected and two coefficients are calculated. C1 determines how well the tilted sensors are tilted (3.7321 is the nominal coefficient for a perfect 15° tilt) and C2 determines how well each pair of sensors (0° and 90°, 90° and 180°, 180° and 270°, 270° and 0°) are spaced (0.25 is the nominal coefficient for a 90° spacing around the payload).

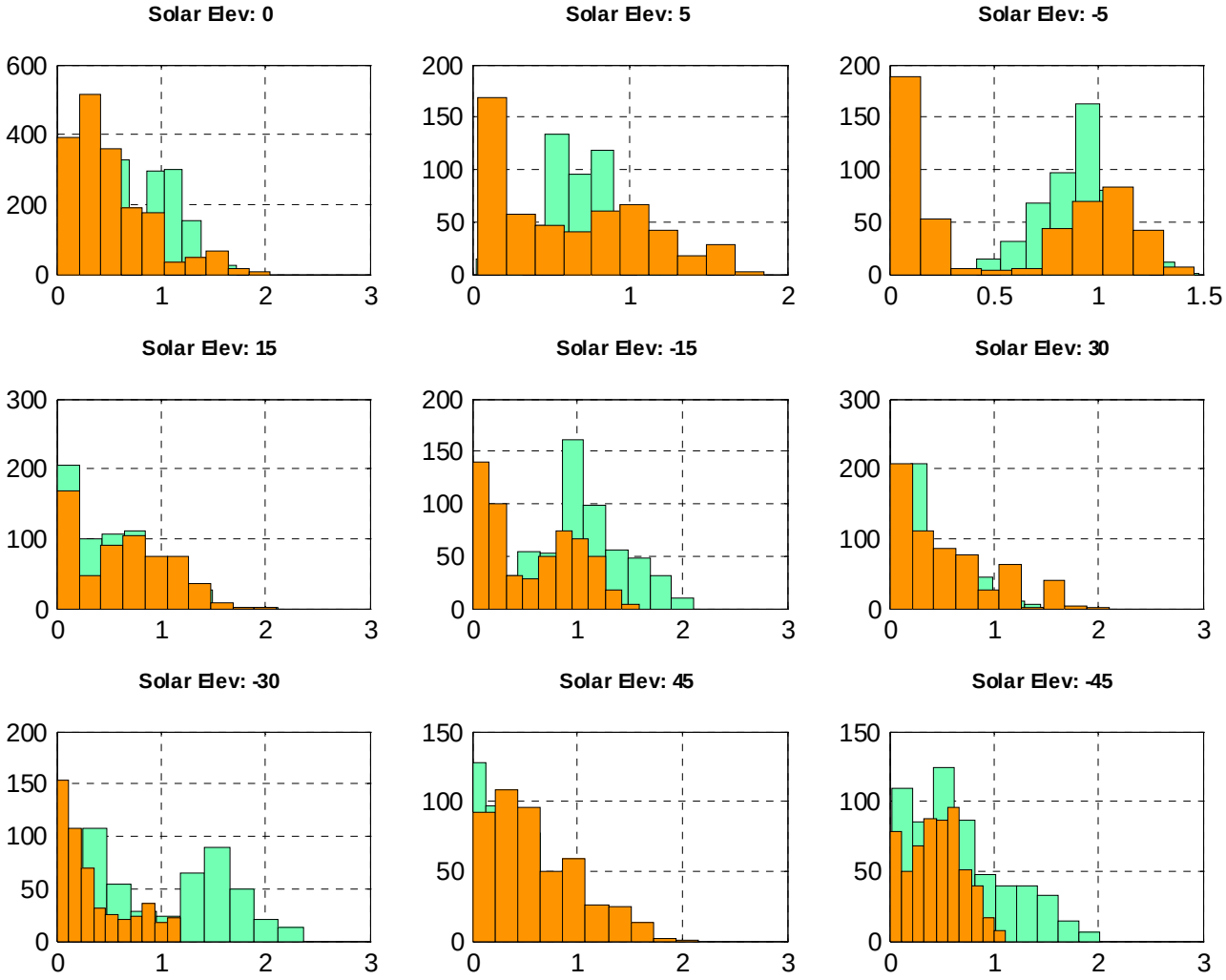

Figure 11. Solar Sensor Calibration Errors at Elevations

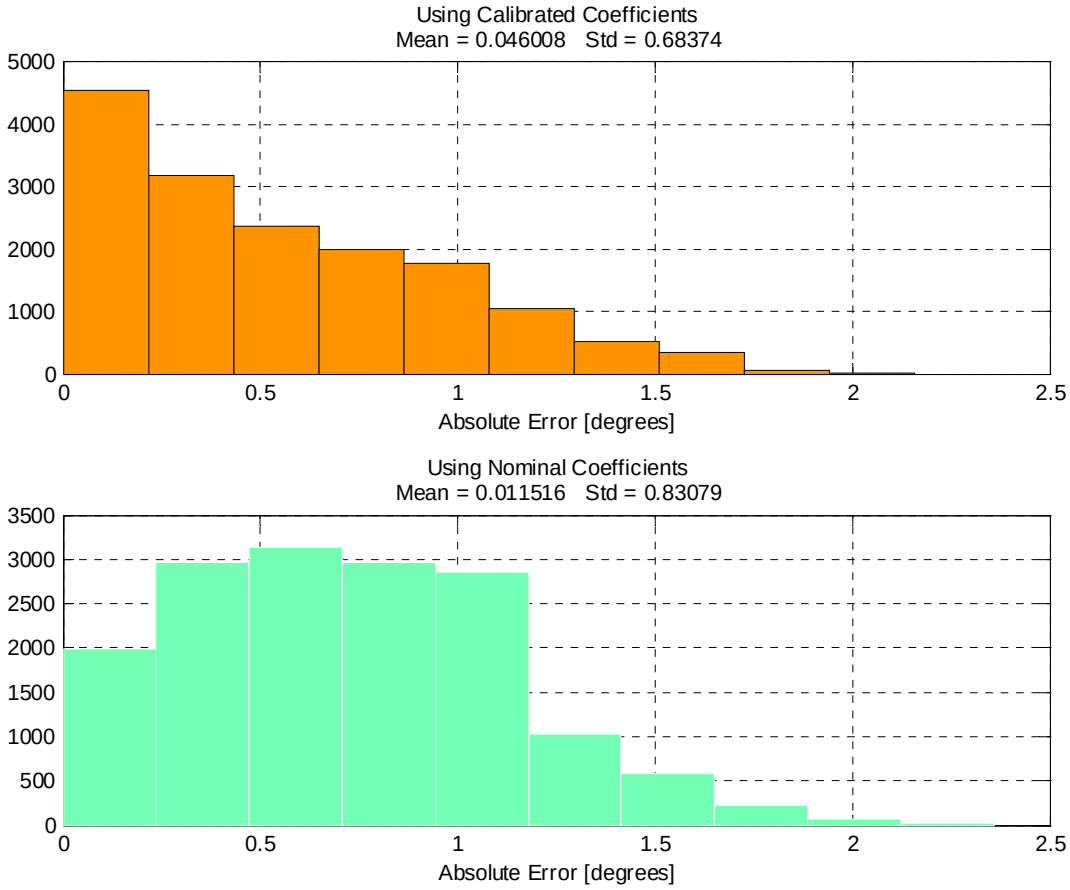

Figure 12. Solar Sensor Calibration Error Summary

Figure 11 shows the errors of the solar elevation angle measured by the solar sensors (green represents uncalibrated data and orange represents calibrated data). For each elevation, the uncalibrated error is under 3° with the calibrated error being under 2° with most results under 1°. Figure 11 also shows that the error distribution varies based on the solar elevation angle. Since angles greater than $\pm$ 45° could not be tested (tilting the rate table more than 45° was deemed as a potential risk since the test section could fall at large angles or produce poor data), there is an uncertainty in the accuracy for angles greater than 45°.

Figure 12 shows the collected results of the error distribution. For the data shown in Figure 12, the error with nominal coefficients is under 2° on average and close to 0.5° for an absolute error. Calibrated coefficients bring the average error closer to 0°. Nominal coefficients (3.7321 for C1 and 0.25 for C2) create a mean of 0.032° with a standard deviation of 0.835°. Calibrated coefficients have a mean of 0.057° with a standard deviation of 0.68°.

Coefficients from this calibration are the following:

	Pair 1	Pair 2	Pair 3	Pair 4
	0° & 270°	180° & 270°	90° & 180°	0° & 180°
C1	3.62700	3.83270	3.92310	3.79770
C2	0.24938	0.25020	0.25057	0.24985

3. ATTITUDE ANALYSIS

3.1 Attitude Determination Process

This section will explain in detail how the attitude was determined for this mission. It will provide the assumptions and restrictions used in each solution, the data reduction process, quality determination, and plots of the attitude solutions.

For this mission, a NIACS with a predictive algorithm was used to align the payload by T+184 seconds to where the –B field should be at T+500 seconds.

The attitude solution received from the NIACS system is a DCM, which takes the body frame (NIACS payload frame, shown in Figure 2) and transforms it to the GAN0 reference frame. These DCMs were transformed to take the Flight Performance body frame to the GAN0 frame, and this FP body frame is defined as follows:

- X-Axis: Out of the nose of the rocket
- Y-Axis: Completes Right Hand triad (at 90° perimeter)
- Z-Axis: Away from rail (at 180° perimeter)

Data provided by the GLNMAC comes from an asynchronous stream and therefore is not part of the same clock as the TM. In order for the attitude solution to be within 1°, synchronization needs to be performed on the asynchronous data stream. This is particularly important for roll since the roll changes by hundreds of degrees a second. Therefore, the asynchronous clock needs to be synched as closely as possible to the ground based clock to avoid any large error in the roll angle.

In order to synchronize the data, the GLNMAC sends a 1 pulse per second discrete signal. This pulse is recorded in the GLNMAC's discrete output. The TM contains a time event deck which sends 1 pulse each second and is recorded. Ideally, both of these pulses should be sent at the same time. However, during flight the two clocks drift apart and this causes error in the time, which makes the timing of the asynchronous attitude solution questionable if it is not synched properly.

Since the rocket is moving fast relative to the ground based clock and it is known that the onboard clocks contain drift (due to a number of factors with heating being a major contributor), it is assumed that the ground based clock contains the ideal time. Therefore, the asynchronous time stream will be synched to the ground based time stamps. In order to do this, the actual offsets between the GLNMAC and time event deck 1 pulse per second are calculated. Then a best fit offset function is calculated based on the error of the timing. Once this function is calculated, it is applied to the asynchronous time stream. To determine the accuracy of the new asynchronous clock, offsets are measured again. Ideally, these offsets would be zero but, there are rounding errors in the software which will still have a slight offset. The results of the time synchronization will be discussed further in section 3.3.

3.2 Assumptions and Restrictions

The assumptions underlying the data reduction and restrictions on the use of the attitude solution include the following:

1) Time is defined as elapsed seconds from launch (T0). T0 in GMT was 07:34:00

2) The launcher coordinates are WGS-84 Coordinates:

Launcher: Athena, Andoya, Norway
Latitude: 69.29422 Degrees
Longitude: 16.01925. Degrees
Elevation: 80.28 Degrees
Azimuth: 12.08 Degrees

3) The payload body frame is the Flight Performance body frame.

4) Elevation and Azimuth are with respect to the fixed local geodetic (North/East/Up) frame. Elevation approaches +90 degrees as the Roll axis approaches Zenith (up). Azimuth is zero at due north and goes positive clockwise (approaching east).

5) Euler angles (pitch, yaw, and roll), parameterize body to reference rotation in a 3-2-1 sequence, where roll is the rotation (degrees) of the payload about the longitudinal geometric axis, X, through the nose (FWD); yaw is the rotation (degrees) of the payload about lateral axis, Z, at 180 degrees from the rail; and pitch is the rotation (degrees) of the payload about the lateral axis, Y, at 90 degrees from the rail. The reference frame for this rotation is the payload body frame at launch (T0) assumed to be the orientation of the launcher.

3.3 Data Reduction and Quality

This section will provide an overview of the data that was reduced and used for the attitude solutions. Magnetic data will be shown for the main payload and sub payload to determine how close to the magnetic field the main payload was and how well the measurements match with the theoretical models. If the difference between the theoretical and calibrated fields is greater than 0.25 uT, then a post flight calibration will be performed.

Raw and processed data from the HCI will be shown along with its horizon crossing times. Raw and processed solar sensor data will be shown. Elevation and azimuth aspect angles calculated by the HCI and solar sensor data will be plotted to determine the quality of the data used for the final attitude solution.

An analysis of the HCI data raised suspicions that the HCI used was not properly calibrated for the low roll rate portions. The digital channel failed at low roll rates but did output data at high roll rates. Another issue with this HCI was that during the low roll rate portion of the flight, every other pulse would have a much weaker signal strength than the previous one. Some of these pulses made it hard to determine the exact crossing times since they were near the noise floor of some of the other pulses. For the report, the digital HCI data will not be shown since a solution could not be determined using the digital data during the science portion. Despite the poor data quality, a solution was calculated (using the analog channel) that is within the expected accuracy of ~ $\pm$ 5 - 10°.

3.3.1 Main Payload

3.3.1.1 Honeywell Magnetometer Data

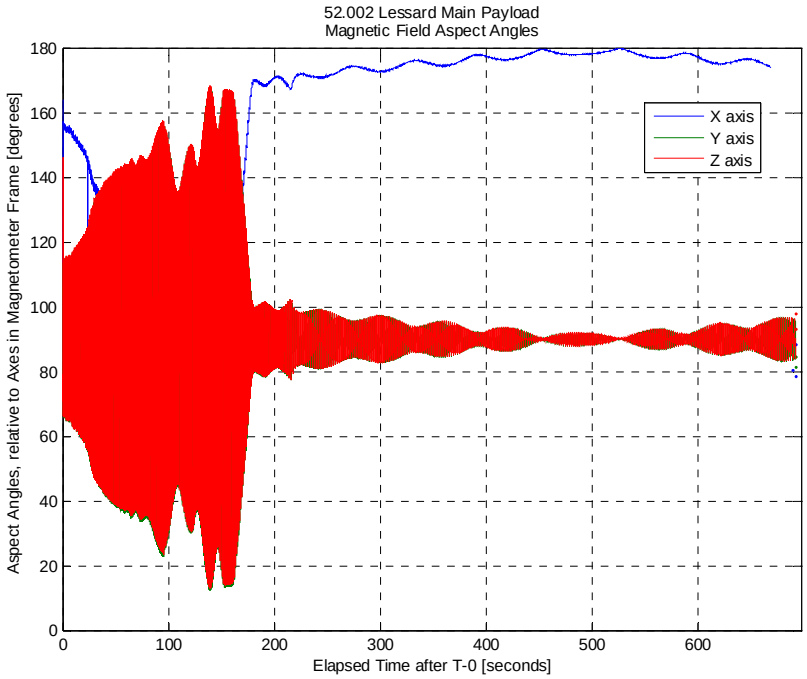

Figure 13. Main Payload HMR: Magnetic Aspect Angles (Full Flight)

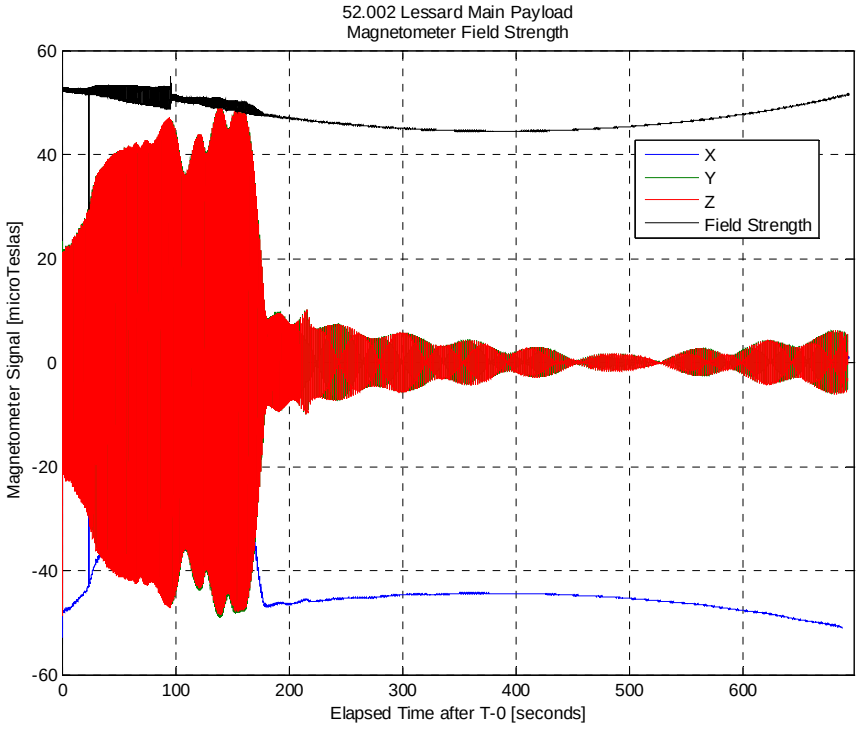

Figure 14. Main Payload HMR: Magnetic Field Strength (Full Flight)

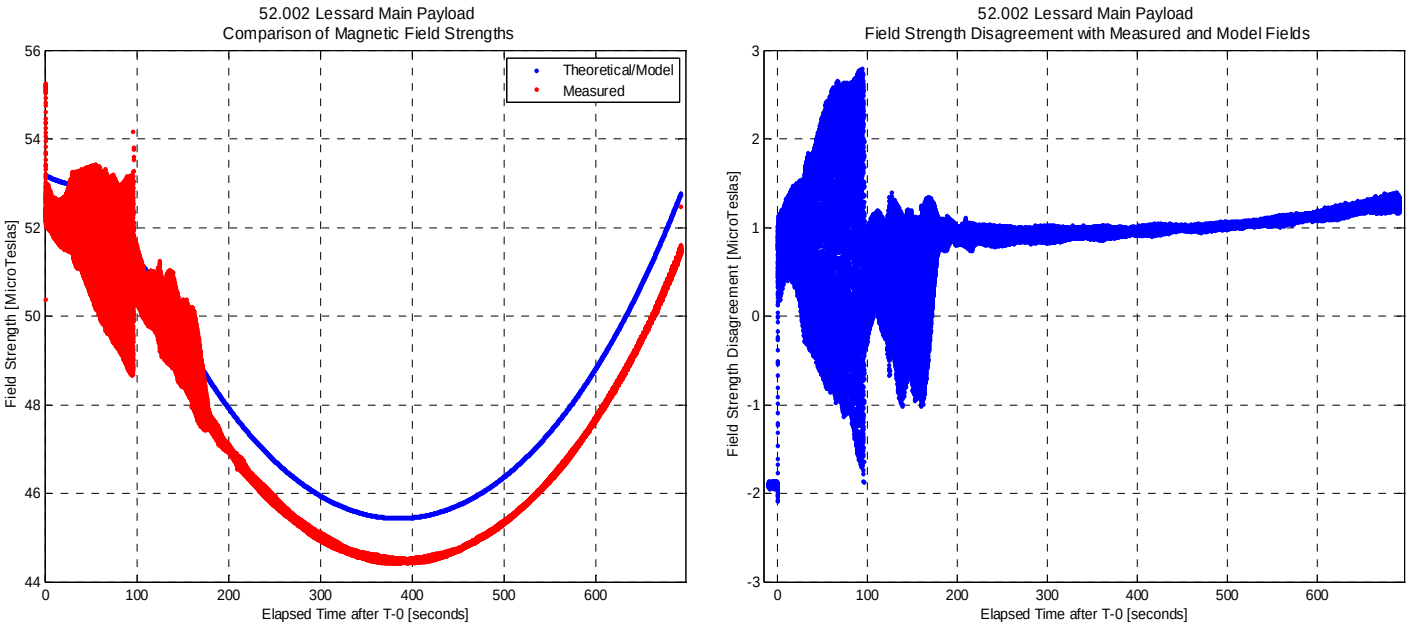

Figure 15. Main Payload HMR: Magnetic Field Strength Comparison (Full Flight)

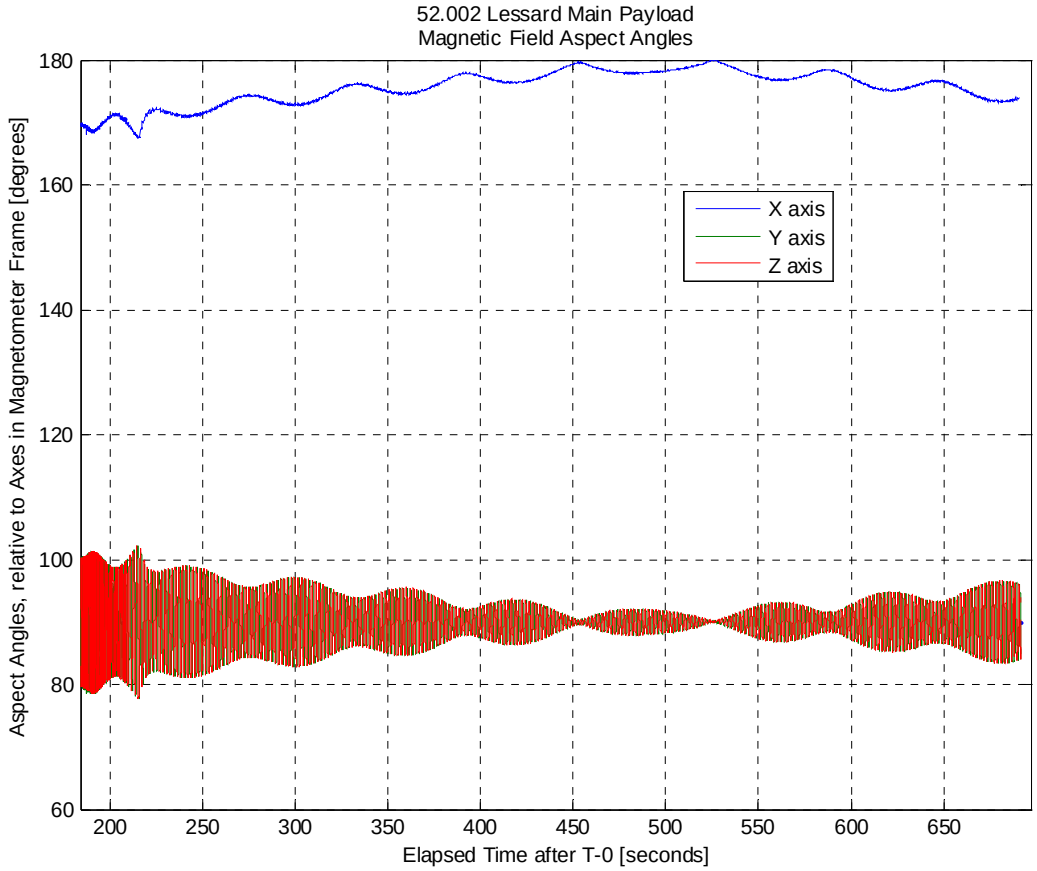

Figure 16. Main Payload HMR: Magnetic Field Aspect Angles (Science – Post Cal)

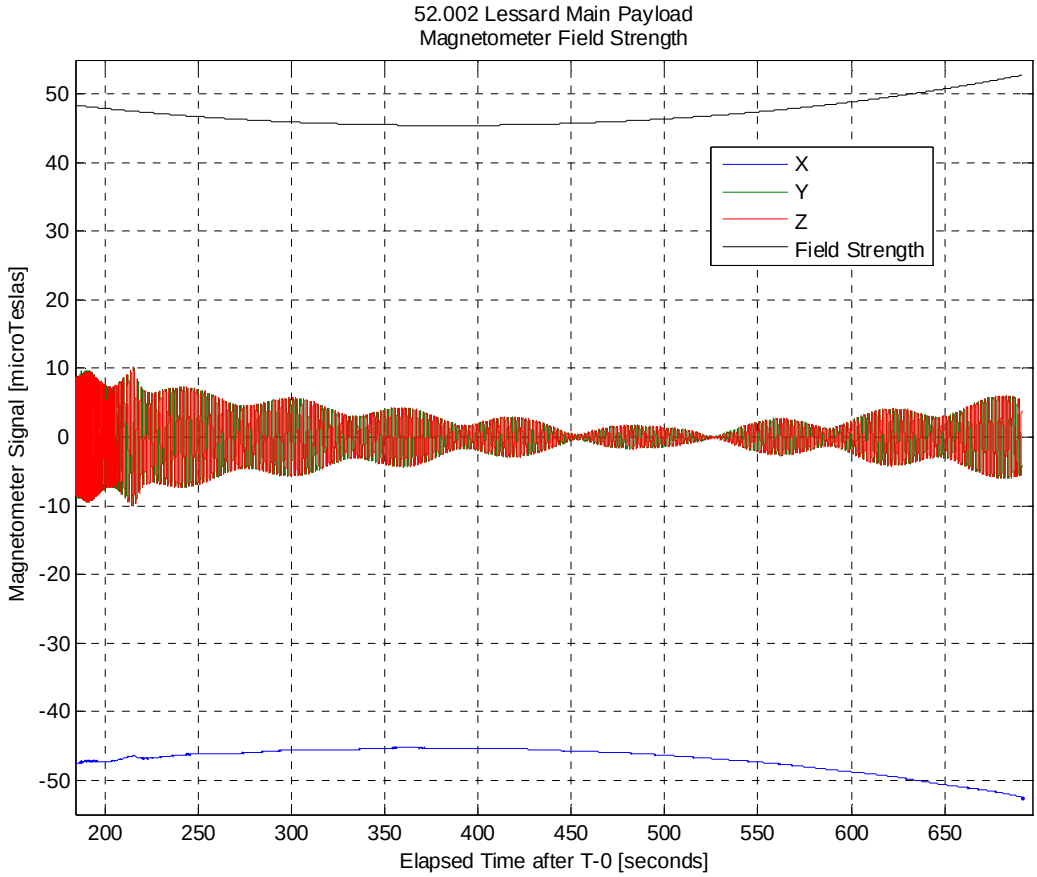

Figure 17. Main Payload HMR: Magnetic Field Strength (Science – Post Cal)

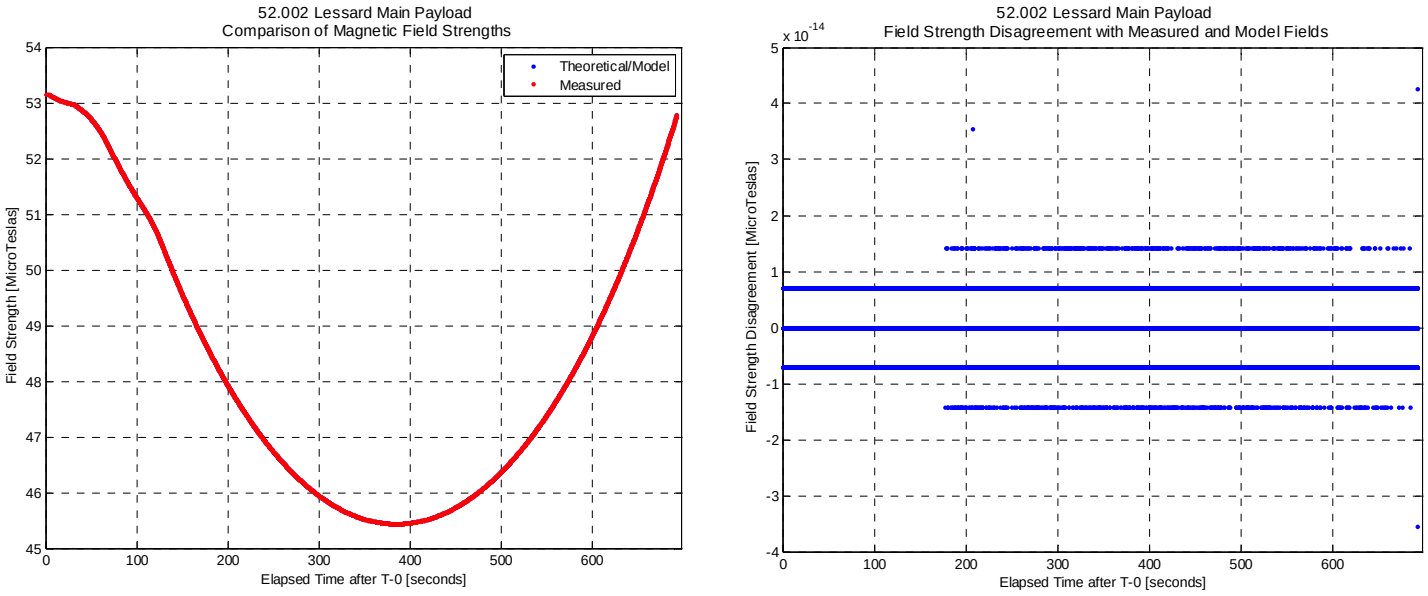

Figure 18. Main Payload HMR: Magnetic Field Strength Comparison (Science – Post Cal)

3.3.1.2 Science Magnetometer Data

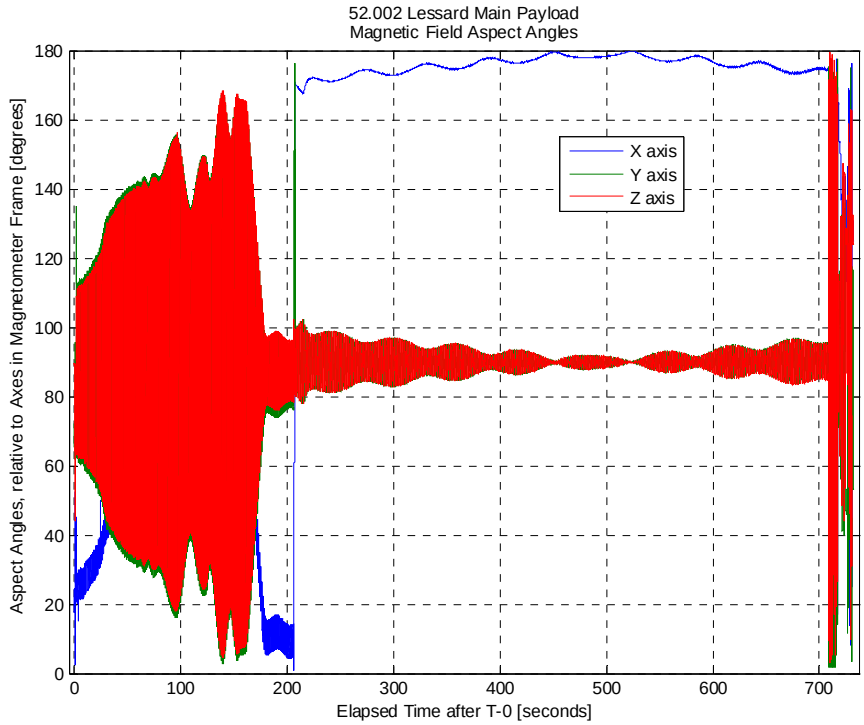

Figure 19. Main Payload Science: Magnetic Aspect Angles (Full Flight)

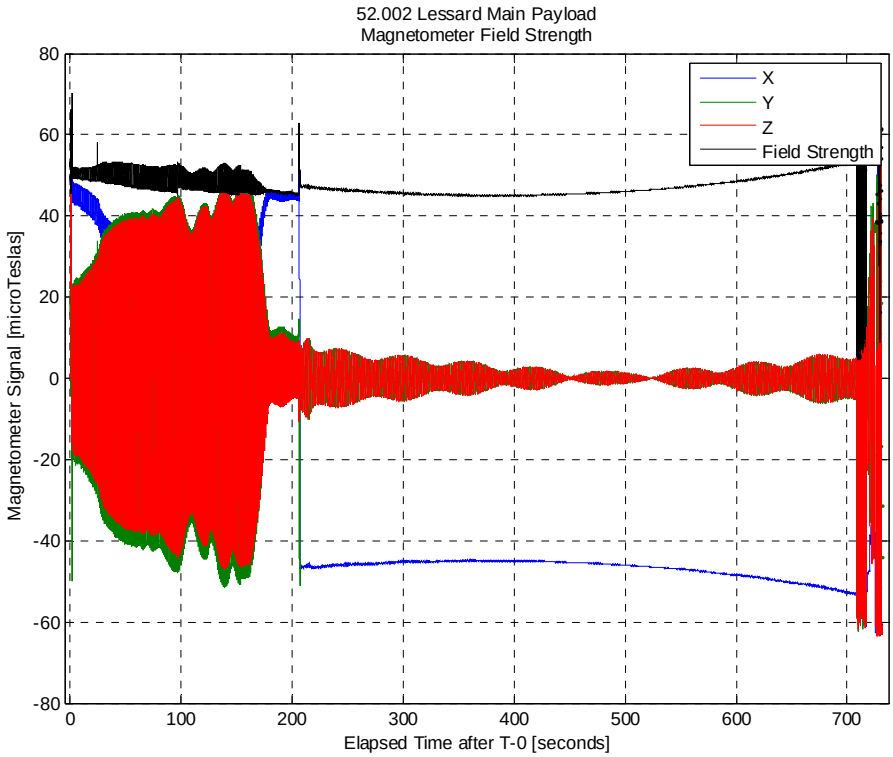

Figure 20. Main Payload Science: Magnetic Field Strength (Full Flight)

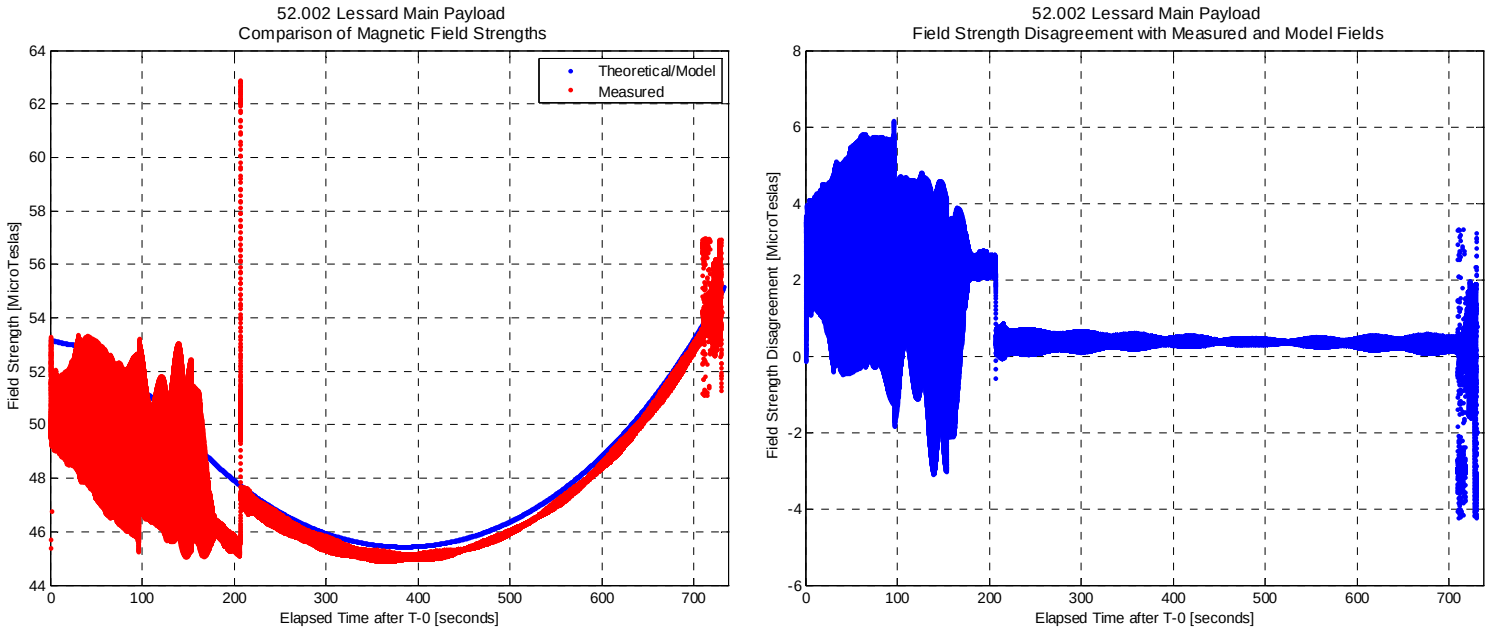

Figure 21. Main Payload Science: Magnetic Field Strength Comparison (Full Flight)

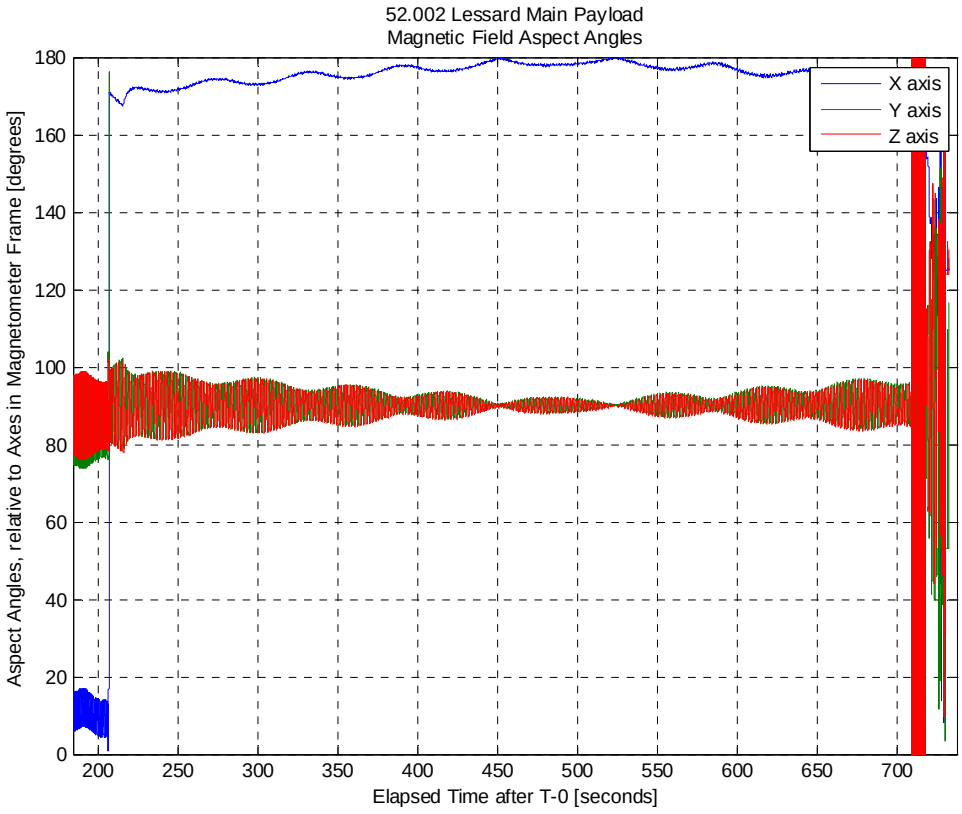

Figure 22. Main Payload Science: Magnetic Field Aspect Angles (Science – Post Cal)

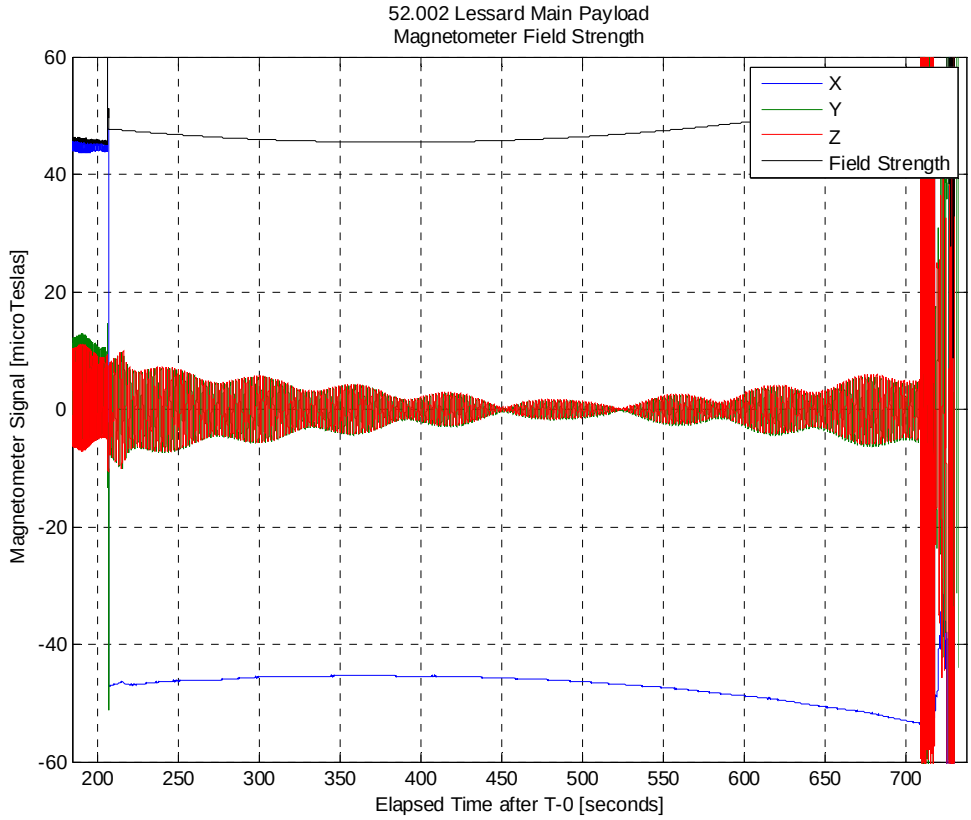

Figure 23. Main Payload Science: Magnetic Field Strength (Science – Post Cal)

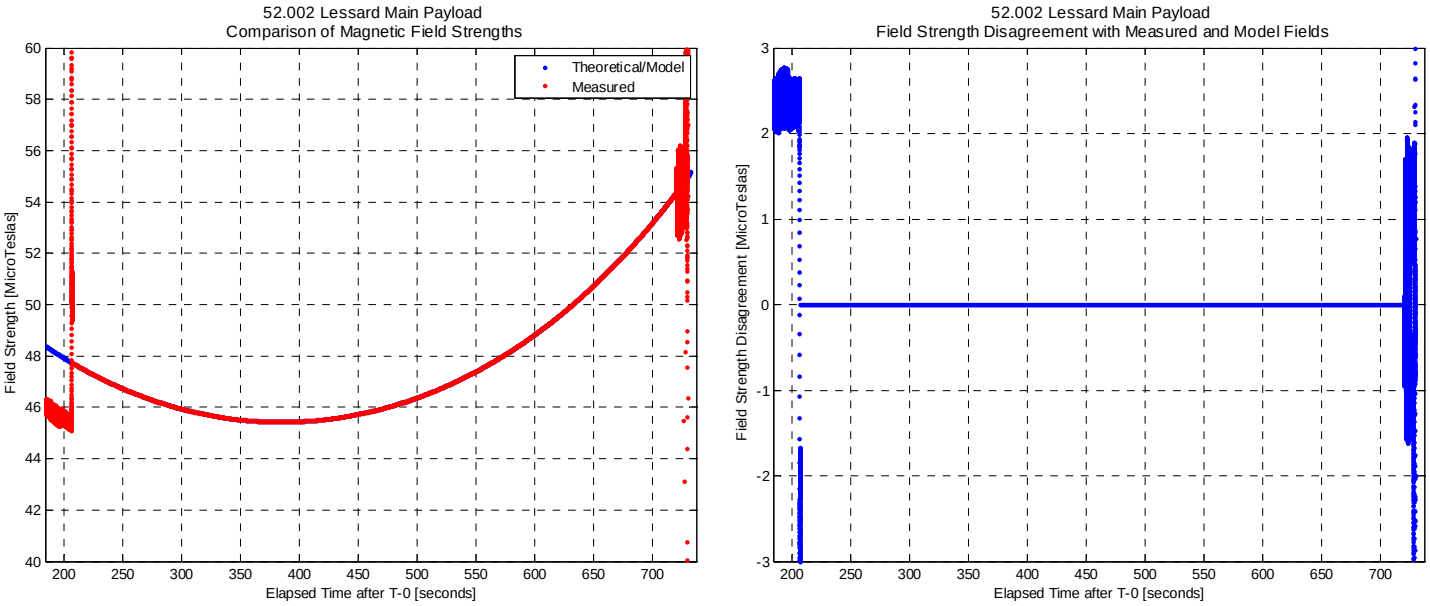

Figure 24. Main Payload Science: Magnetic Field Strength Comparison (Science – Post Cal)

3.3.1.3 Time Synchronization

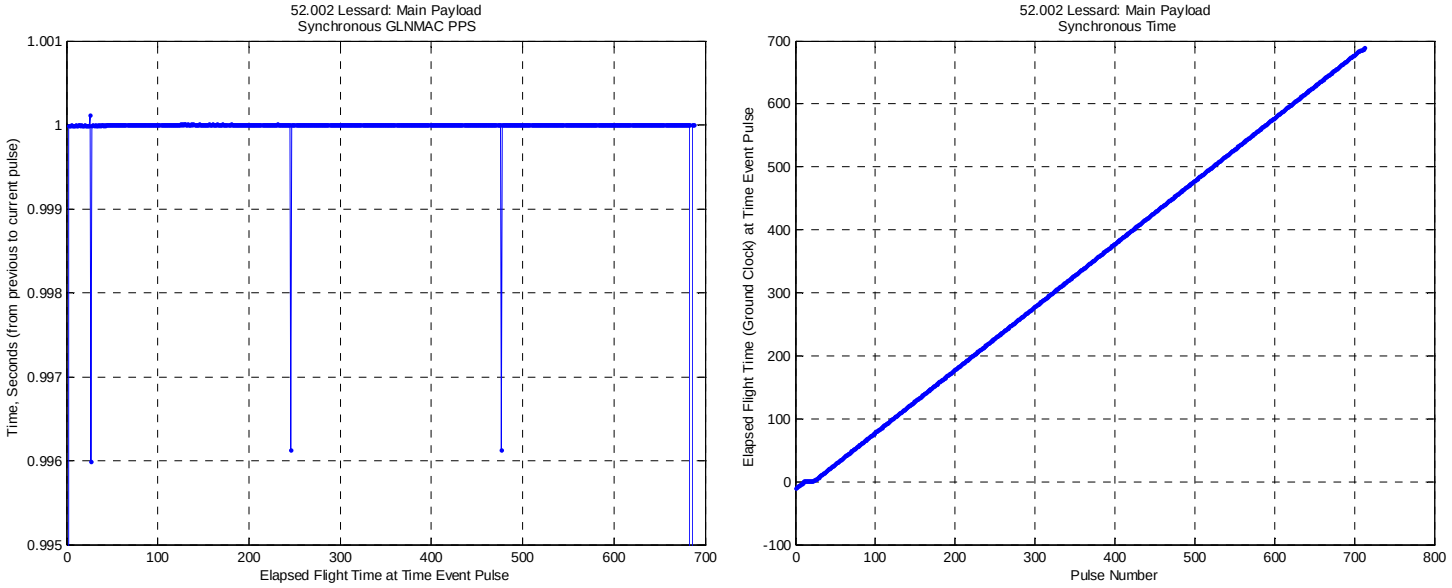

Figure 25 Synchronous Data Quality (Time Event Deck)

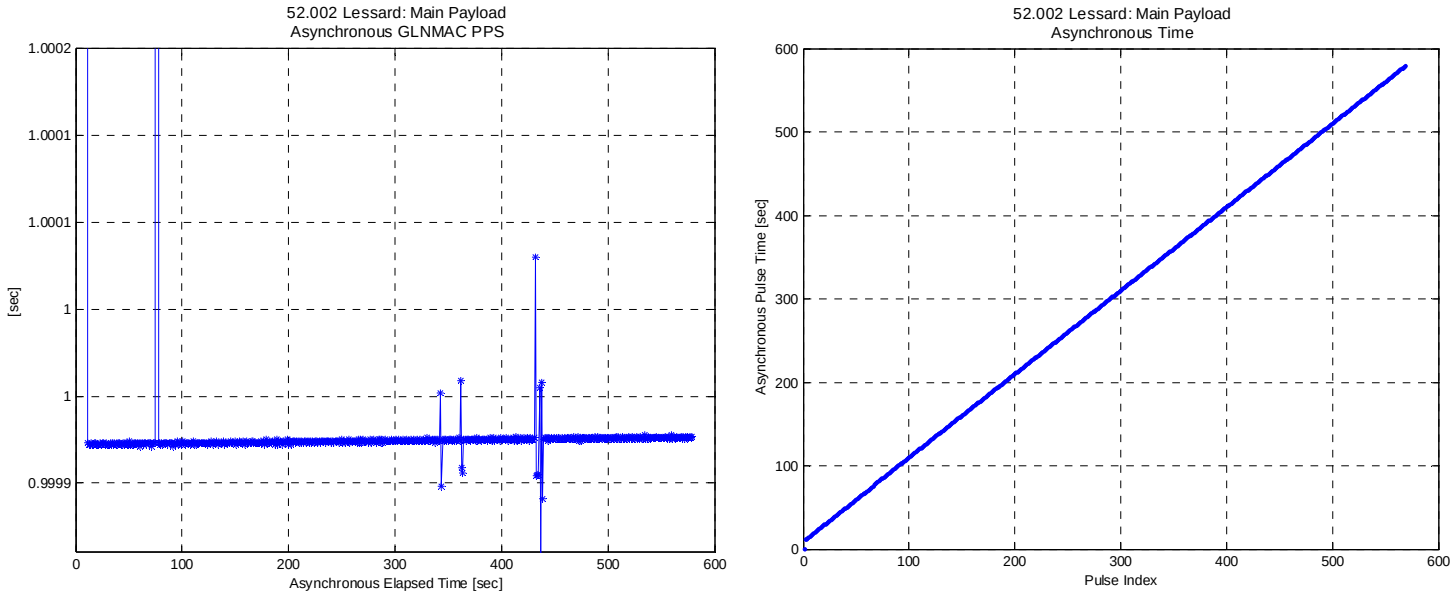

Figure 26. Asynchronous Data Quality (GLNMAC Timer)

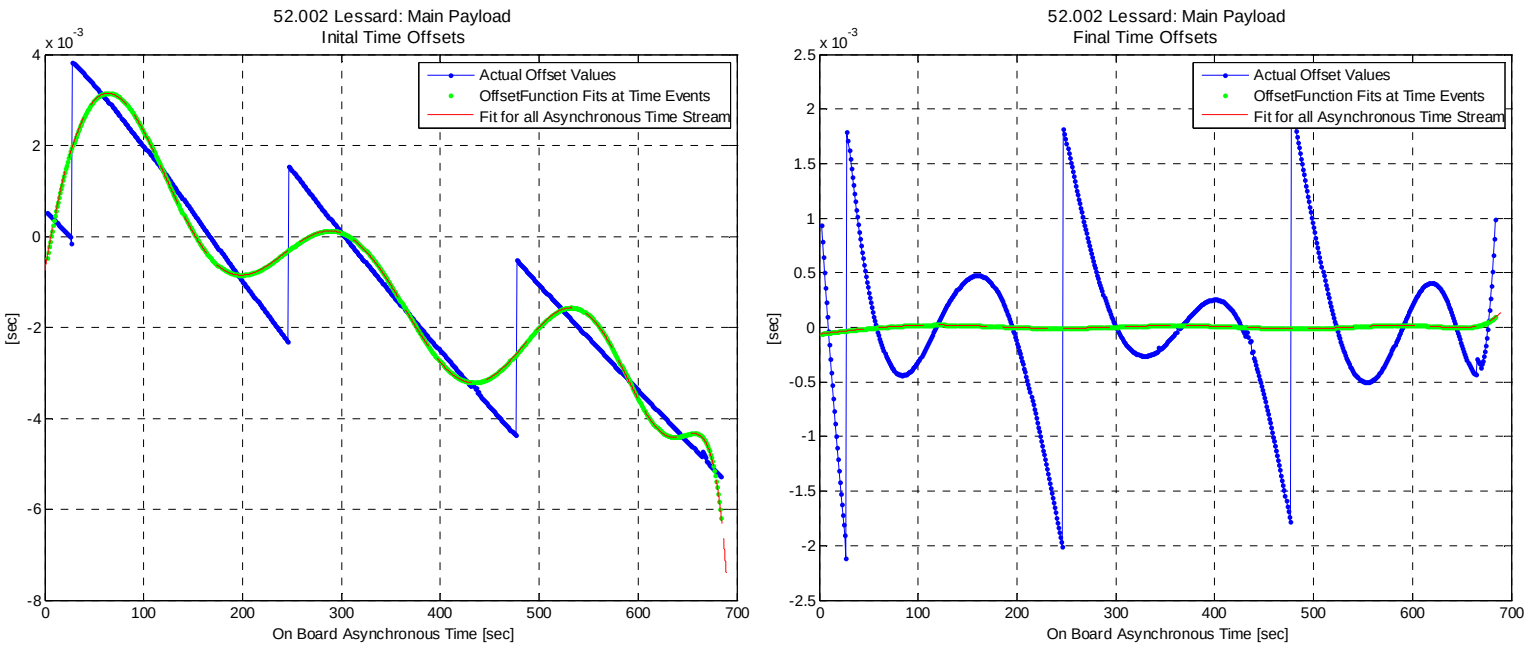

Figure 27. Time Offsets

The plots in Figure 25 show that the main payload had a few missing pulses and not all of the pulses from the time event deck were coming in at exactly one second. A few pulses were off by nearly 4 milliseconds, which is not uncommon. Figure 25 also shows that during the burn phases, the synchronous time had multiple pulses during the first thirty seconds. Figure 26 shows that the GLNMAC's onboard pulses came in at ~1 every second. Since the main payload spins at ~1.0 Hz during the science portion (begins at ~206 seconds, when the booms deploy), the time difference between the PCM clock (synchronous data) and the GLNMAC must not be greater than 2.8 milliseconds in order to measure the roll up to 1° per second. The plot on the left side of Figure 127 shows that prior to the time synchronization, the error was ranging from 4 milliseconds to -5 milliseconds. Once the time synchronization is applied, the error is reduced to no more than ~$\pm$ 2 milliseconds with the average fit offset being under 15 microseconds during the science portion.

3.3.2 Sub Payload

3.3.2.1 WAASP Magnetometer Data

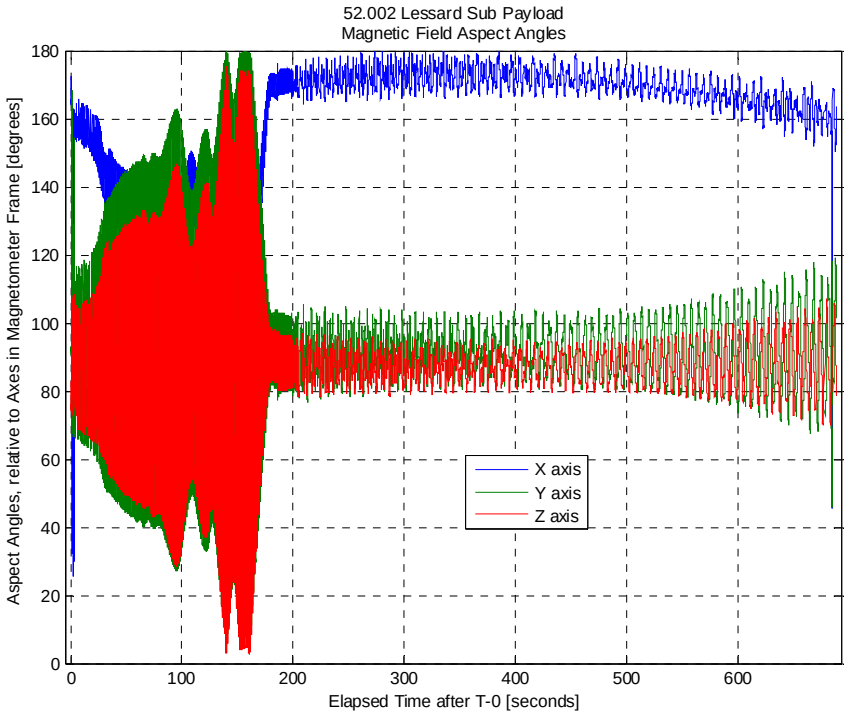

Figure 28. Sub Payload WAASP: Magnetic Aspect Angles (Full Flight)

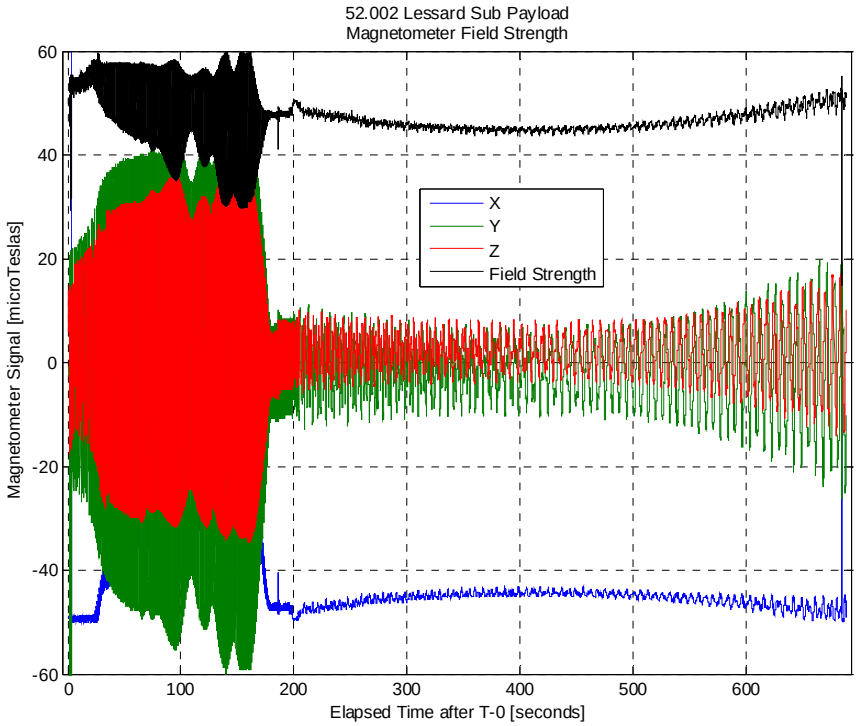

Figure 29. Sub Payload WAASP: Magnetic Field Strength (Full Flight)

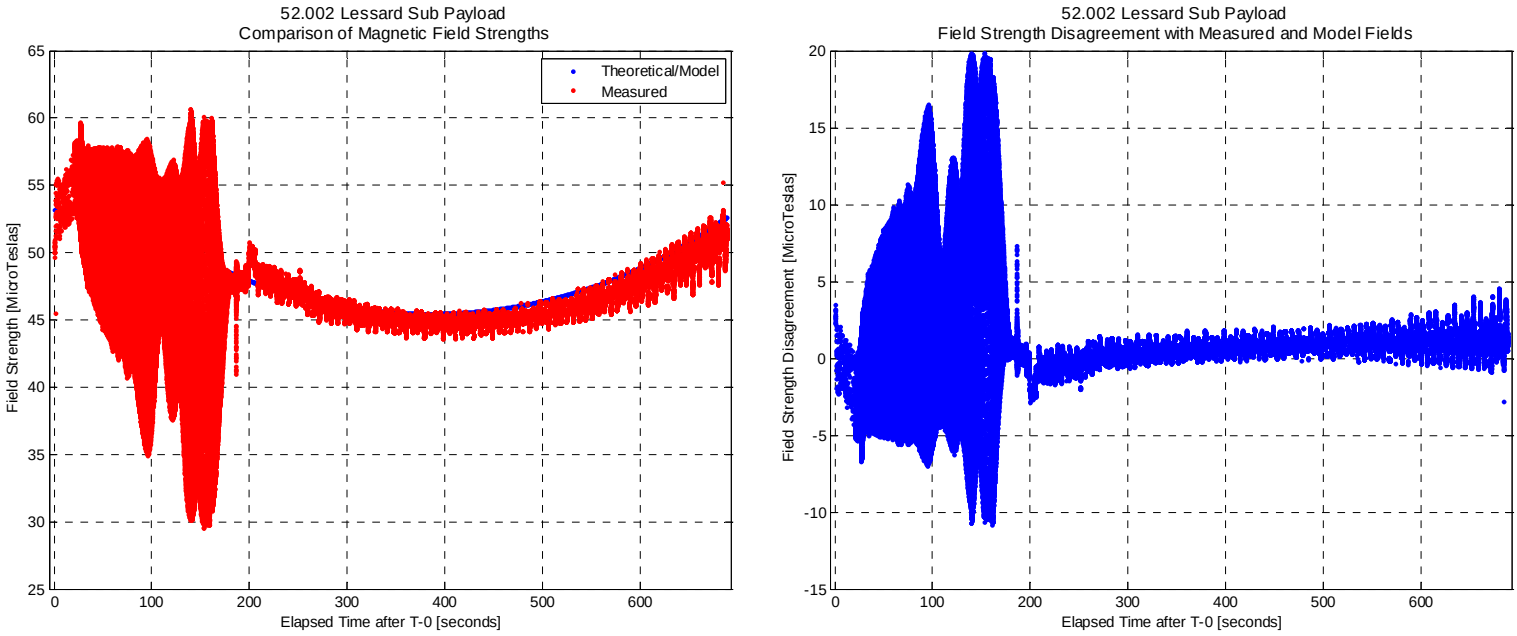

Figure 30. Sub Payload WAASP: Magnetic Field Strength Comparison (Full Flight)

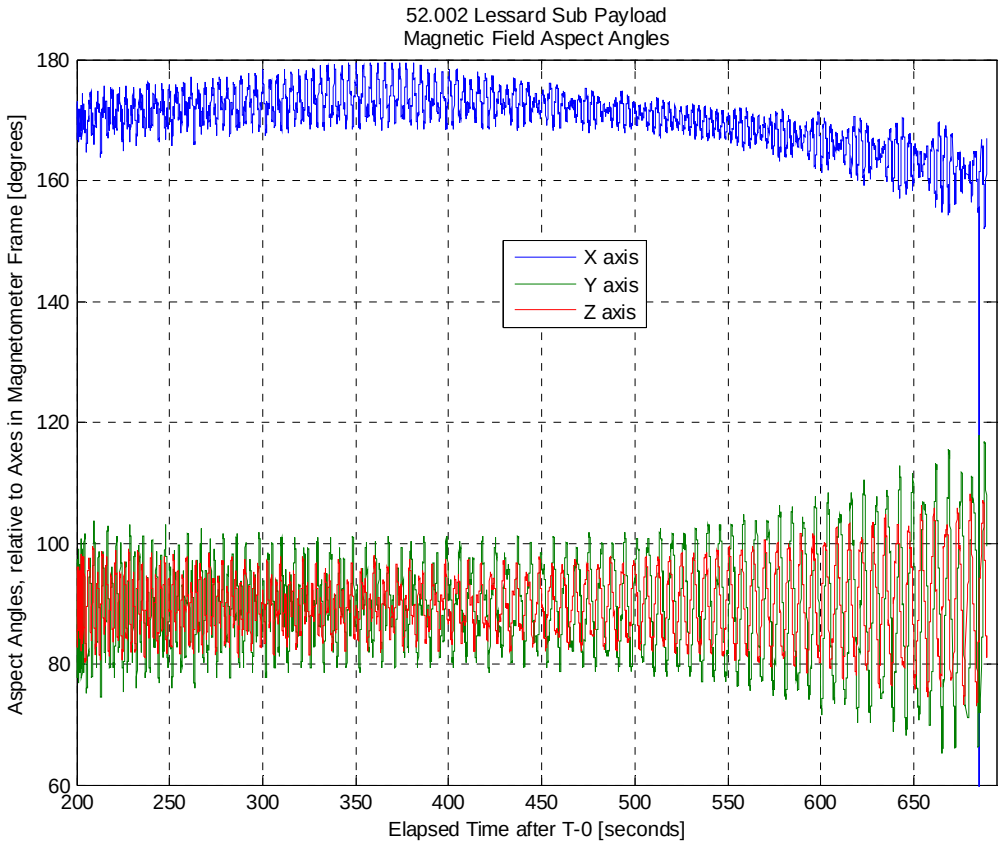

Figure 31. Sub Payload WAASP: Magnetic Field Aspect Angles (Science – Post Cal)

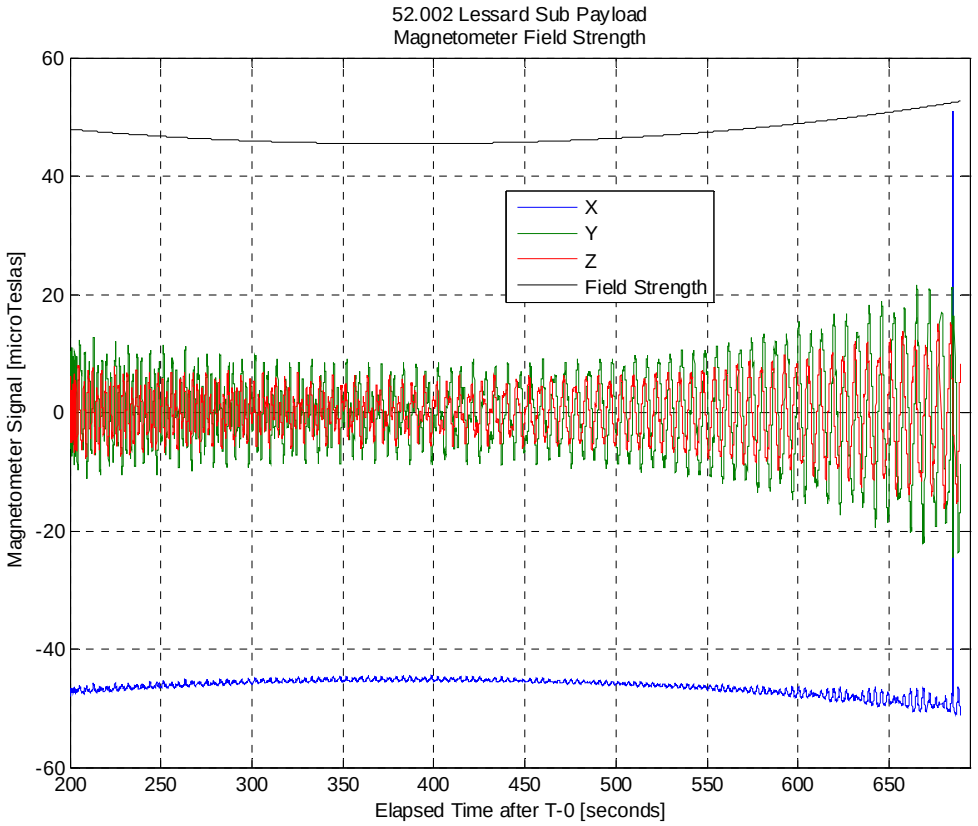

Figure 32. Sub Payload WAASP: Magnetic Field Strength (Science – Post Cal)

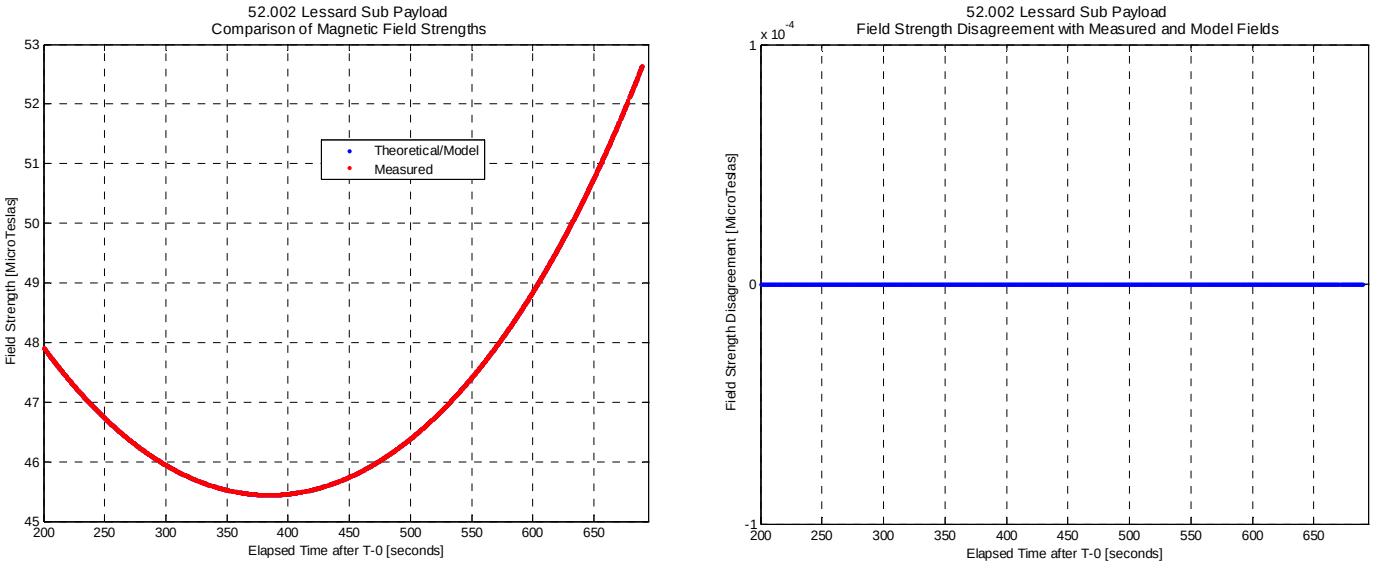

Figure 33. Sub Payload WAASP: Magnetic Field Strength Comparison (Science – Post Cal)

3.3.2.2 Science Magnetometer Data

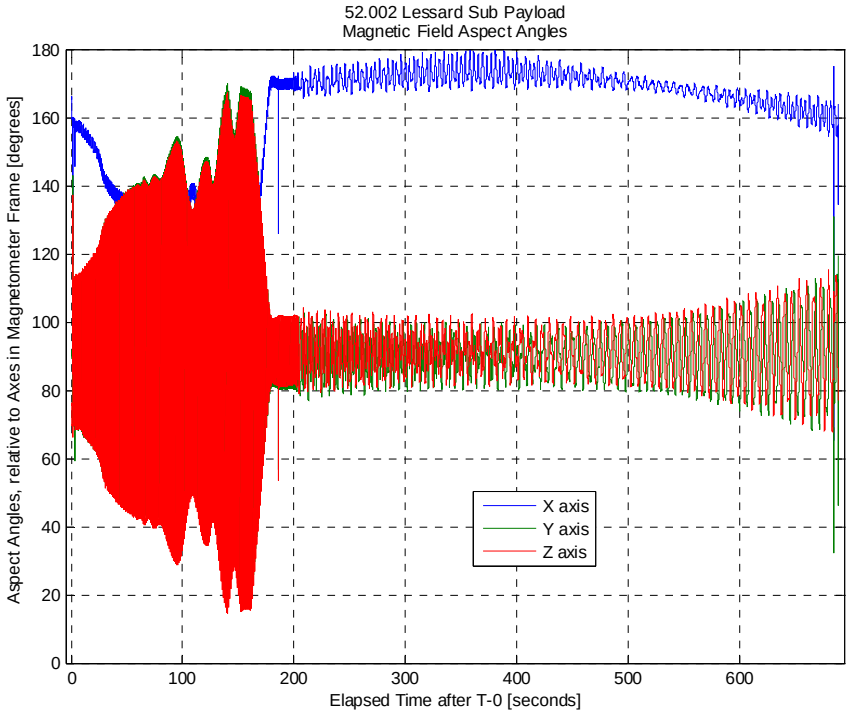

Figure 34. Sub Payload Science: Magnetic Aspect Angles (Full Flight)

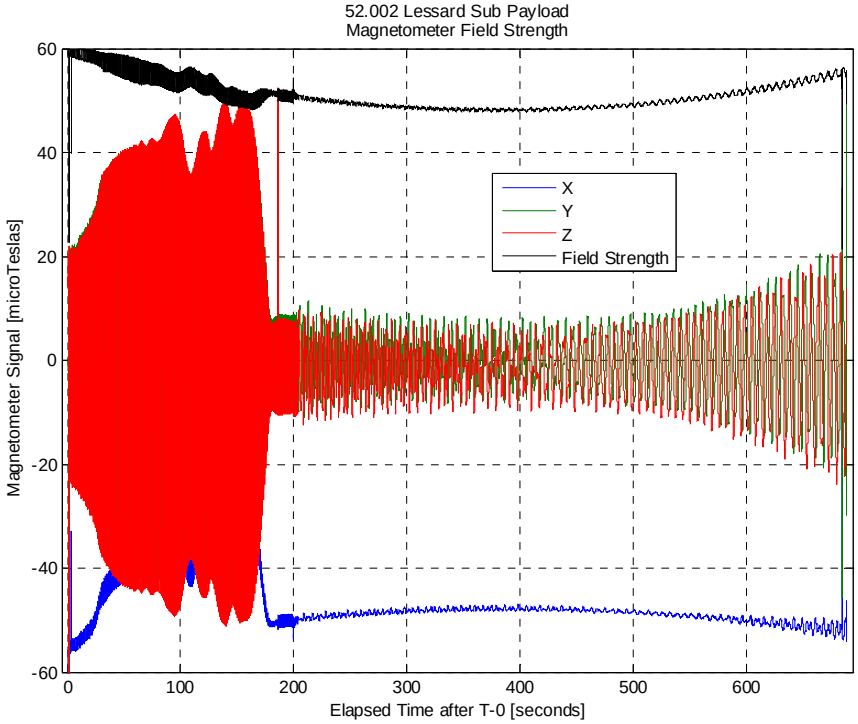

Figure 35. Sub Payload Science: Magnetic Field Strength (Full Flight)

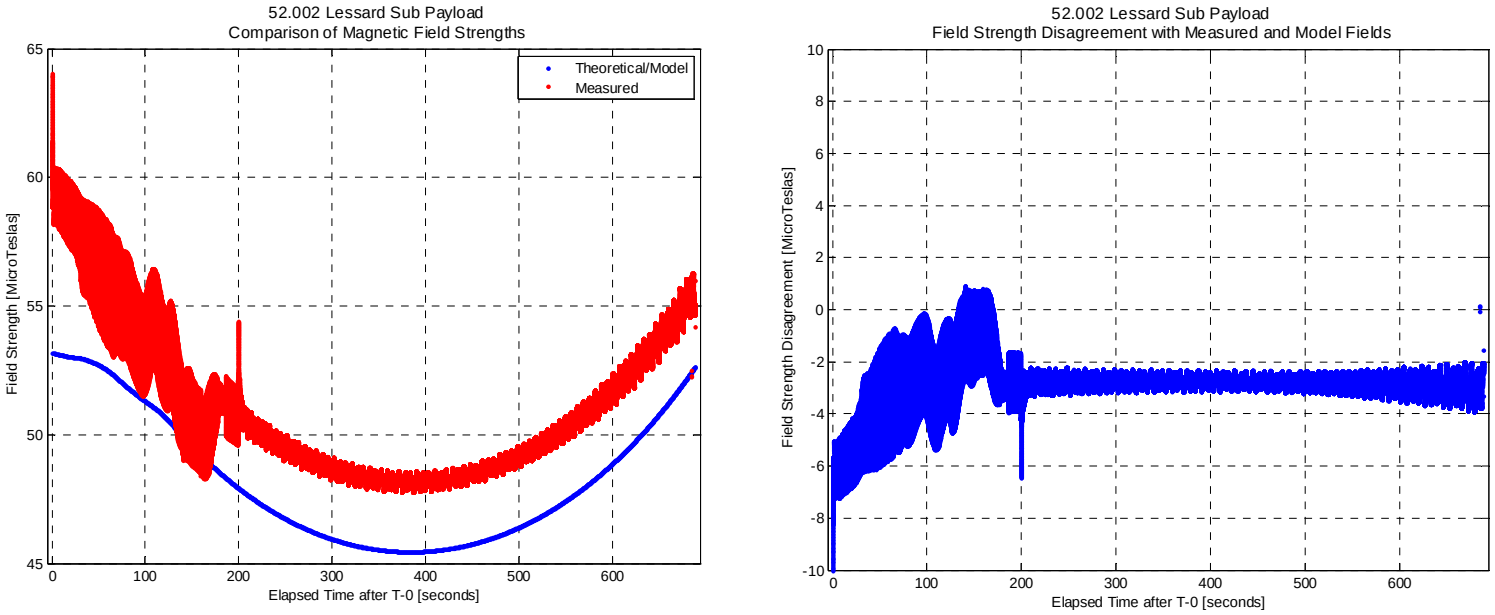

Figure 36. Sub Payload Science: Magnetic Field Strength Comparison (Full Flight)

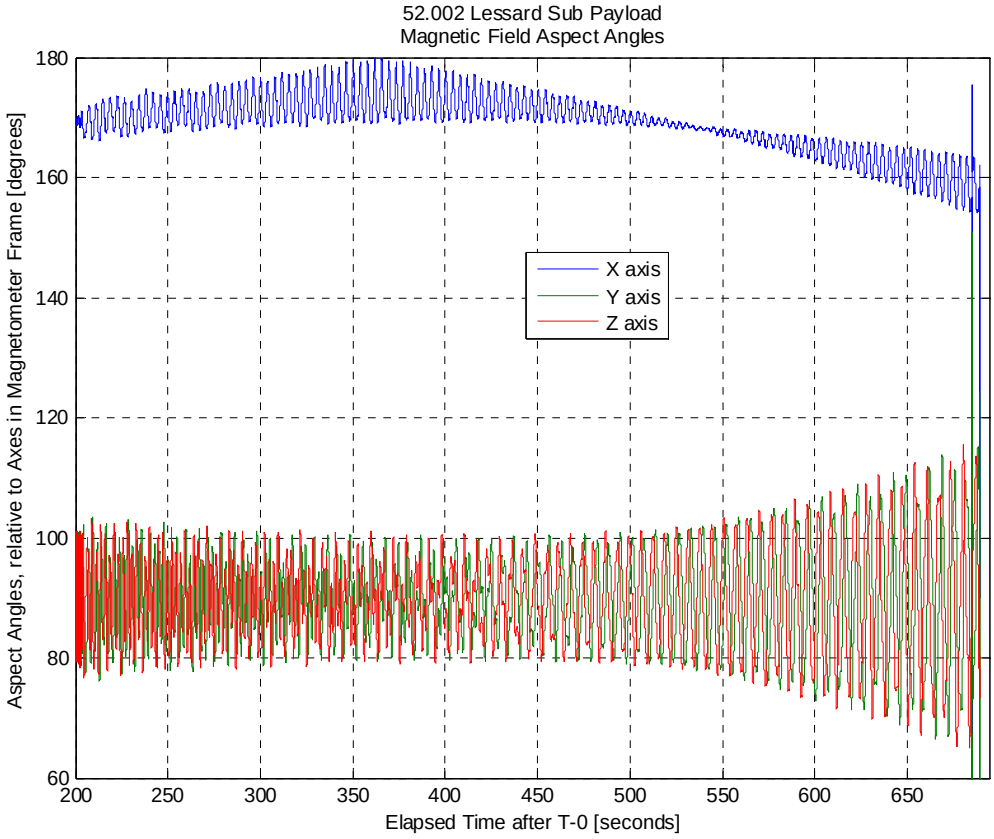

Figure 37. Sub Payload Science: Magnetic Field Aspect Angles (Science – Post Cal)

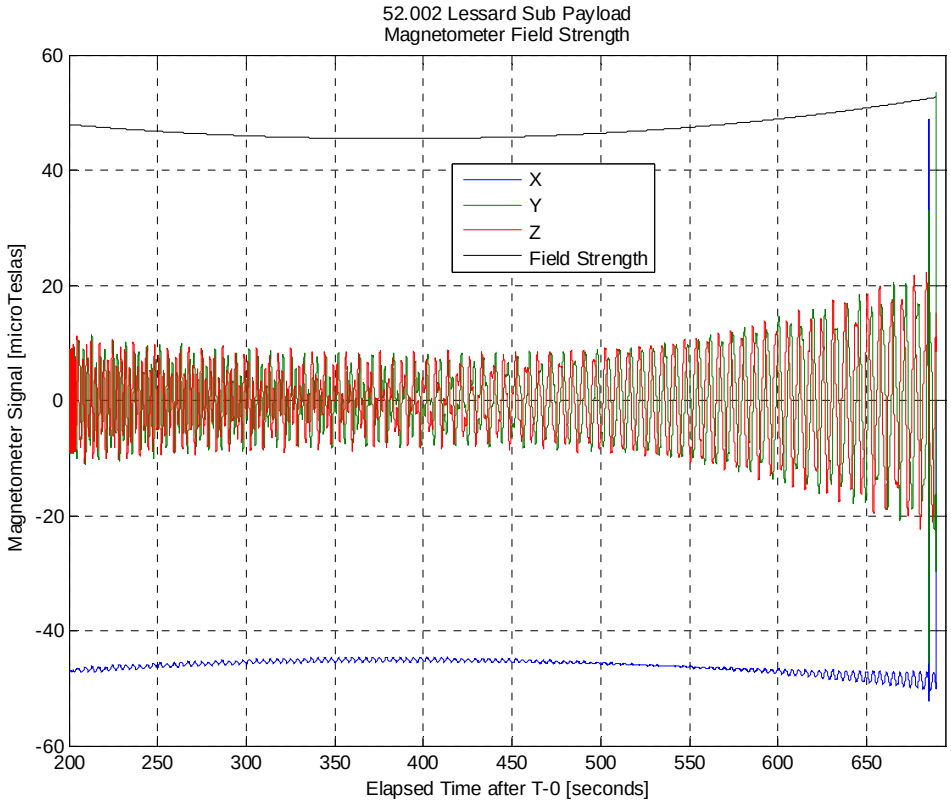

Figure 38. Sub Payload Science: Magnetic Field Strength (Science – Post Cal)

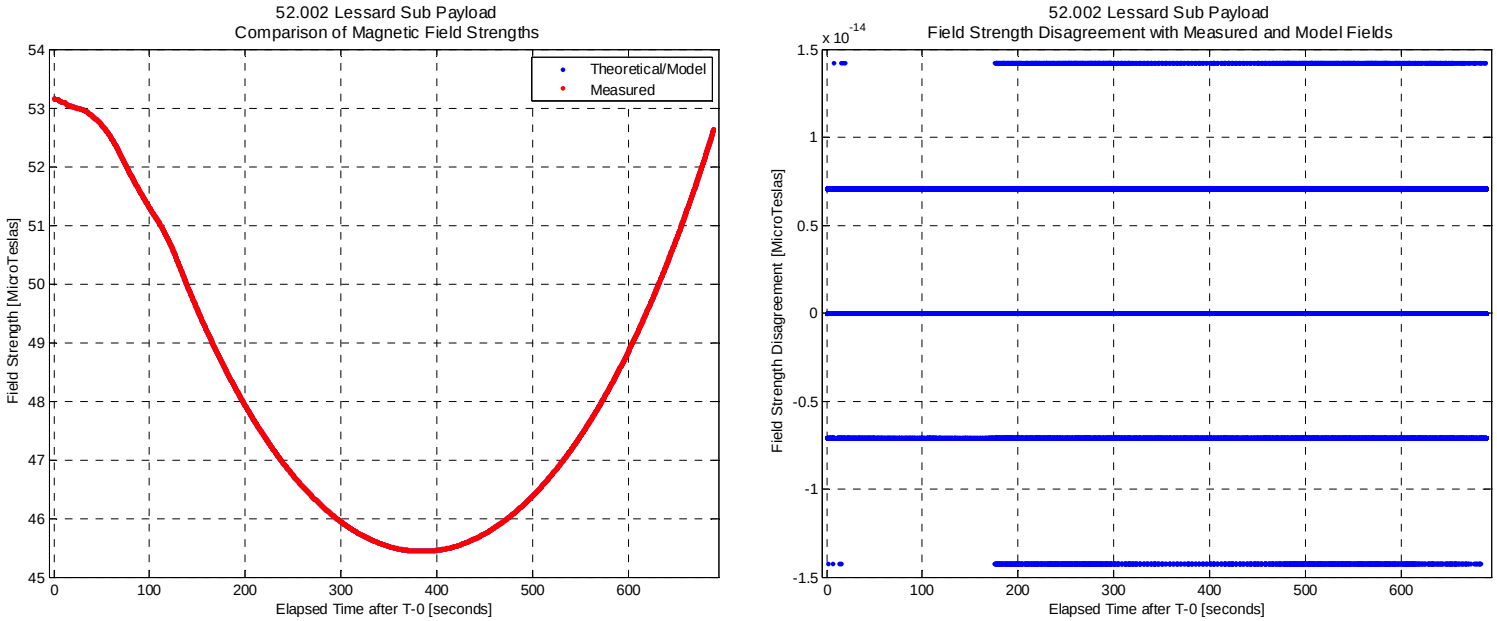

Figure 39. Sub Payload Science: Magnetic Field Strength Comparison (Science – Post Cal)

3.3.2.3 Solar Sensor Data

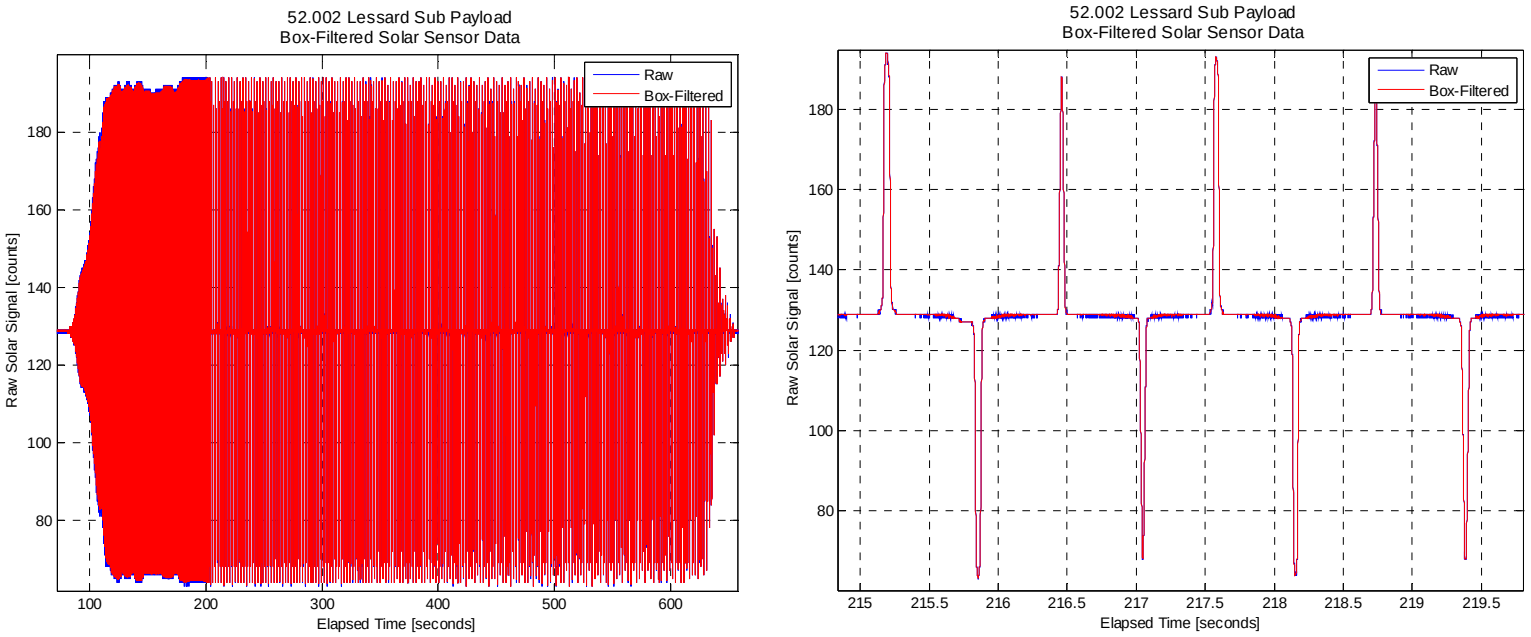

Figure 40. Raw Solar Sensor Data

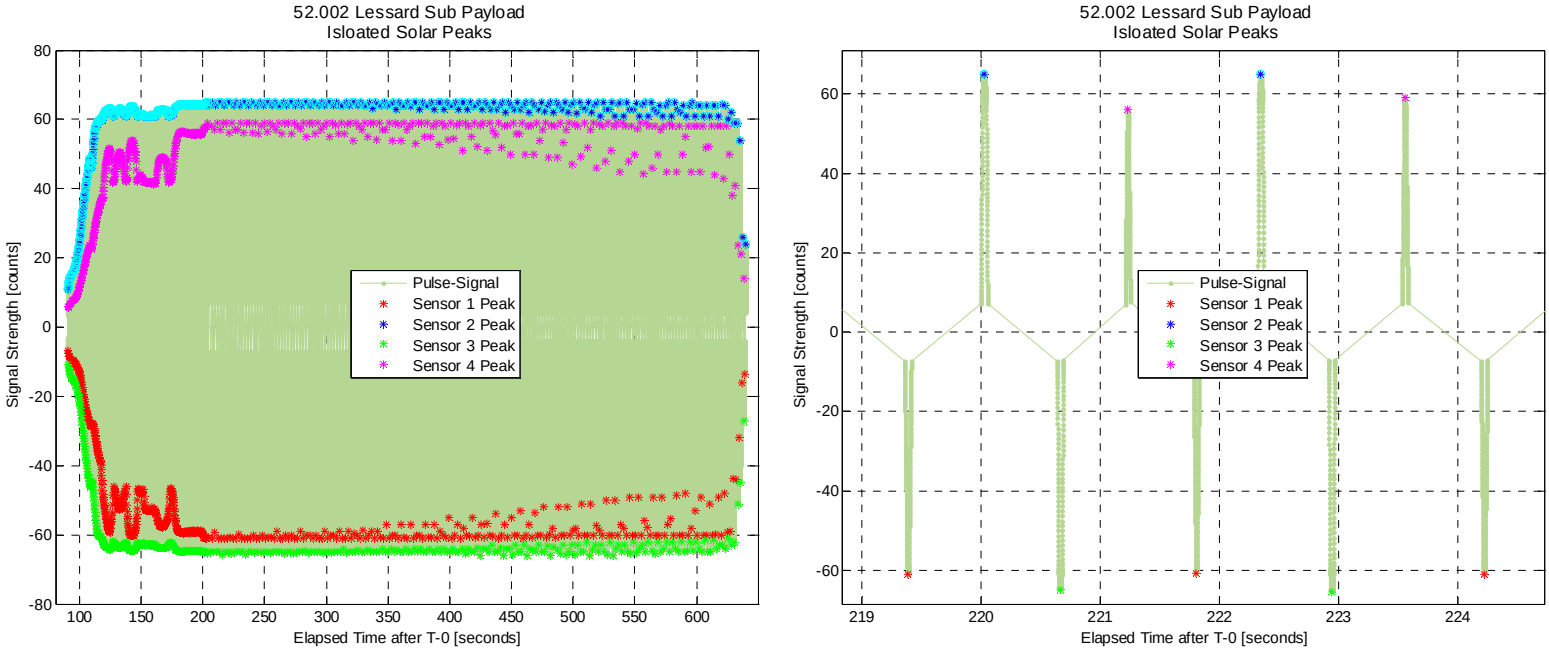

Figure 41. Isolated Solar Peaks

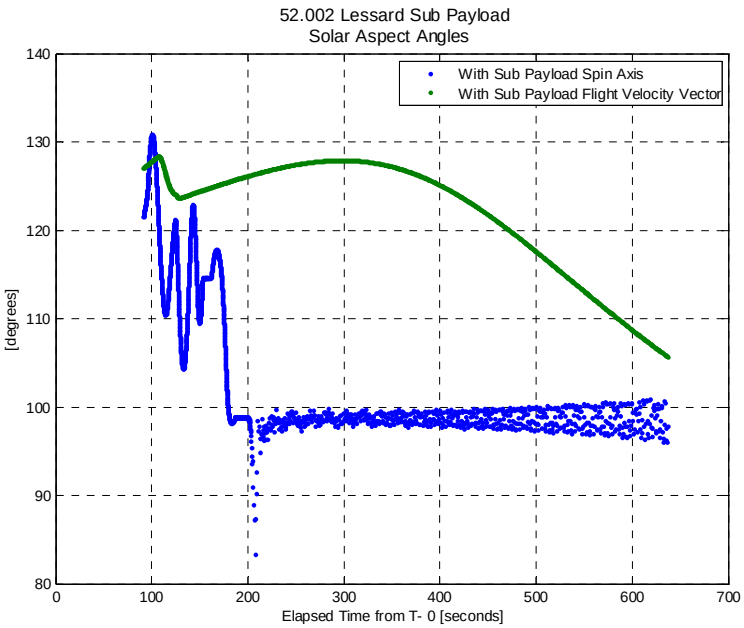

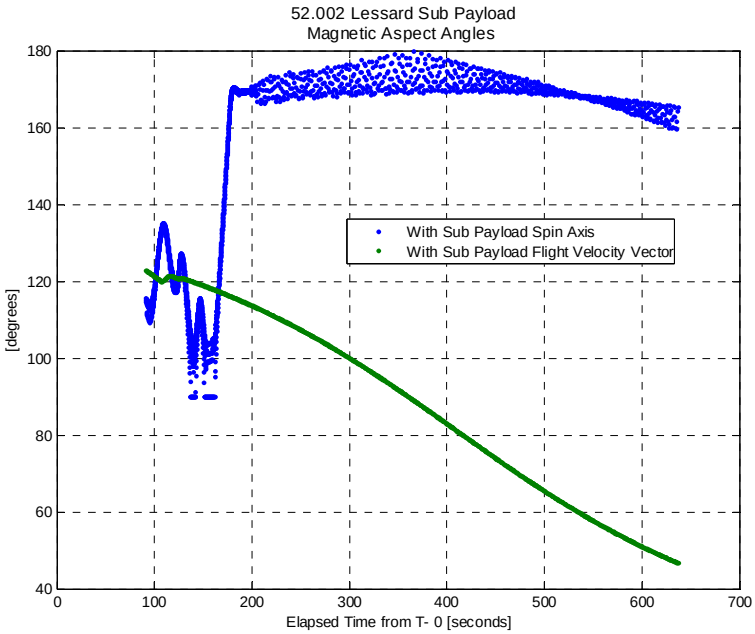

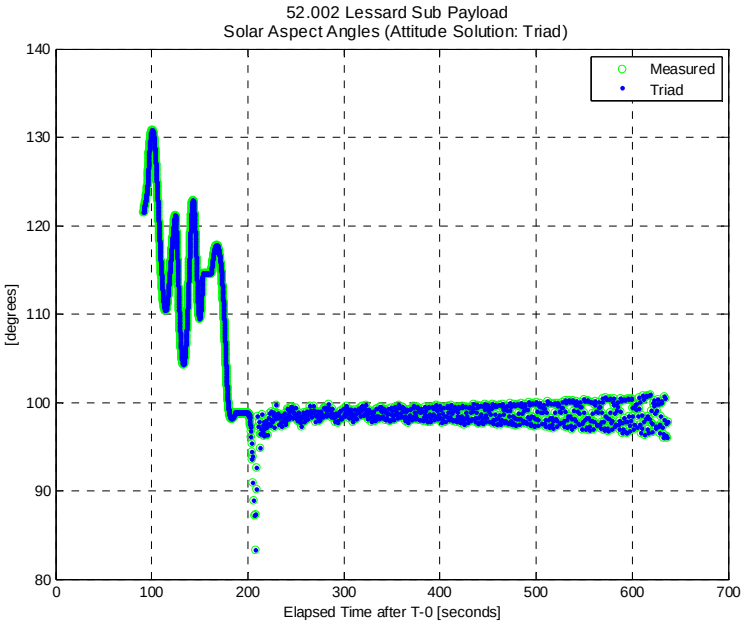

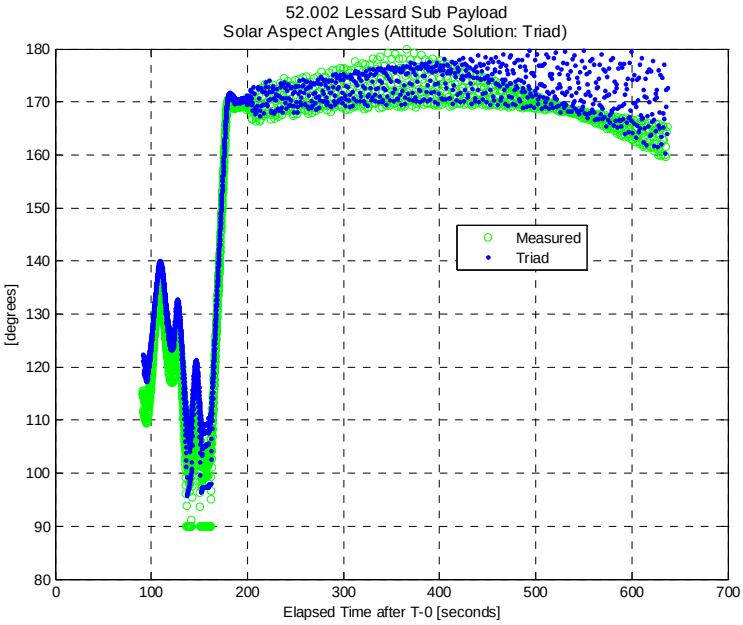

Figure 42. Sol/Mag Aspect Angles

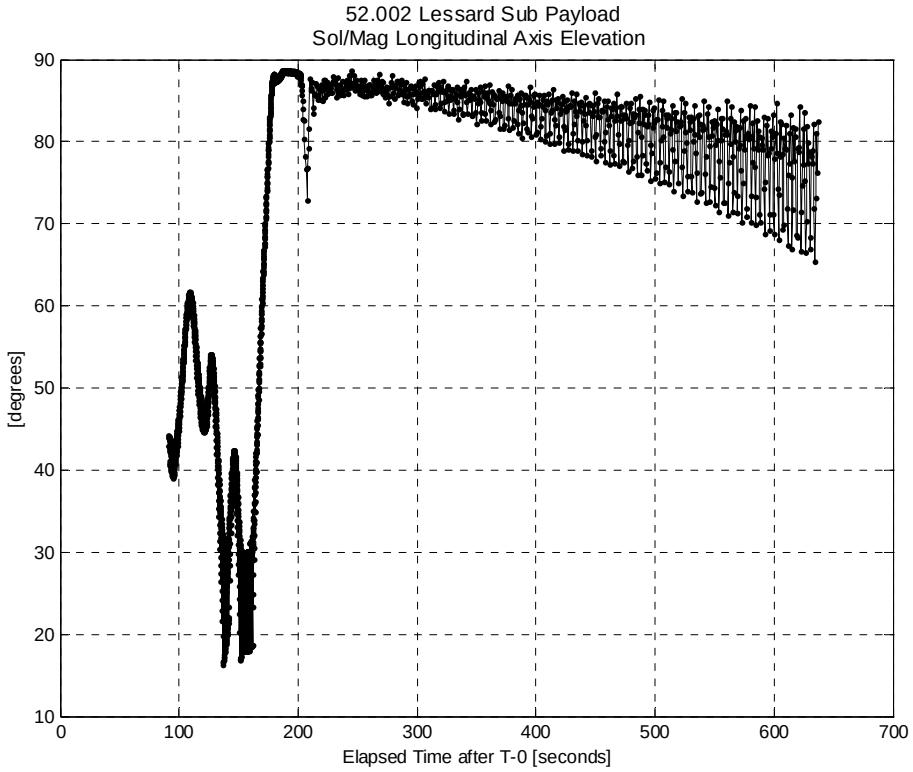

Figure 43. Sol/Mag Elevation Angle

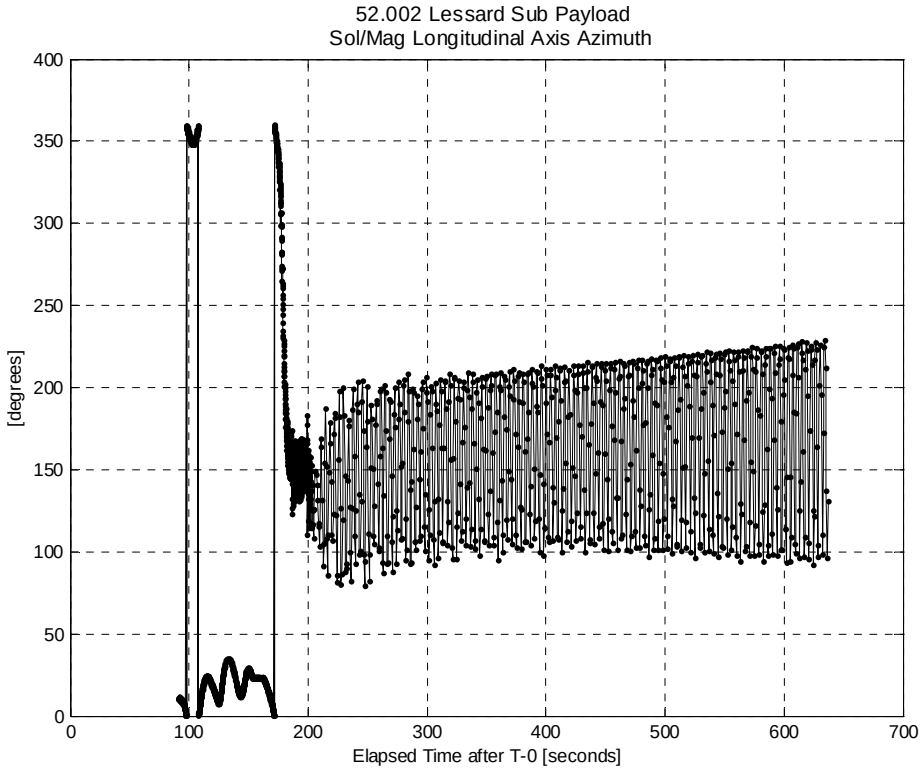

Figure 44. Sol/Mag Azimuth Angle

3.3.2.4 HCI Sensor Data

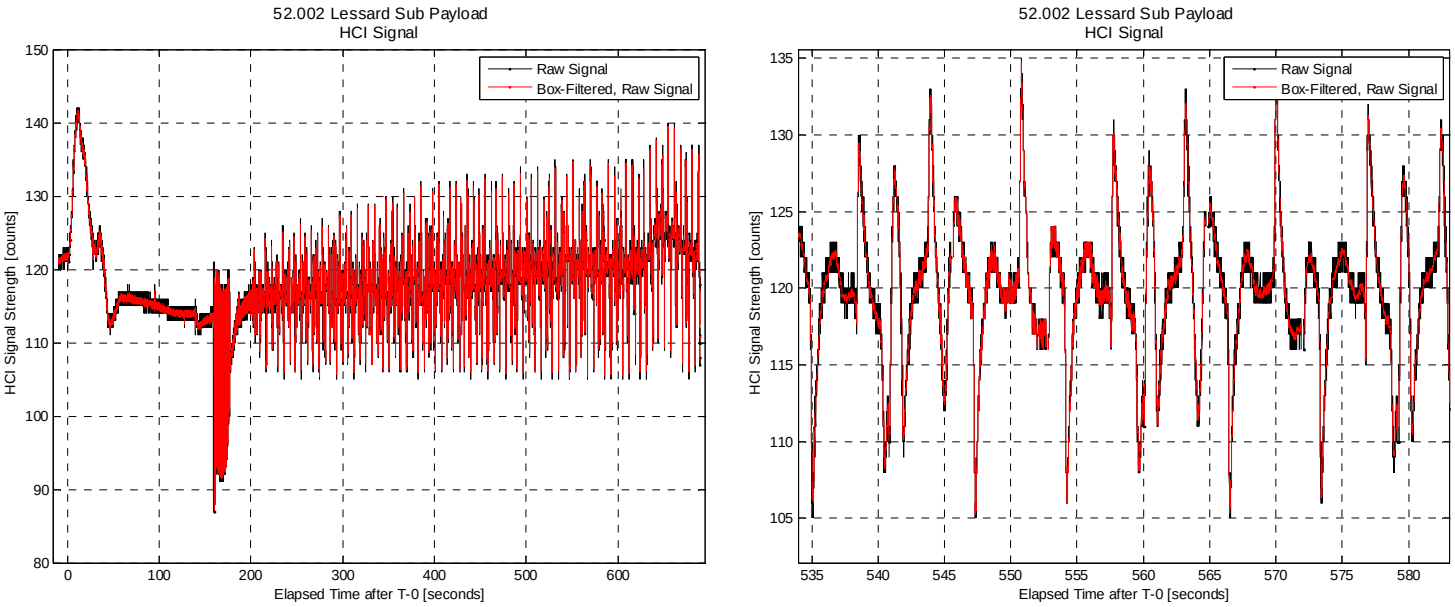

Figure 45. Raw HCI Sensor Data

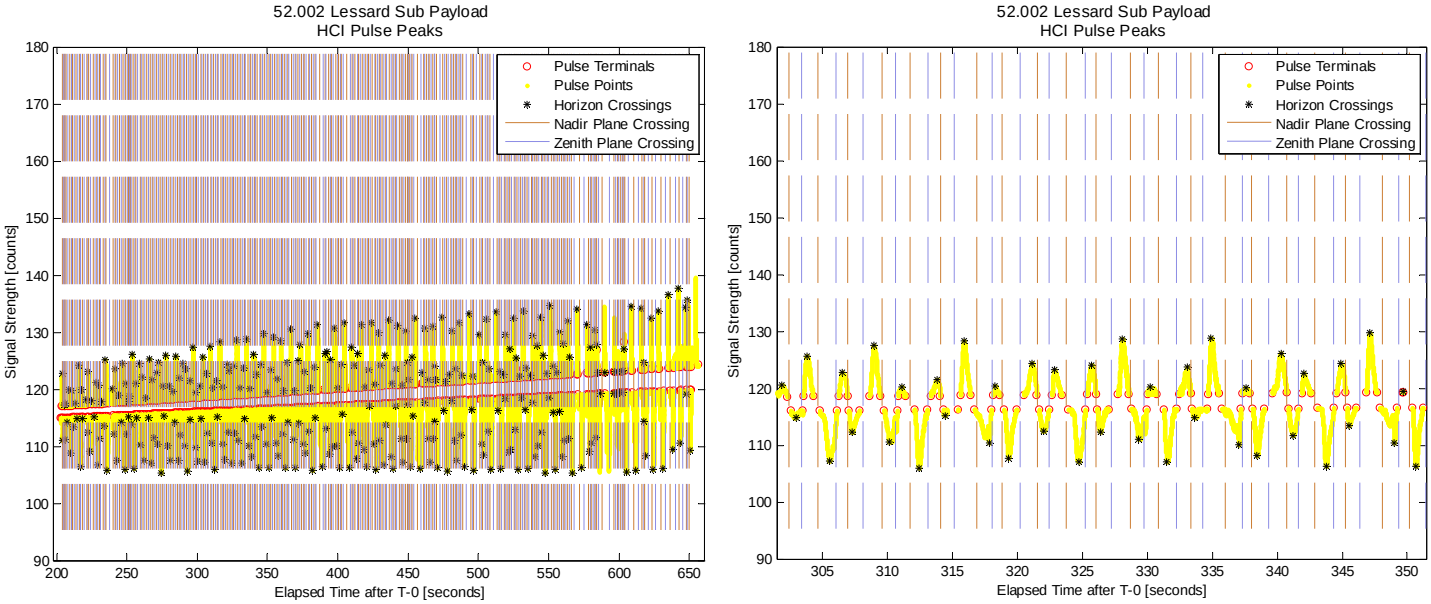

Figure 46. Isolated HCI Peaks

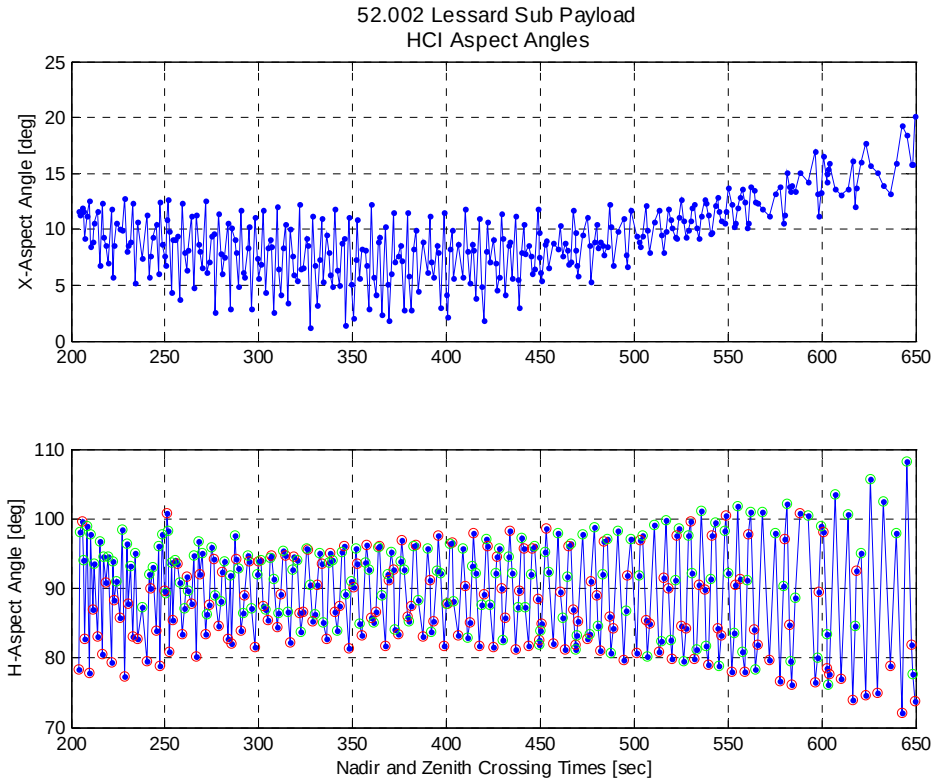

Figure 47. HCI/Mag Aspect Angles

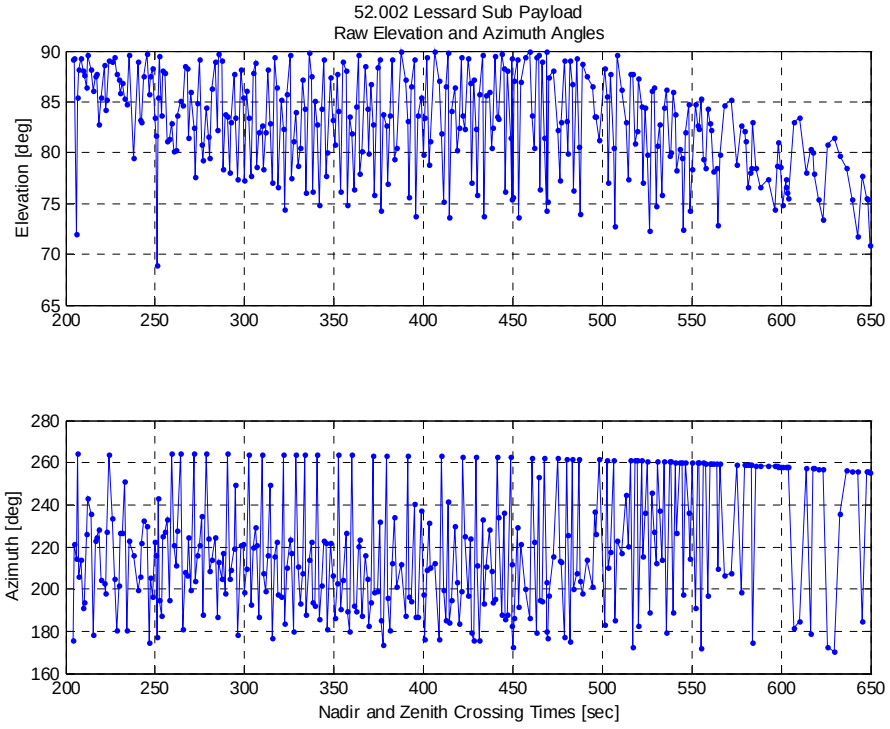

Figure 48. HCI/Mag Elevation and Azimuth

3.4 ATTITUDE

3.4.1 Main Payload

Attitude data was delivered through the asynchronous stream of the GLNMAC in the form of a DCM relative to the NIACS frame. This DCM was transformed to a DCM relative to the Flight Performance frame. That DCM was used in the attitude determination script to determine the final attitude solution which consists of the DCM in the local geodetic ENU frame, local geodetic elevation and azimuth and body relative Euler angles.

For the attitude determination post flight report, the attitude figures presented will show the whole flight and science portions for the main and the sub payload. There will also be a set of plots for the when sub and main payloads are attached and a solution can be obtained. This set of plots will be used to show that the sol/mag is within its expected accuracy (a good HCI solution could not be obtained due to the magnetic field alignment maneuver in this section and poor pulse behavior (the pulse band became very small and narrow, thus making the solution questionable during the magnetic field alignment)). A comparison of the HCI/mag and sol/mag solution is also performed to show the confidence in the HCI/mag solution (this solution tends to be questionable with sounding rockets).

Attitude plots are arranged in the following sections: roll rate, angle of attack (relative to the velocity vector), local geodetic attitude, and inertial attitude. The roll rate section presents the roll rate derived from the GLNMAC's attitude solution. The local geodetic attitude section presents the local geodetic azimuth attitude, which contains the velocity vector, payload longitudinal axis azimuth, and magnetic azimuth. In addition to local geodetic azimuth, the local geodetic elevation is presented. The inertial attitude section consists of the Euler angles with respect to the body frame at launch.

3.4.1.1 Full Flight

Roll Rate

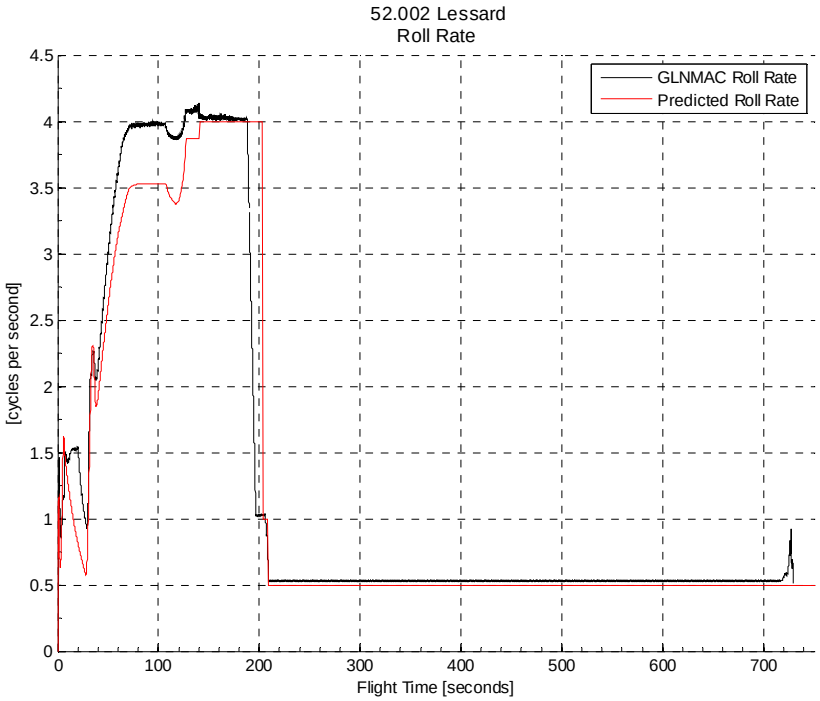

Figure 49. Main Payload Full Flight: Roll Rate

Angle of Attack

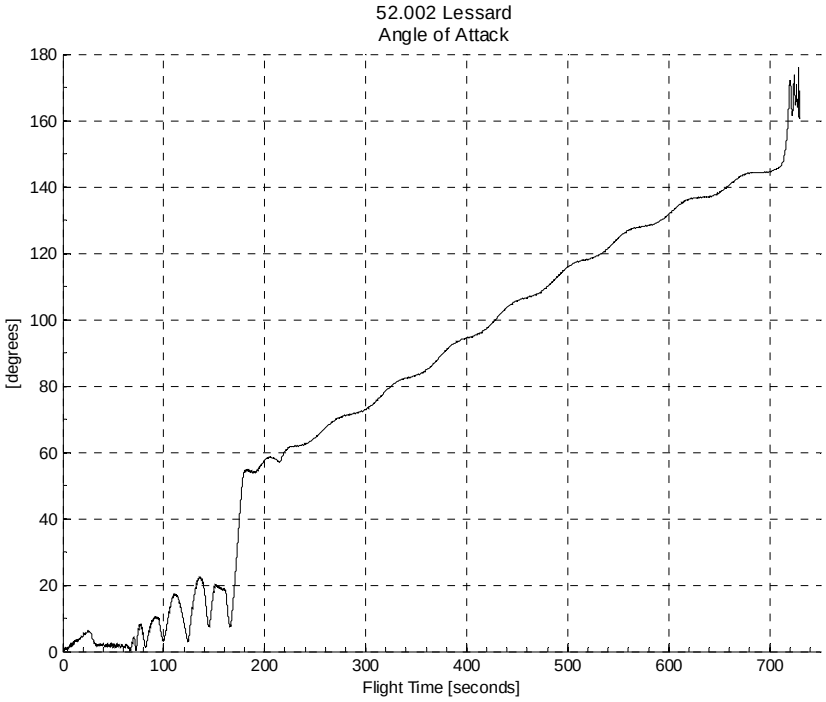

Figure 50. Main Payload Full Flight: Angle of Attack

Local Geodetic Attitude

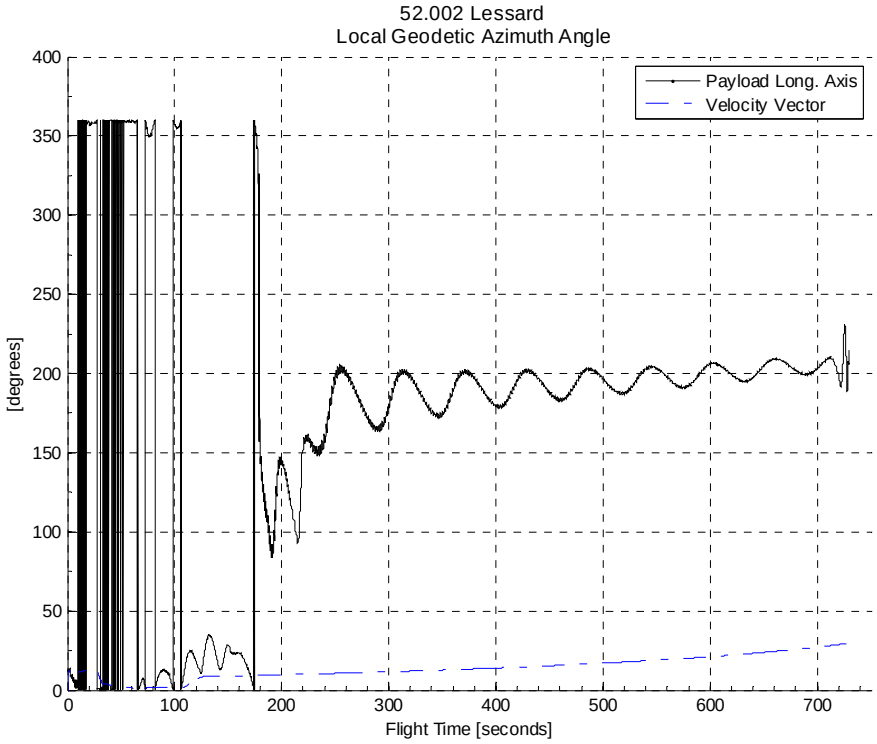

Figure 51. Main Payload Full Flight: Local Geodetic Azimuth Attitude

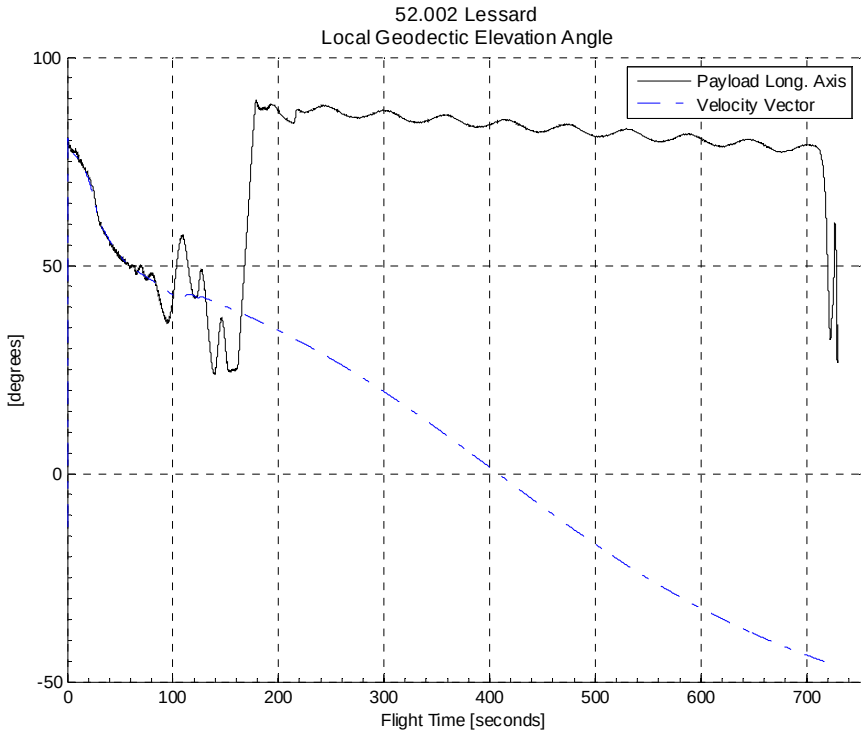

Figure 52. Main Payload Full Flight: Local Geodetic Elevation Attitude

Inertial Attitude

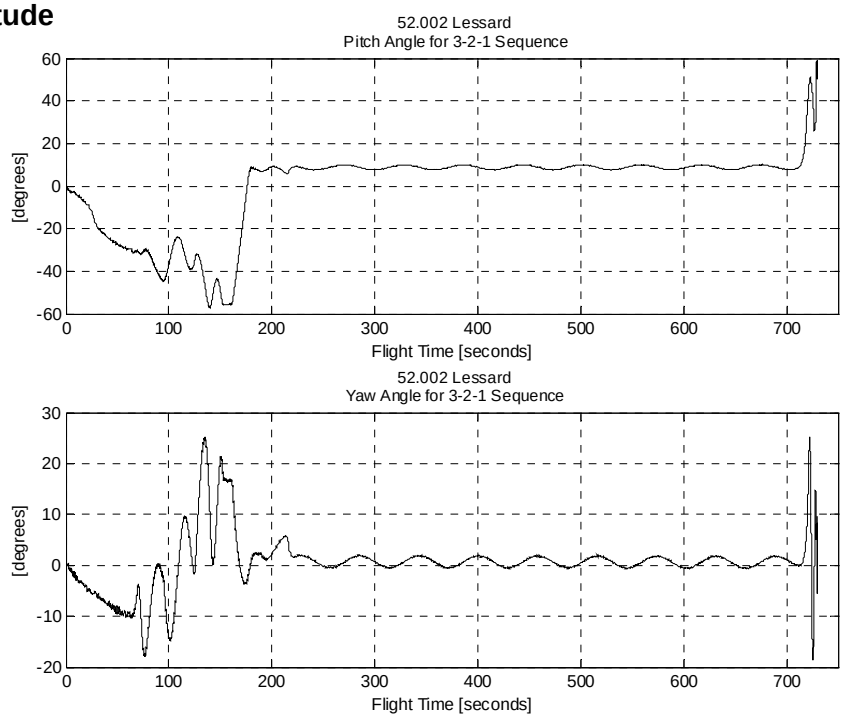

Figure 53. Main Payload Full Flight: Pitch and Yaw

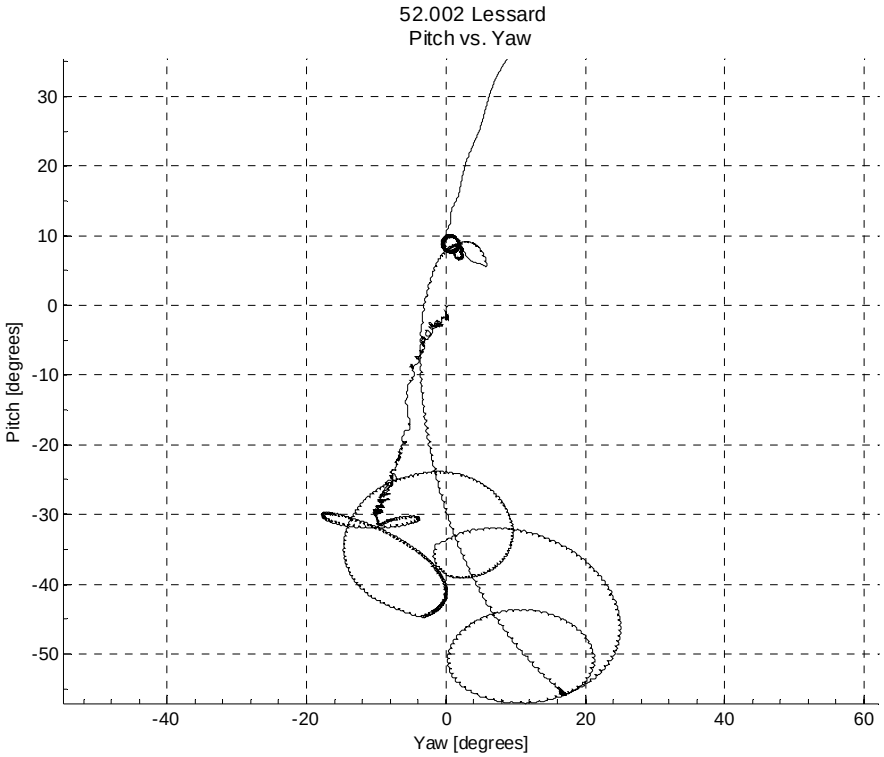

Figure 54. Main Payload Full Flight: Pitch vs. Yaw

3.4.1.2 Main Payload: Science (T+184 – T+730)

Roll Rate

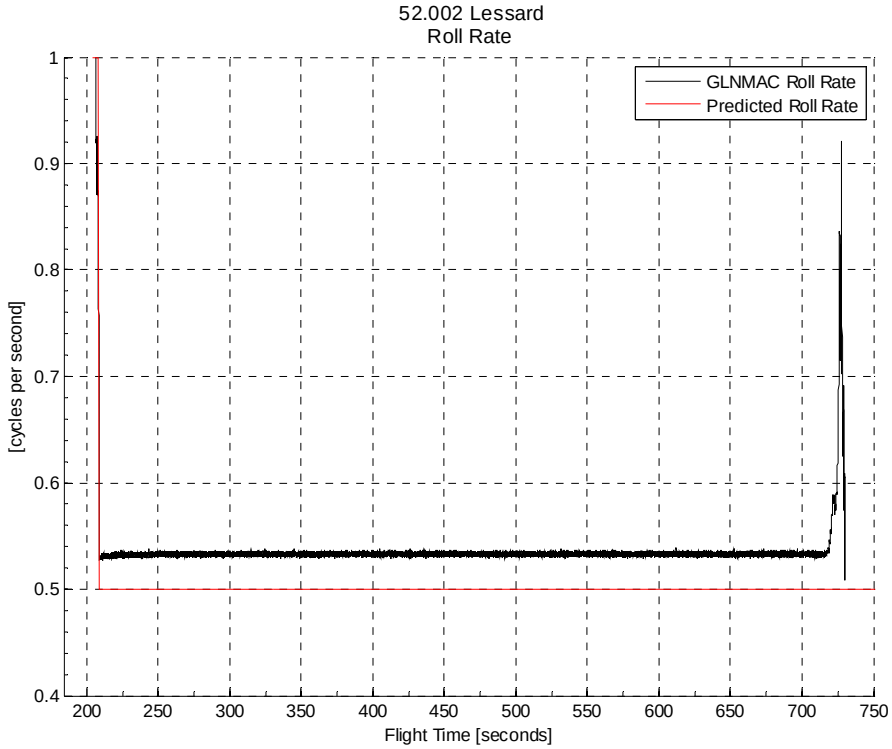

Figure 55. Main Payload Science: Roll Rate

Angle of Attack

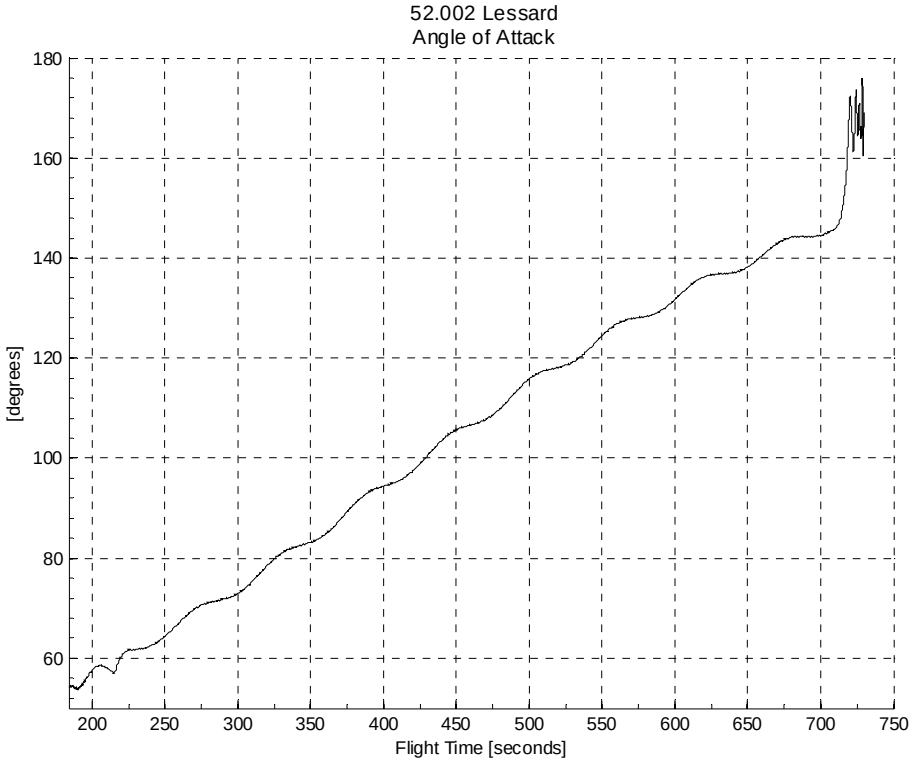

Figure 56. Main Payload Science: Angle of Attack

Local Geodetic Attitude

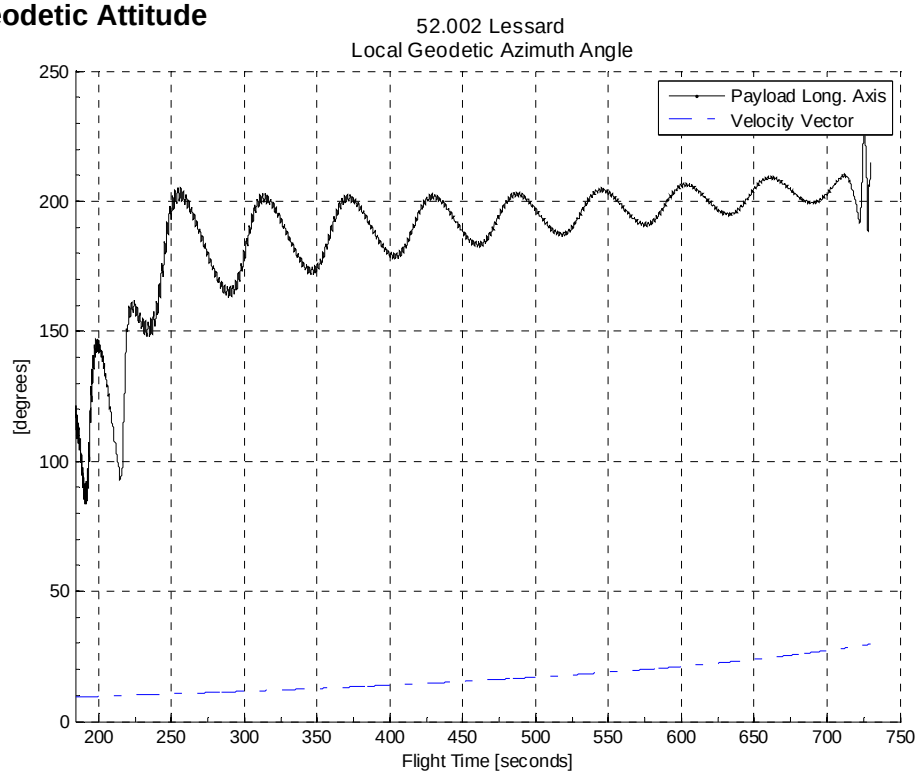

Figure 57. Main Payload Science: Local Geodetic Azimuth Attitude

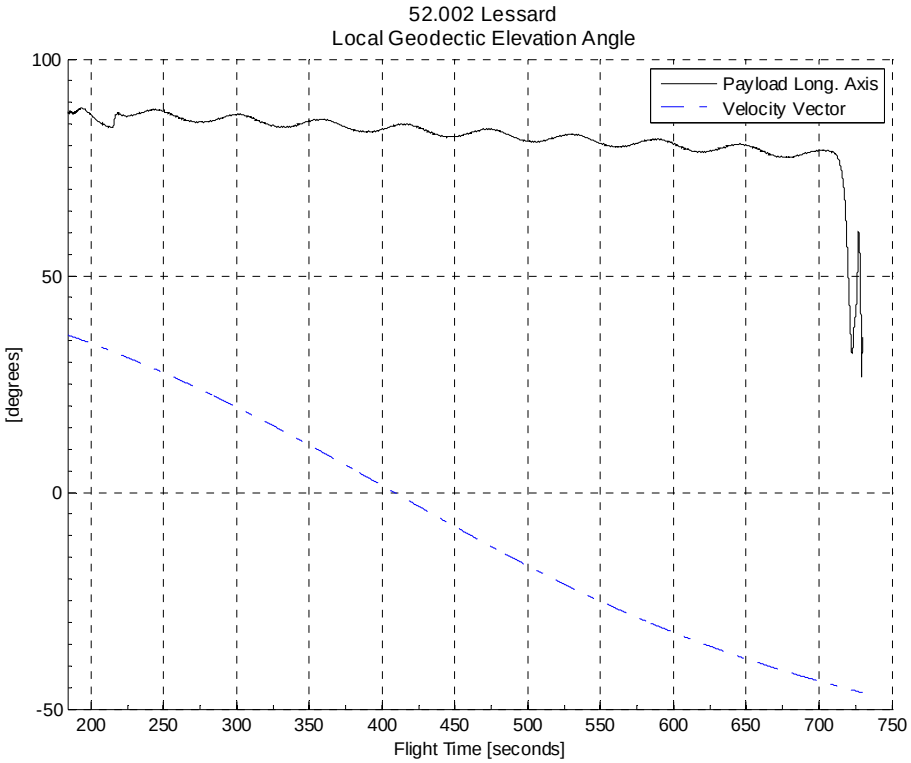

Figure 58. Main Payload Science: Local Geodetic Elevation Attitude

Inertial Attitude

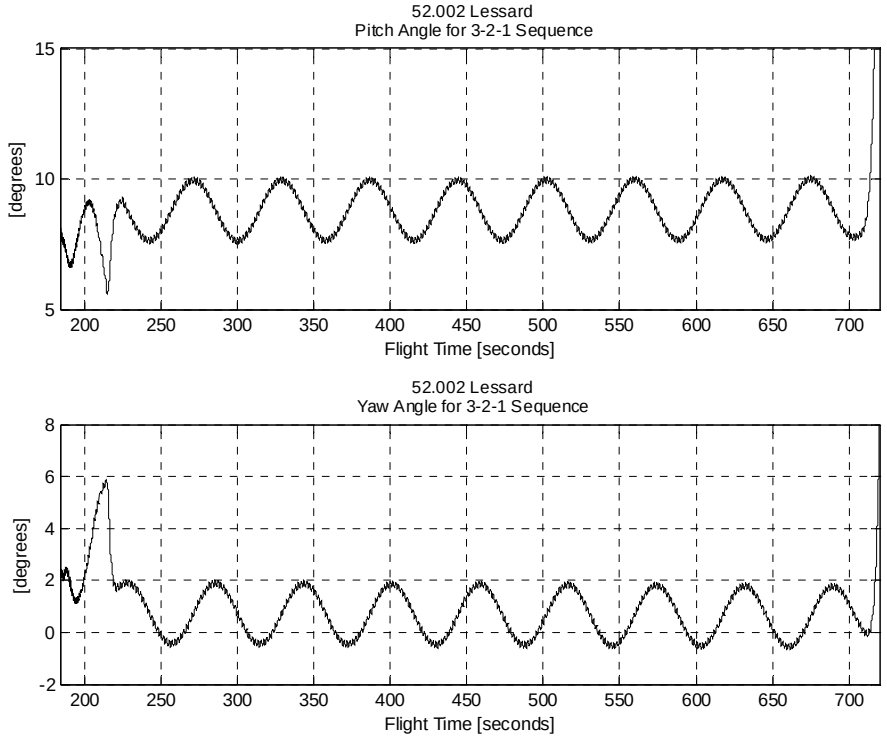

Figure 59. Main Payload Science: Pitch and Yaw

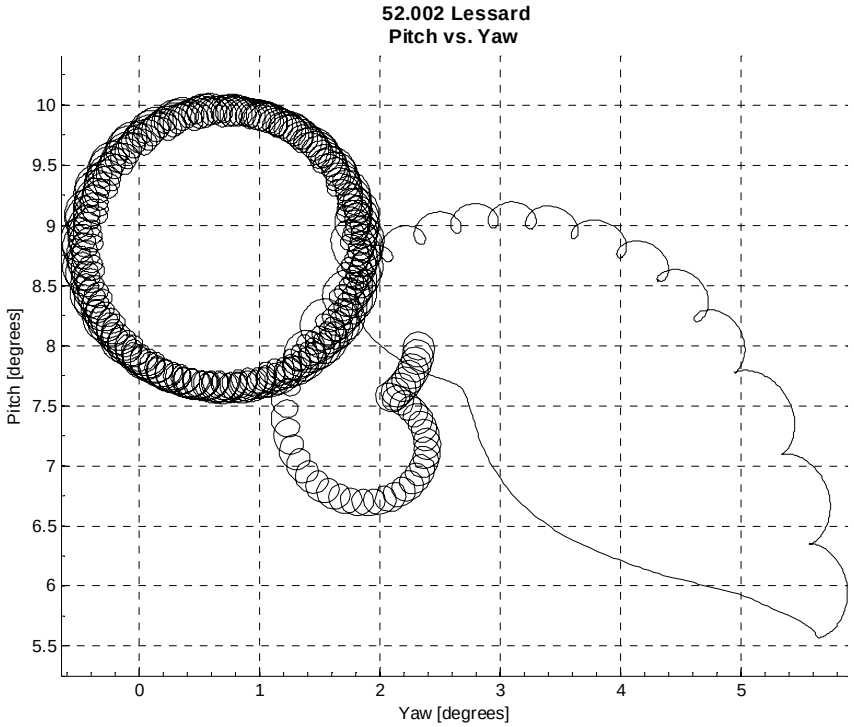

Figure 60. Main Payload Science: Pitch vs. Yaw

3.4.2 Main & Sub Payload Attached (T+160 – 186)

3.4.2.1 GLNMAC: Sol/Mag

Roll Rate

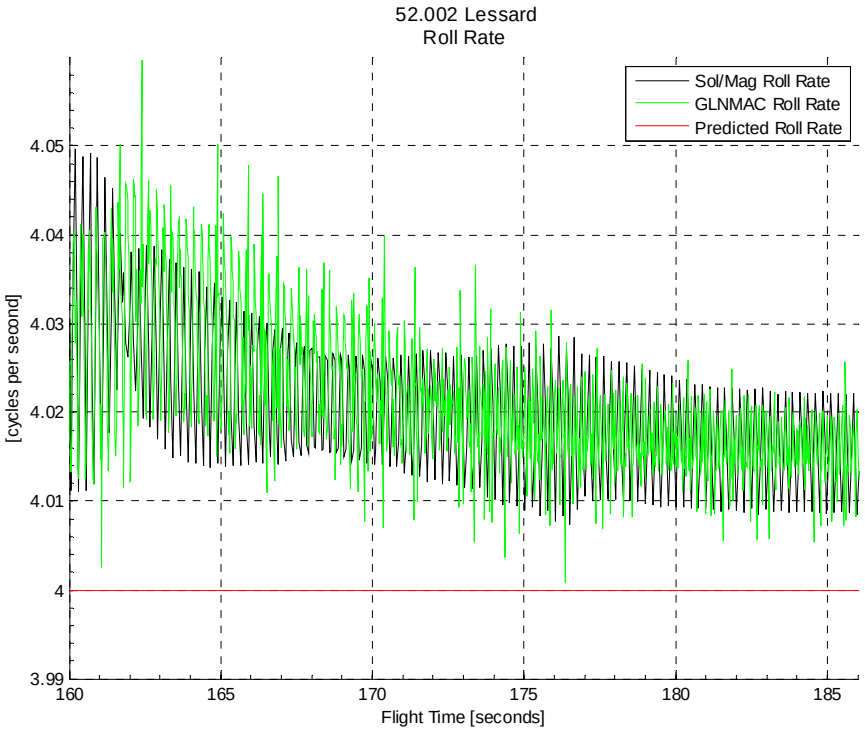

Figure 61. Sub Payload Attached, GLNMAC:Sol/Mag: Roll Rate

Angle of Attack

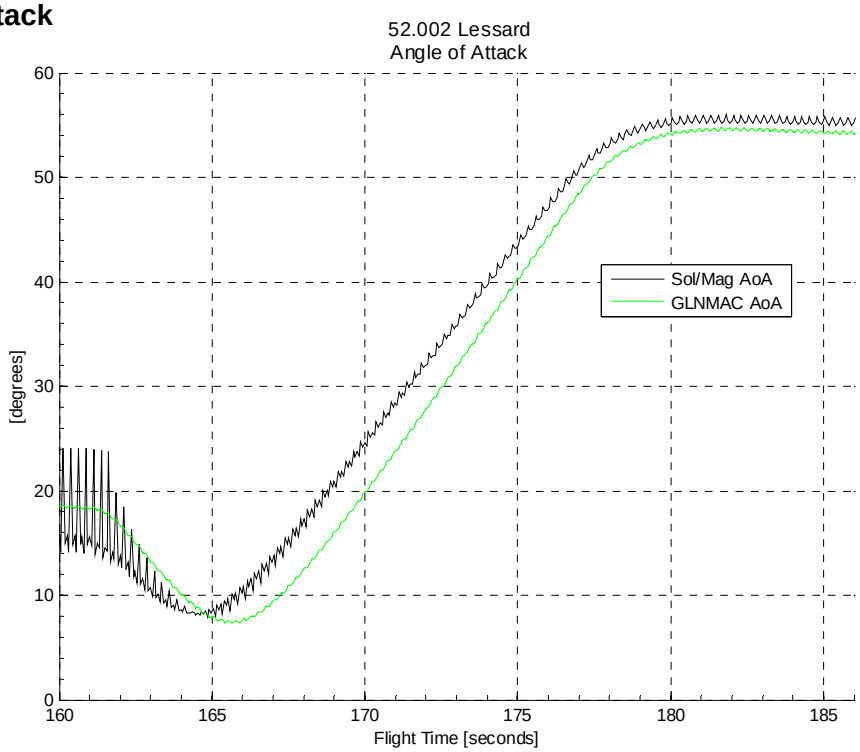

Figure 61. Sub Payload Attached, GLNMAC:Sol/Mag: Angle of Attack

Local Geodetic Attitude

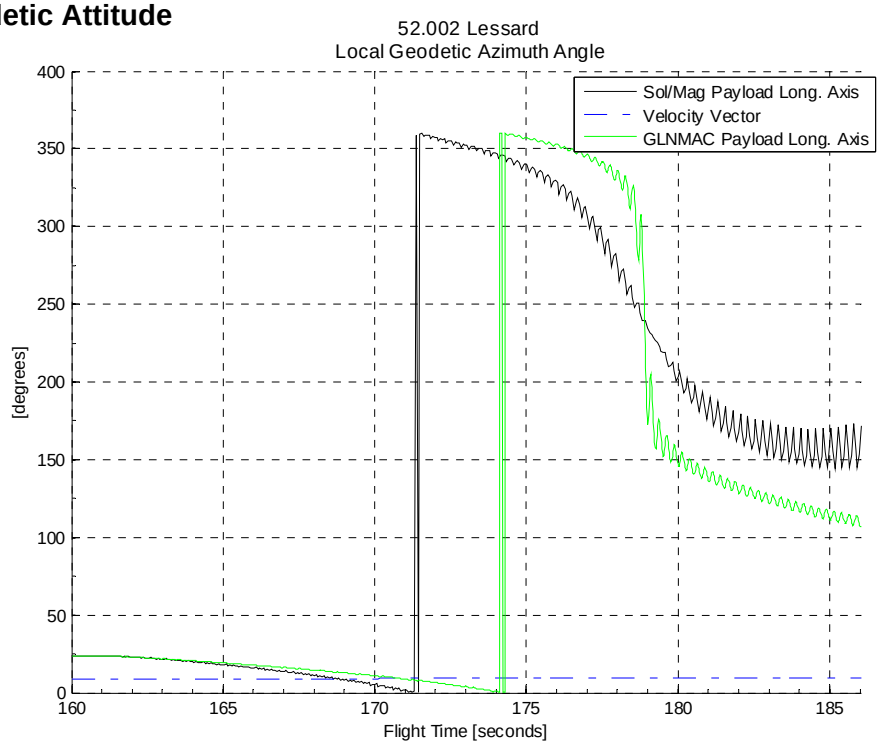

Figure 63. Sub Payload Attached, GLNMAC:Sol/Mag: Local Geodetic Azimuth Attitude

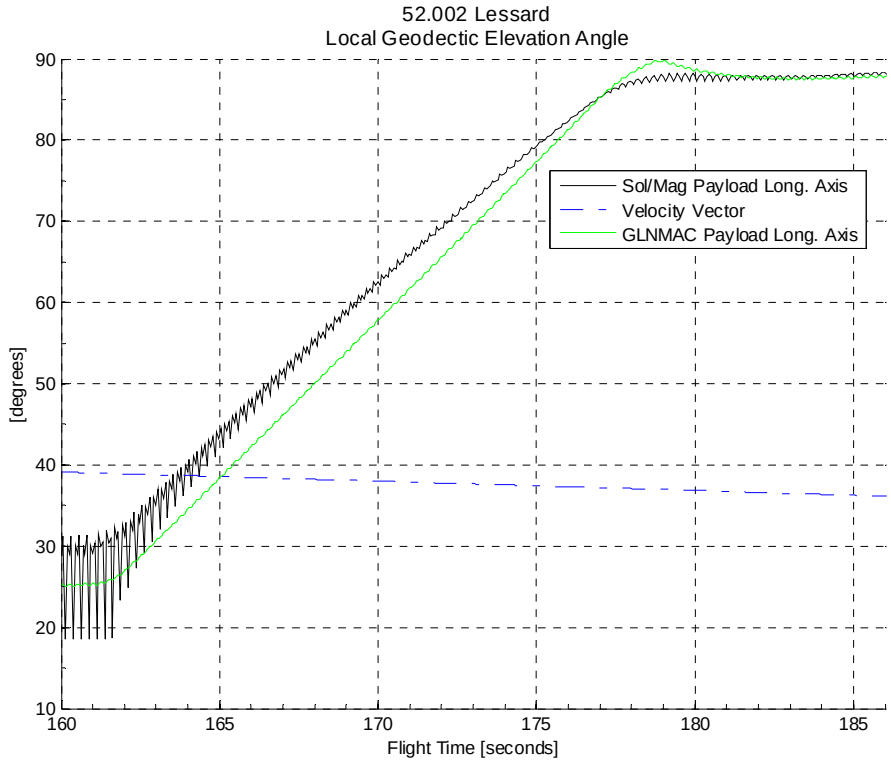

Figure 64. Sub Payload Attached, GLNMAC:Sol/Mag: Local Geodetic Elevation Attitude

Inertial Attitude

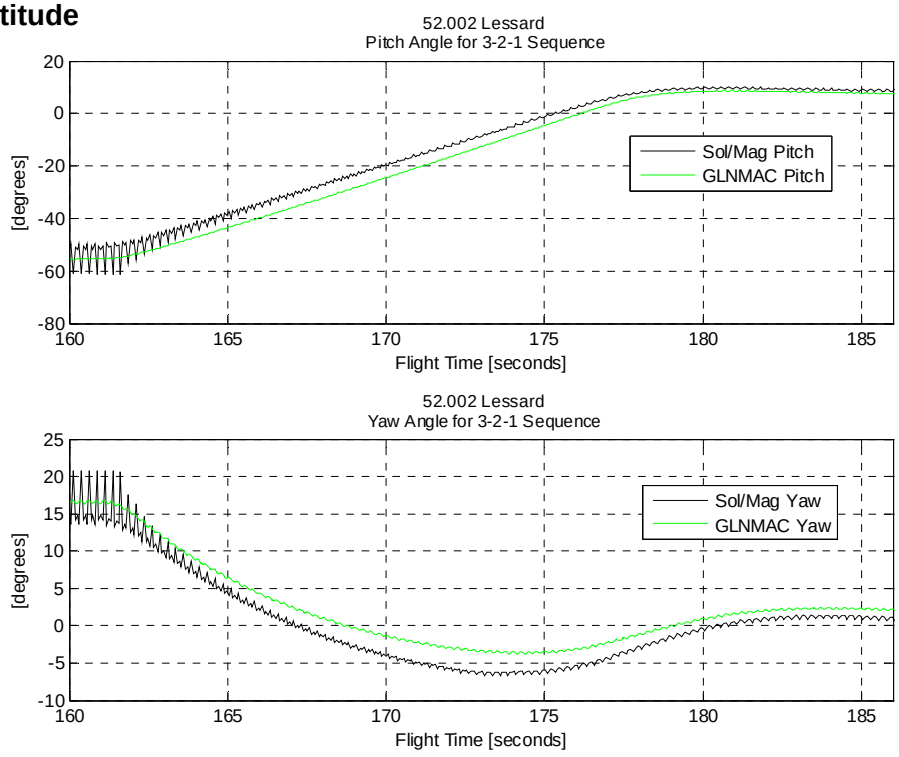

Figure 65. Sub Payload Attached, GLNMAC:Sol/Mag: Pitch and Yaw

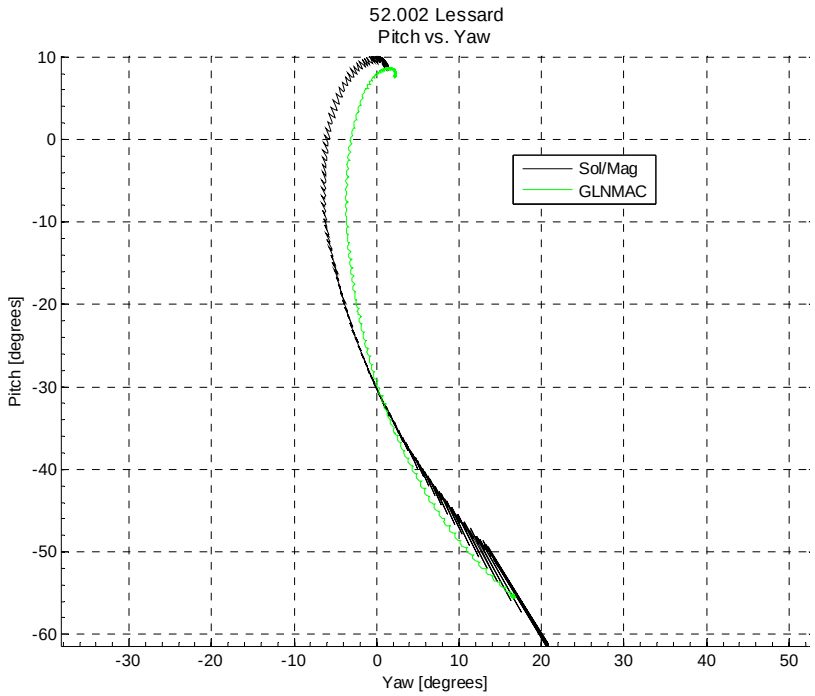

Figure 66. Sub Payload Attached, GLNMAC:Sol/Mag: Pitch vs. Yaw

3.4.3 Sub Payload

3.4.3.1 Sol/Mag

Roll Rate

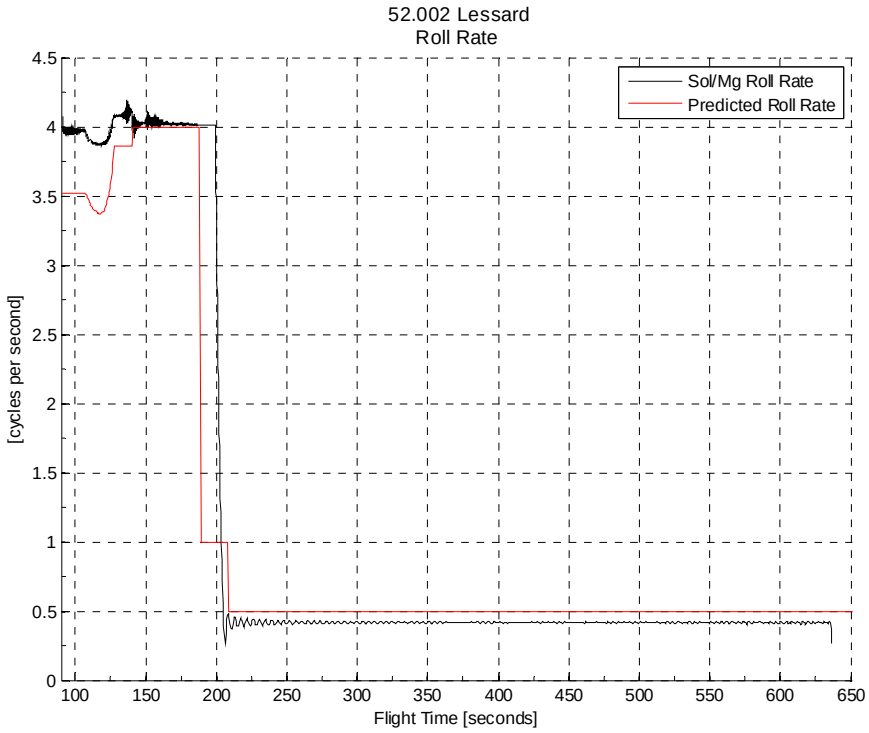

Figure 67. Sub Payload Sol/Mag: Roll Rate

Angle of Attack

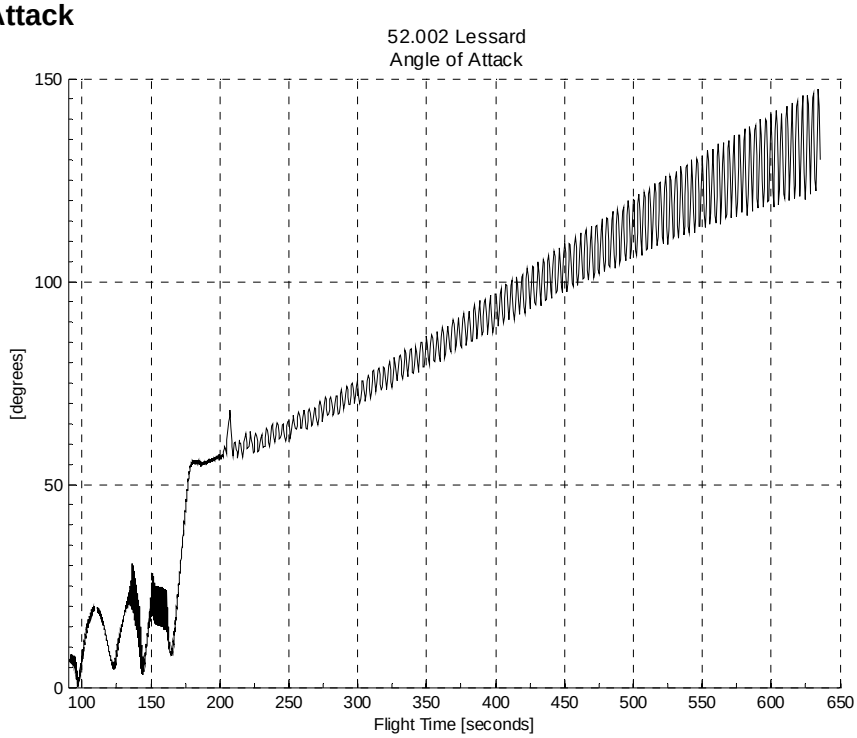

Figure 68. Sub Payload Sol/Mag: Angle of Attack

Local Geodetic Attitude

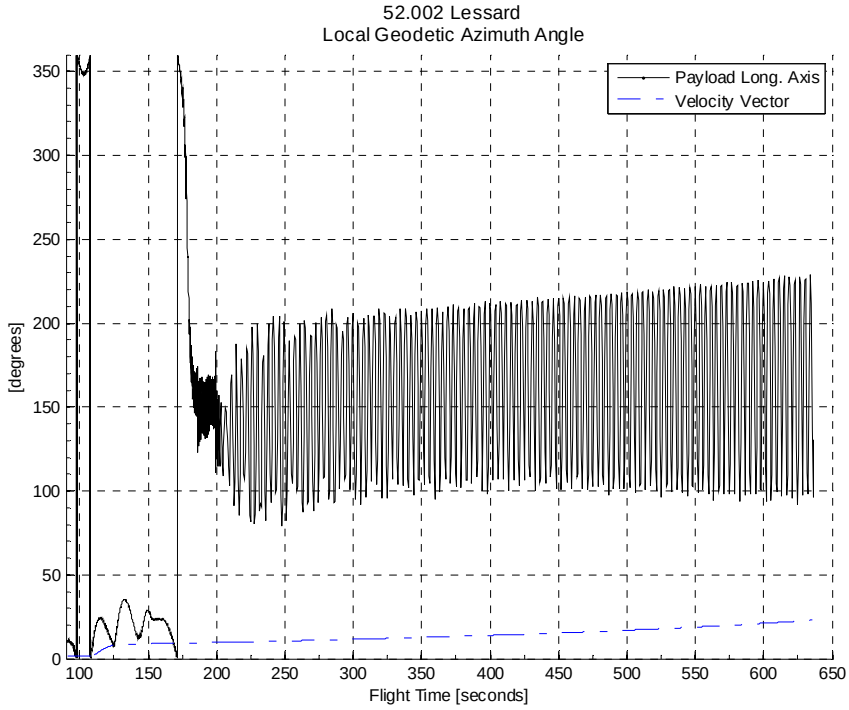

Figure 69. Sub Payload Sol/Mag: Local Geodetic Azimuth Attitude

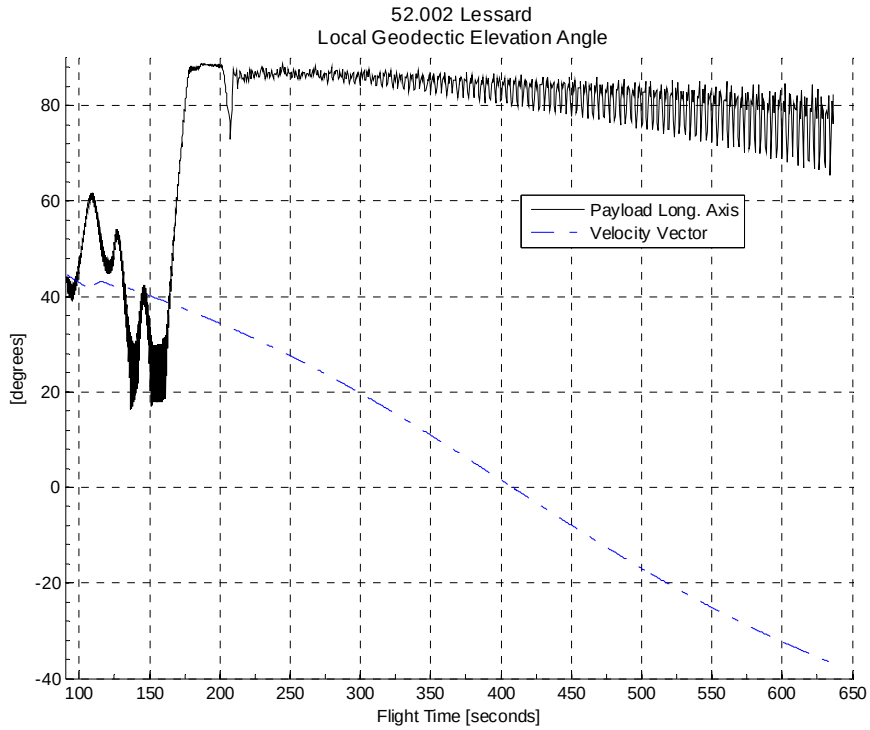

Figure 70. Sub Payload Sol/Mag: Local Geodetic Elevation Attitude

Inertial Attitude

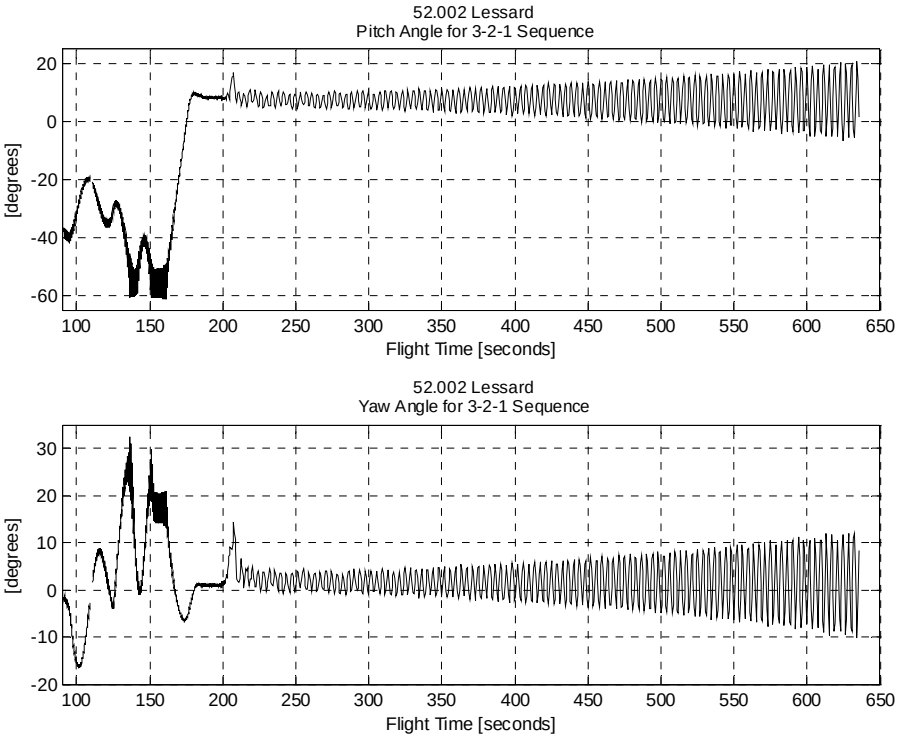

Figure 71. Sub Payload Sol/Mag: Pitch and Yaw

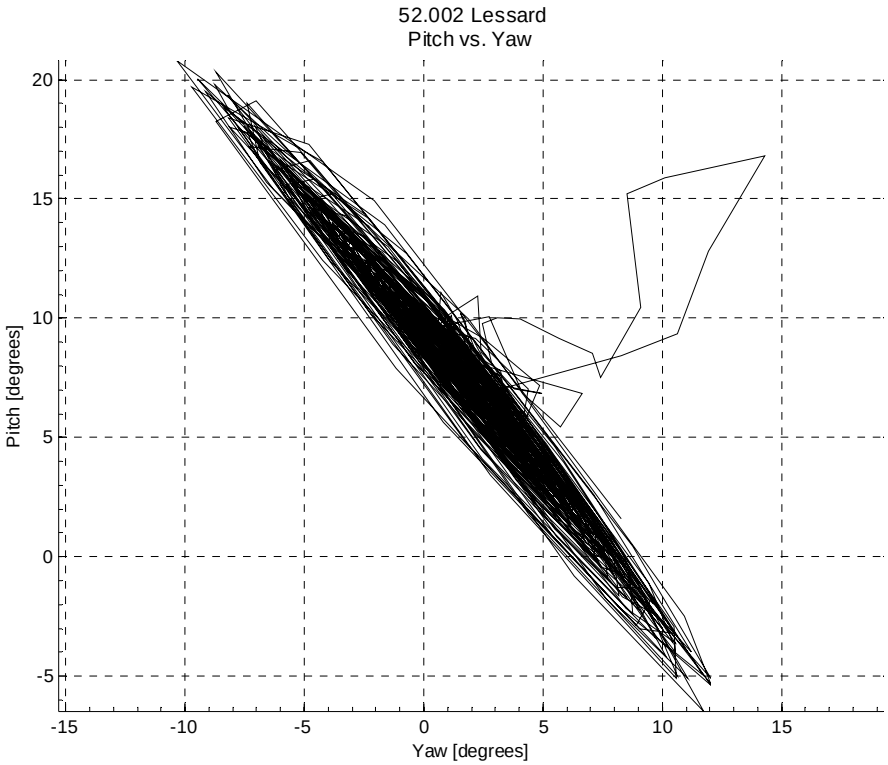

Figure 72. Sub Payload Sol/Mag: Pitch vs. Yaw

3.4.3.2 HCI/Mag

Roll Rate

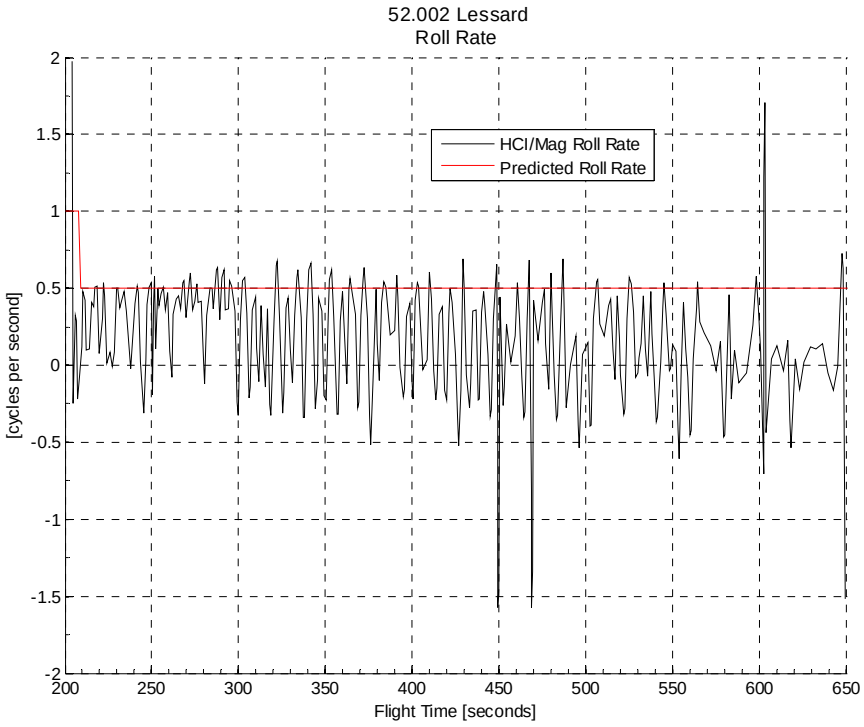

Figure 73. Sub Payload HCI/Mag: Roll Rate

Angle of Attack

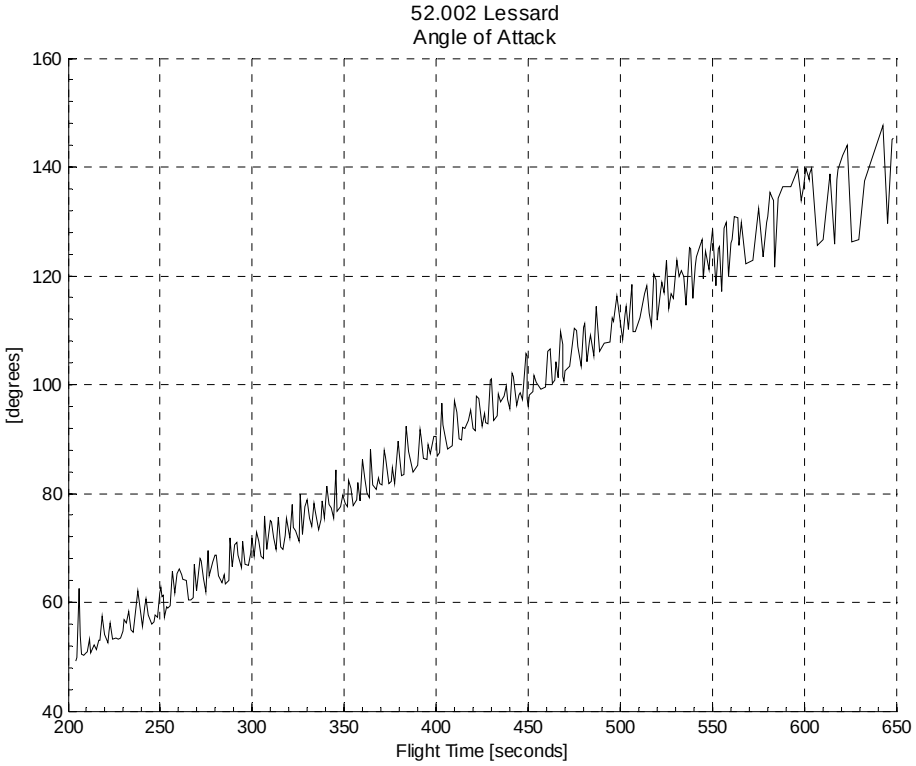

Figure 74. Sub Payload HCI/Mag: Angle of Attack

Local Geodetic Attitude

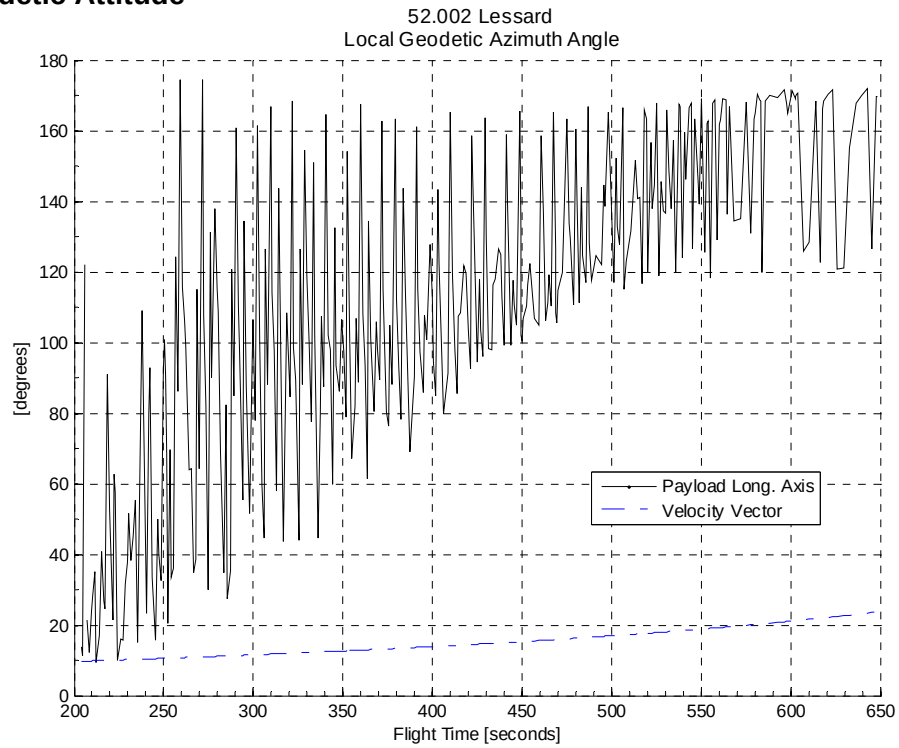

Figure 75. Sub Payload HCI/Mag: Local Geodetic Azimuth Attitude

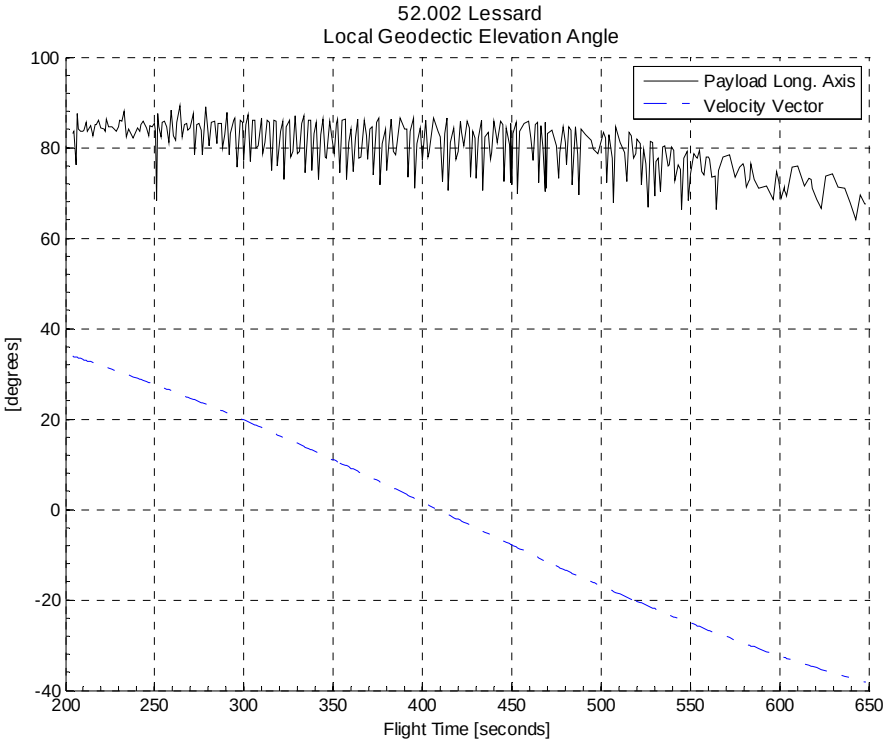

Figure 76. Sub Payload HCI/Mag: Local Geodetic Elevation Attitude

Inertial Attitude

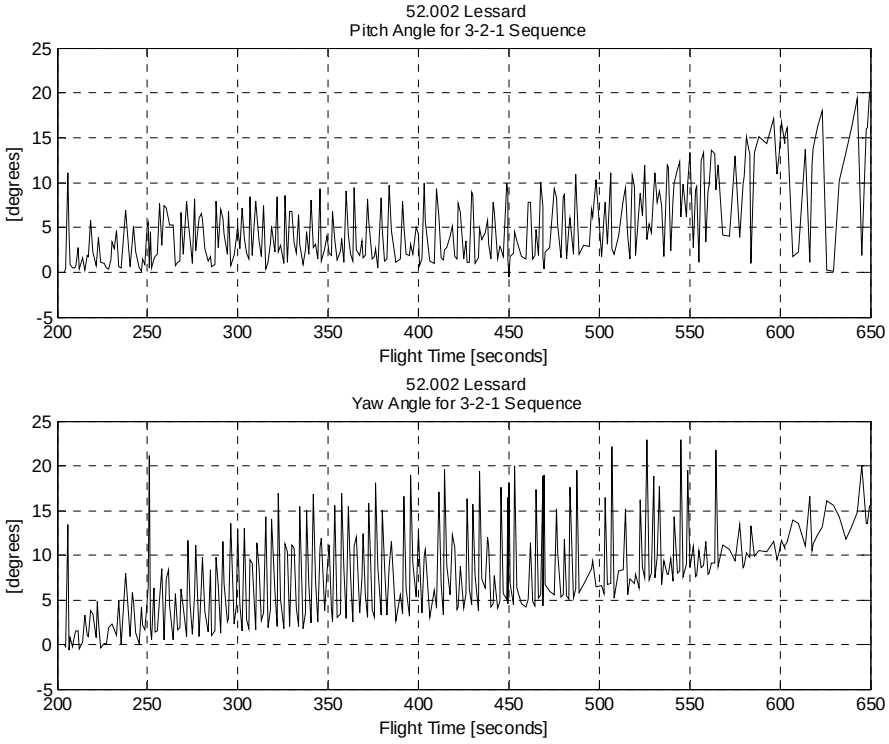

Figure 77. Sub Payload HCI/Mag: Pitch and Yaw

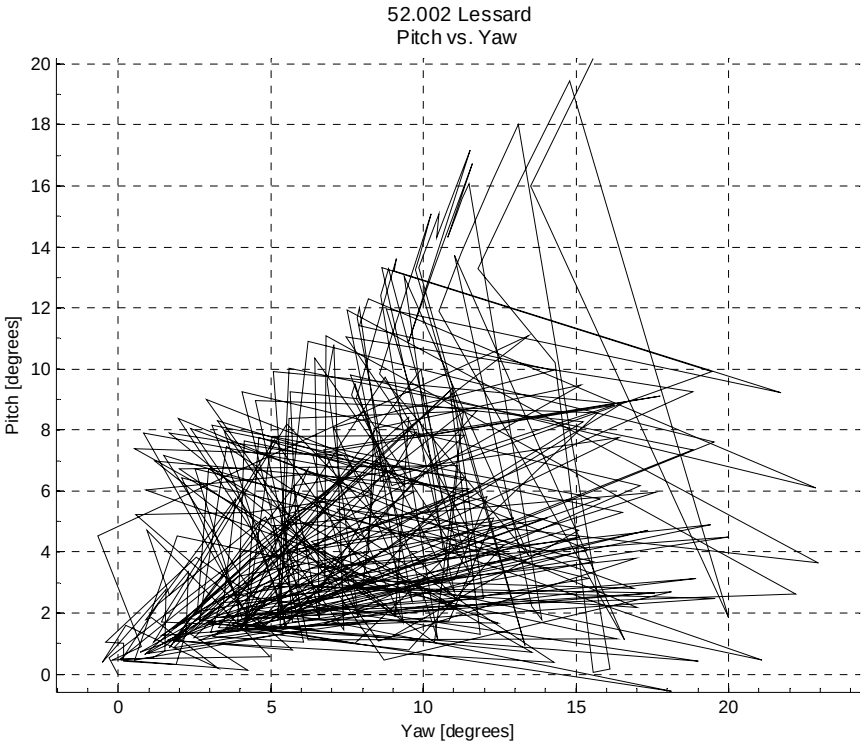

Figure 78. Sub Payload HCI/Mag: Pitch vs. Yaw

3.4.3.3 HCI/Mag: Sol/Mag

Roll Rate

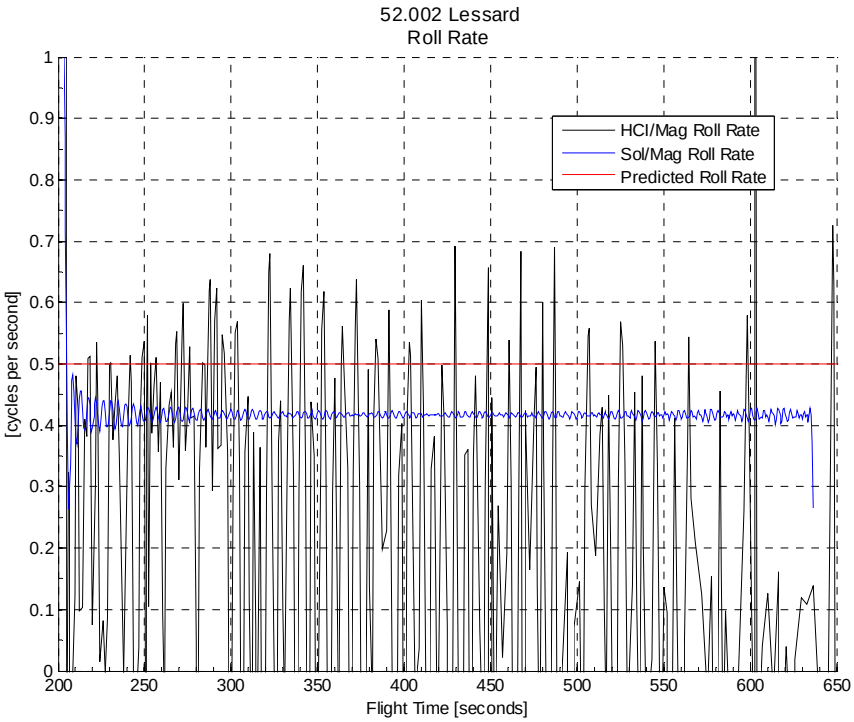

Figure 79. HCI/Mag: Sol/Mag: Roll Rate

Angle of Attack

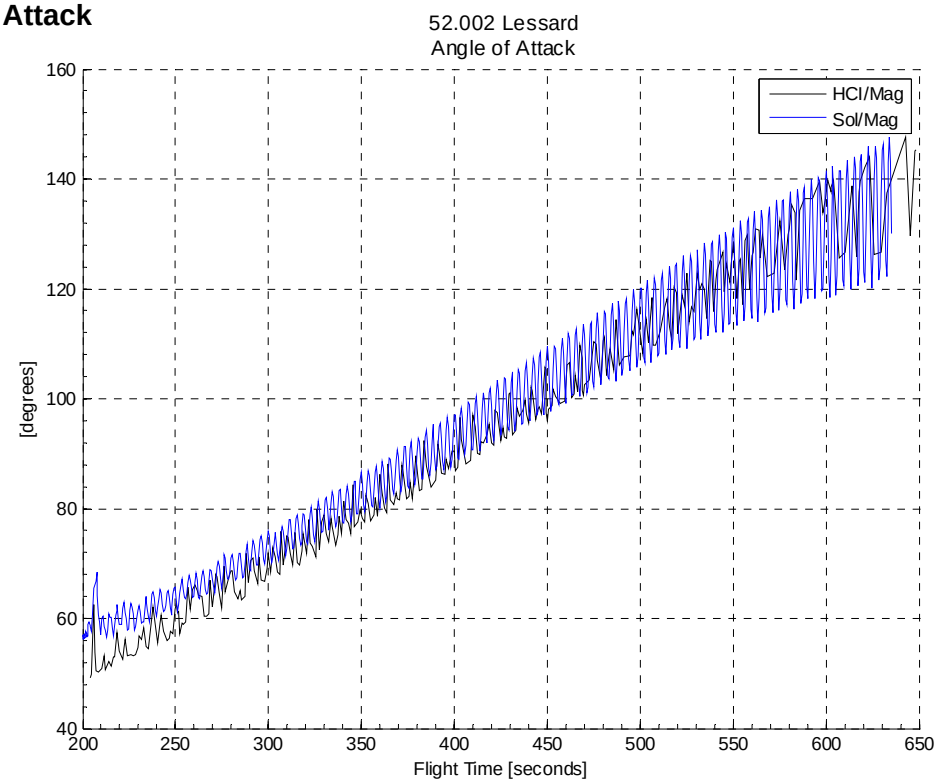

Figure 80. HCI/Mag: Sol/Mag: Angle of Attack

Local Geodetic Attitude

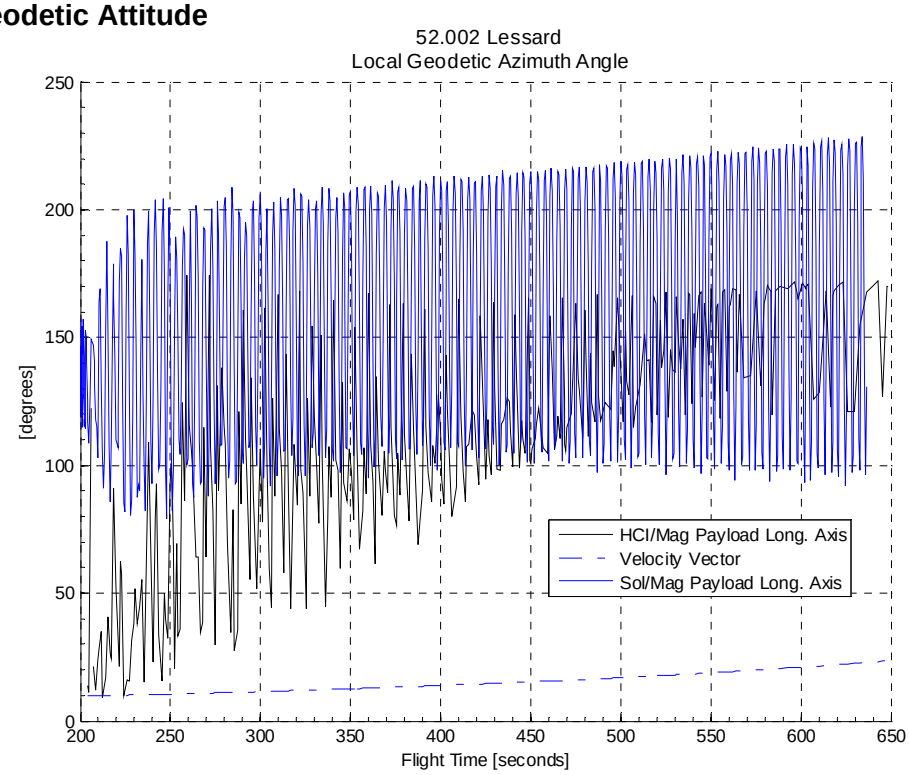

Figure 81. HCI/Mag: Sol/Mag: Local Geodetic Azimuth Attitude

a

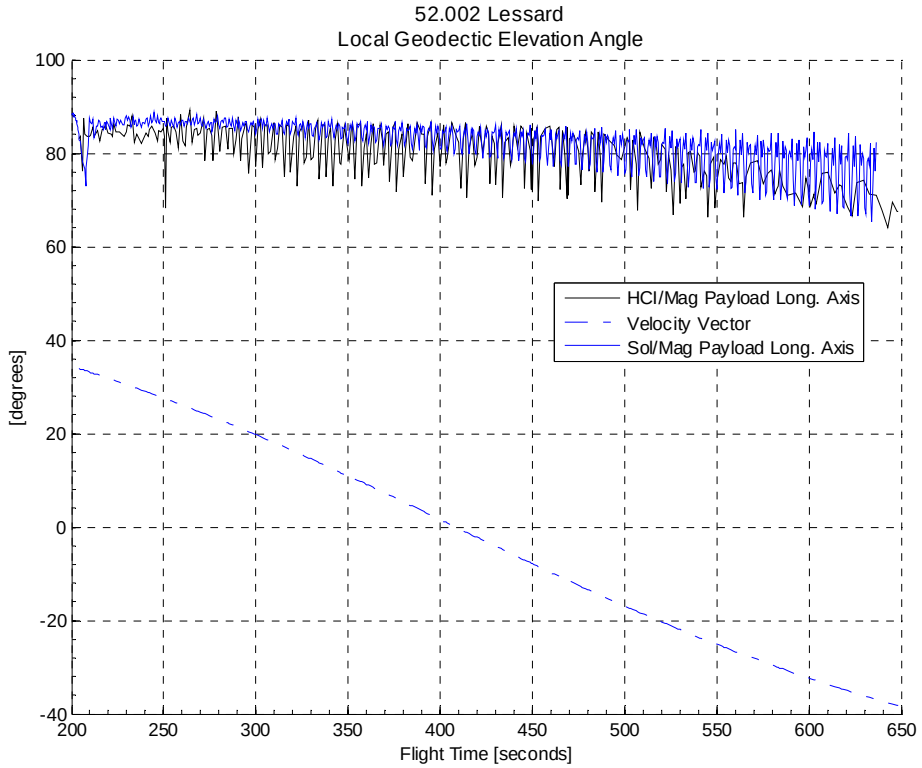

Figure 82. HCI/Mag: Sol/Mag: Local Geodetic Elevation Attitude

Inertial Attitude

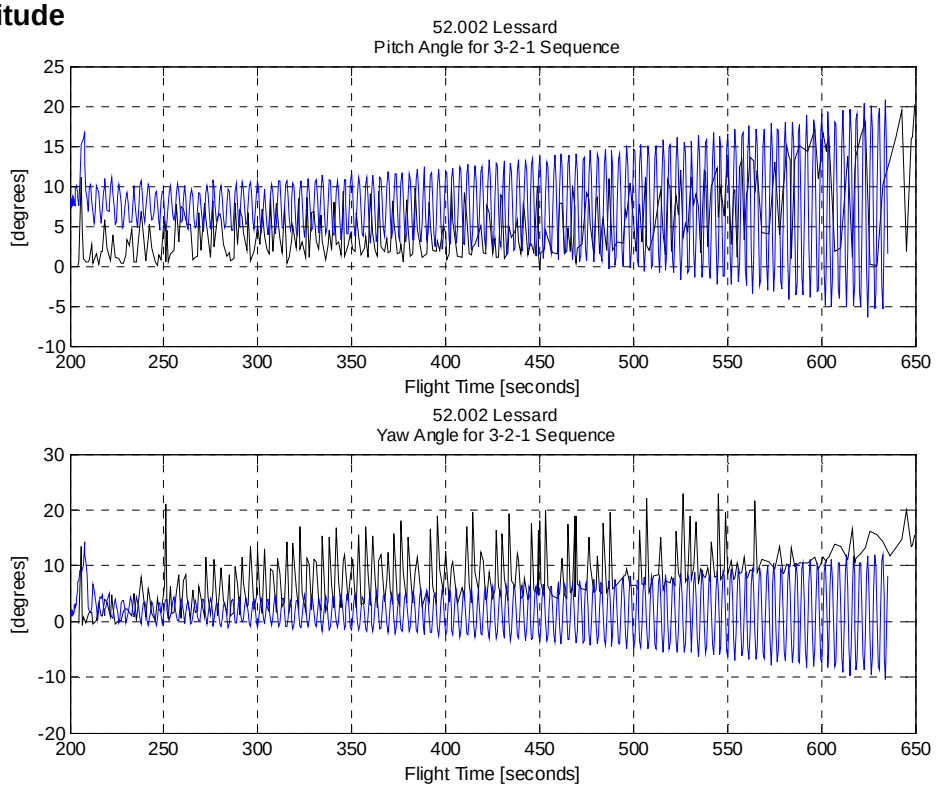

Figure 83. HCI/Mag: Sol/Mag: Pitch and Yaw

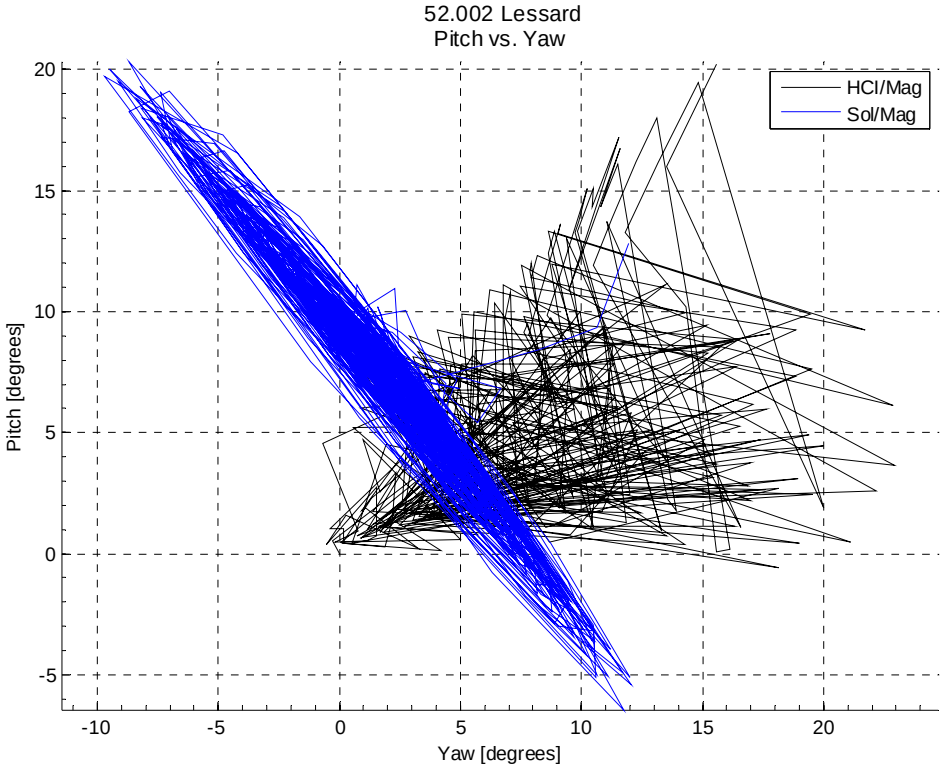

Figure 84. HCI/Mag: Sol/Mag: Pitch vs. Yaw

4. CONCLUSIONS

4.1 Final Conclusions

- Three axis attitude solution was finalized for the main payload on February 11th, 2016. Sol/Mag solution for the sub payload was finalized on March 1st, 2016. HCI Attitude was finalized on March 4th, 2016. HCI/Mag and Sol/Mag solutions are being improved with better methods and these solutions can be sent upon request. (Plots of the magnetic field with respect to the calculated spin axis will be shown to verify that the attitude solutions are valid when compared to data measured by the magnetometer).
- Main payload burnout roll rate was trimmed to 4 $\pm$ 0.5 Hz.
- Lateral rates were dampened to below 0.01 deg/sec for sub payload skirt deployment.
- Main payload was aligned to T+500 –B field for sub-payload deployment.
- Coning half angle was ~0.81° prior to sub payload deployment.
- Main payload roll rate was ~0.53 Hz between T+209 and T+717, which is within the tolerance of 0.5 $\pm$ 0.05 Hz.

4.2 Attitude Solution Verifications with Measured Mag Field

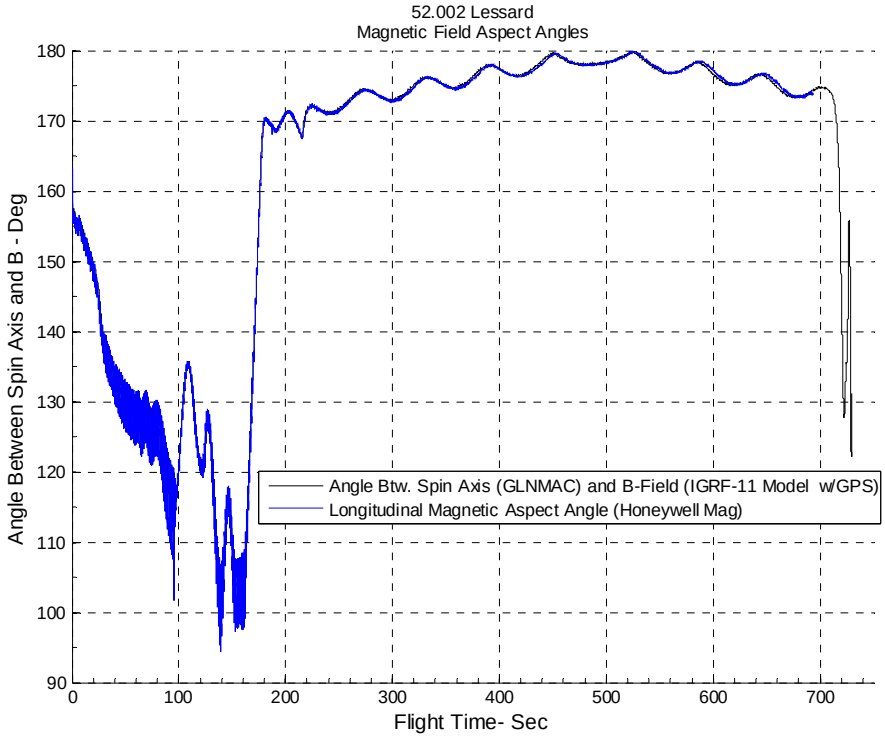

Figure 85. Main Payload Magnetic Field Pointing: GLNMAC Full Flight

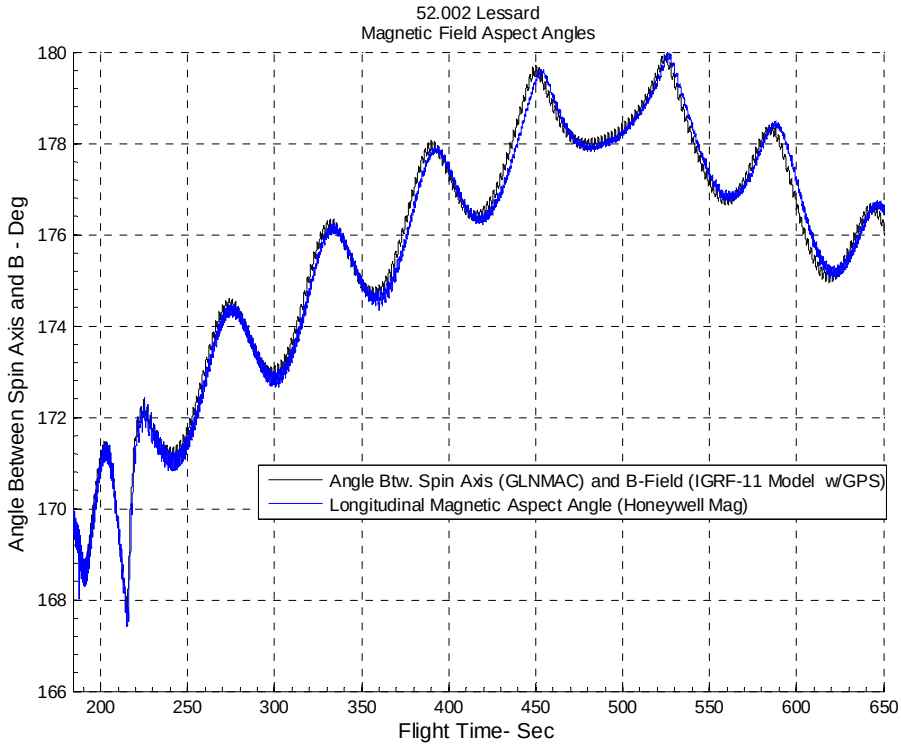

Figure 86. Main Payload Magnetic Field Pointing: GLNMAC Science

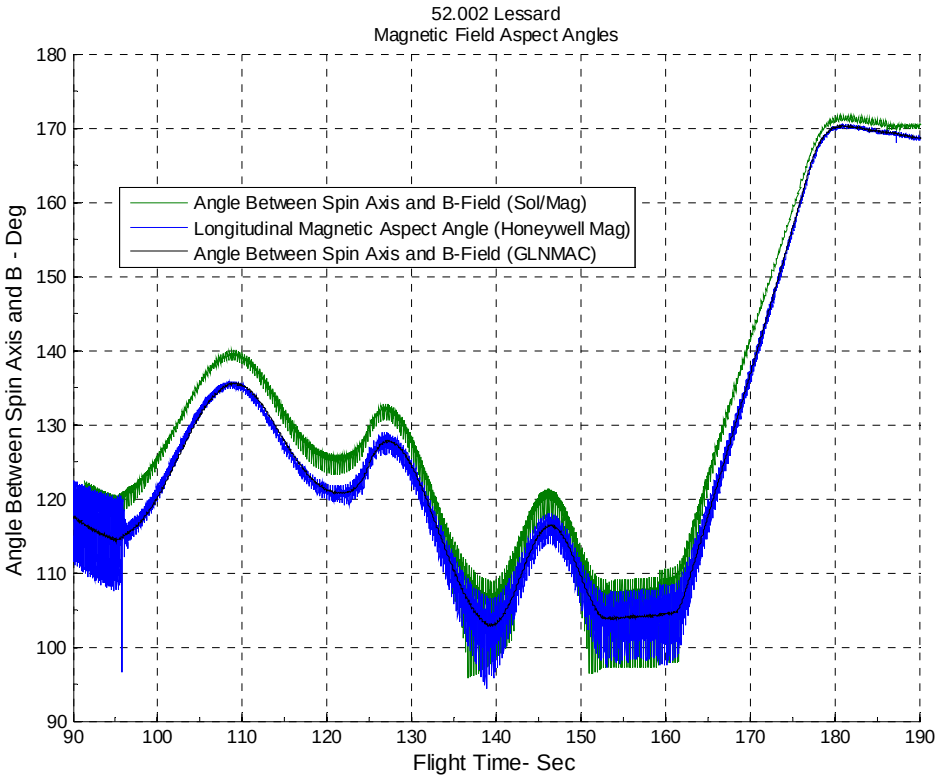

Figure 87. Main Payload Magnetic Field Pointing: GLNMAC: Sol/Mag (Sub Attached)

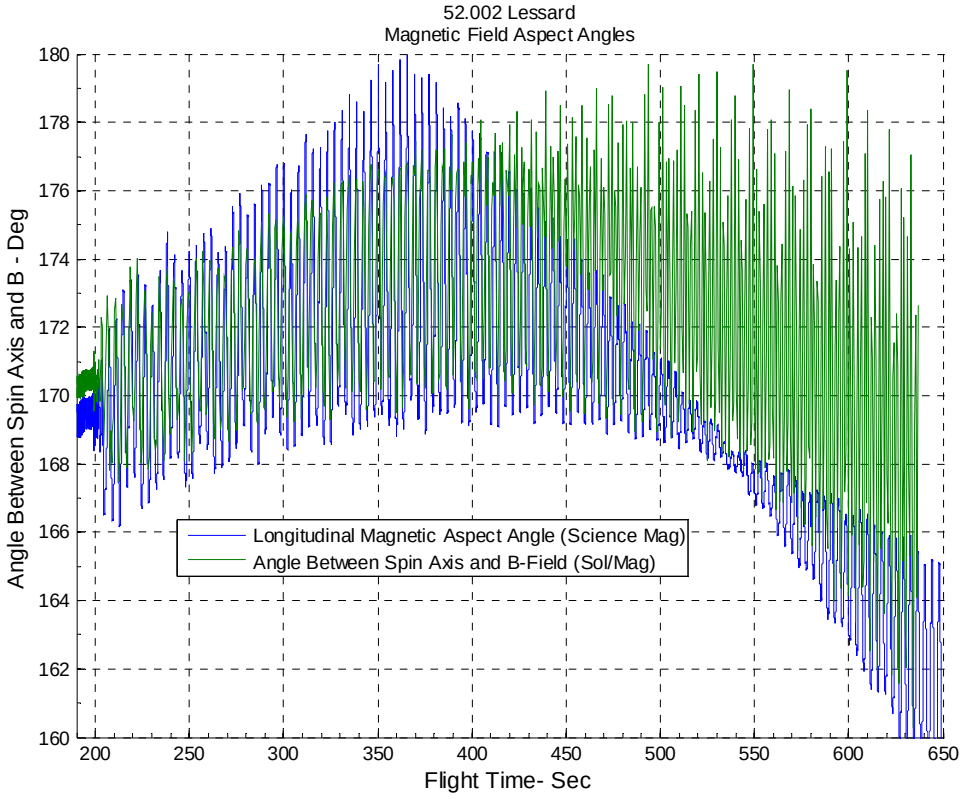

Figure 88. Sub Payload Magnetic Field Pointing: Sol/Mag

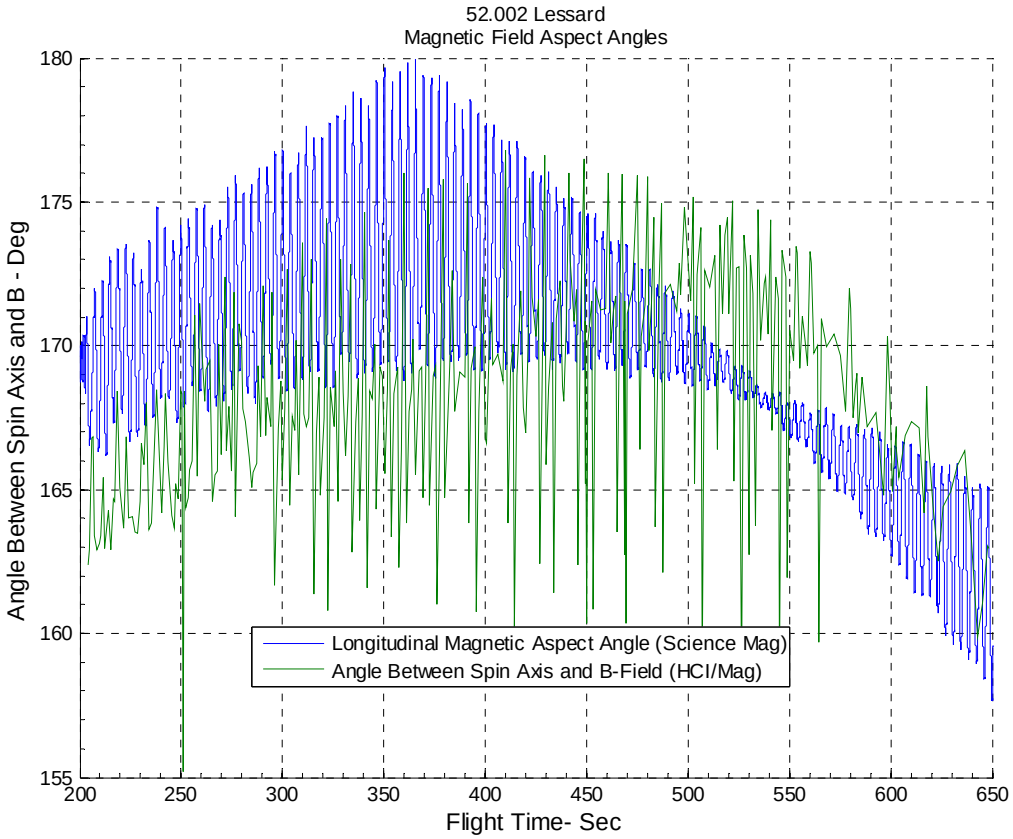

Figure 89. Sub Payload Magnetic Field Pointing: HCI/Mag

5. GLNMAC Housekeeping

This section will provide plots detailing the housekeeping data received by the Gyro. Data shown here is used to evaluate the quality of GLNMAC data and the performance of the GLNMAC throughout the flight.

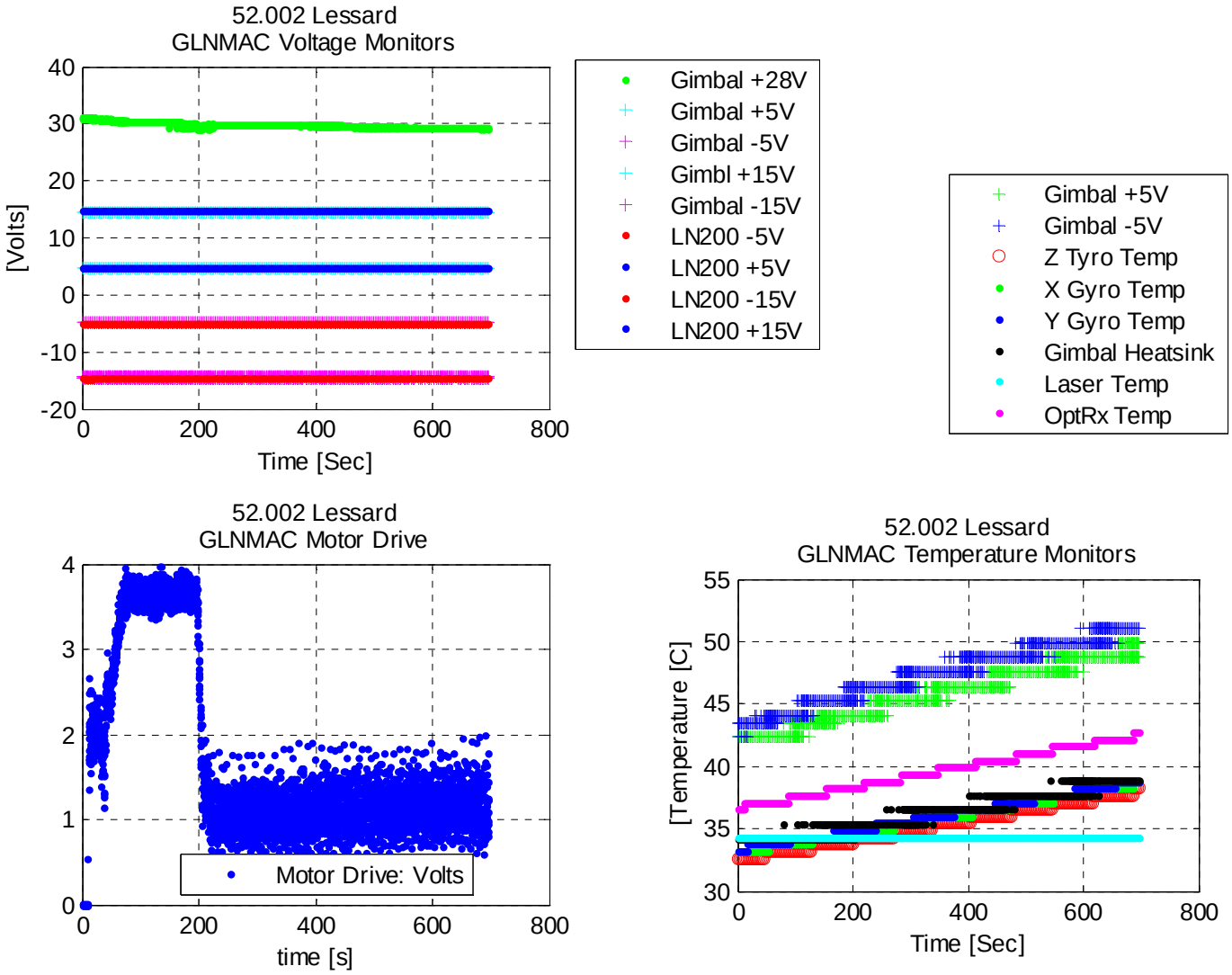

Figure 90. Main Payload: GLNMAC Voltage and Temperature Monitors

Figure 90 shows that the GLNMAC voltage stayed fairly constant throughout the flight. It also shows that there was a slight increase in the temperature, which is normal for the GLNMAC to experience. The last plot shows the motor drive which shows the areas where the GLNMAC picked up changes in the dynamics of the vehicle. Changes in the motor drive correspond to times when the attitude was seen to change, thus verifying that the GLNMAC was working nominally.

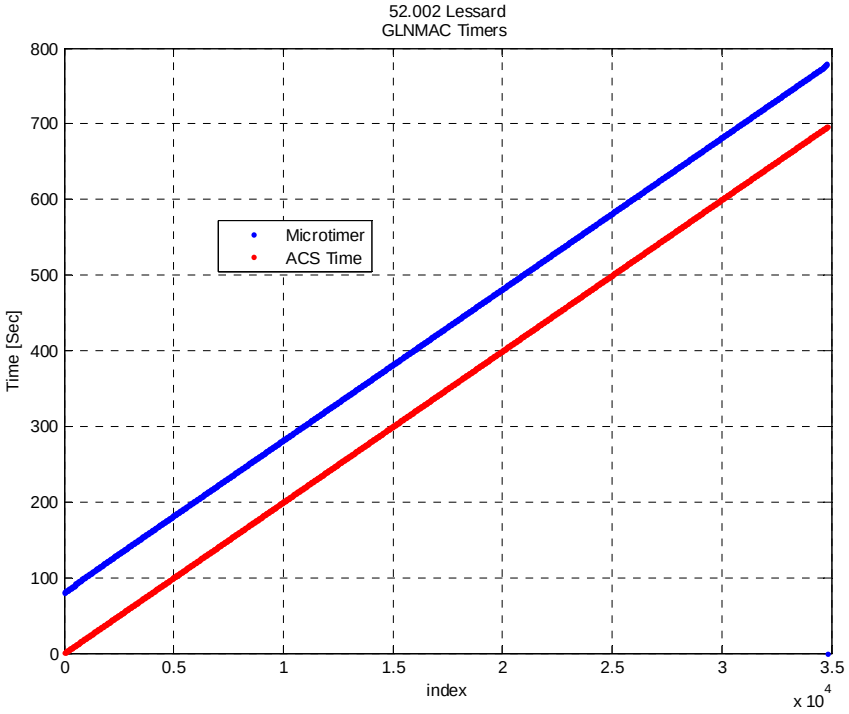

Figure 91. Main Payload: GLNMAC Timers

Figure 91 shows the GLNMAC timing information. This plot was used to determine the correct indexes to use for the microtimer time domain used in the synchronization process. It also shows that during the flight (up until reentry), there were no significant dropouts with timer data.

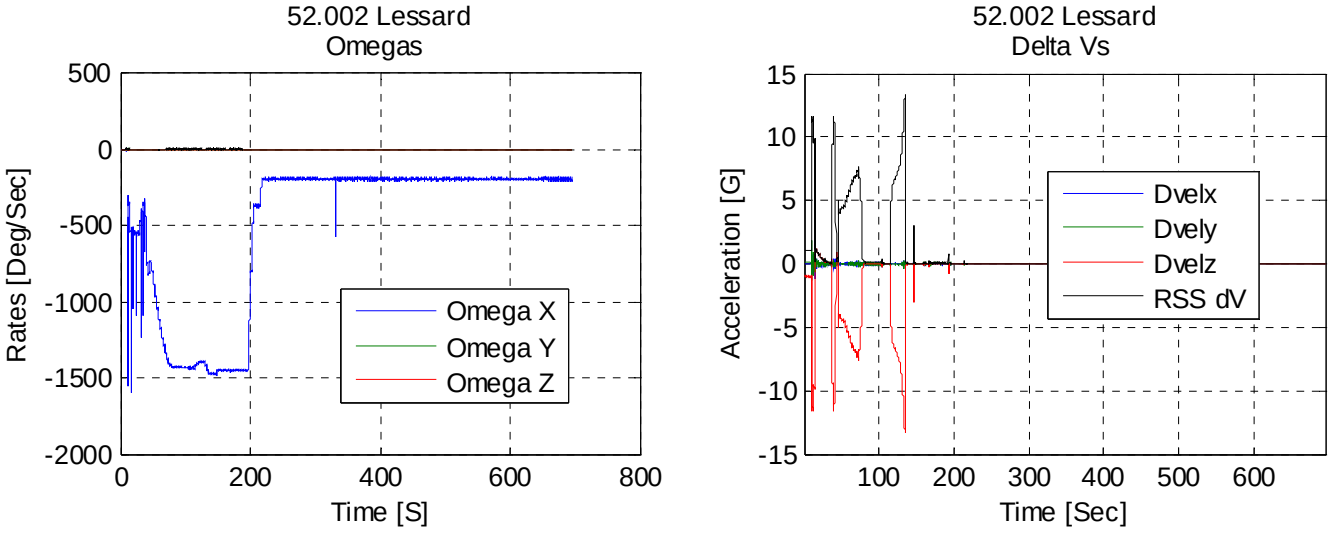

Figure 92. Main Payload: GLNMAC Calculated Omega and Delta Velocity

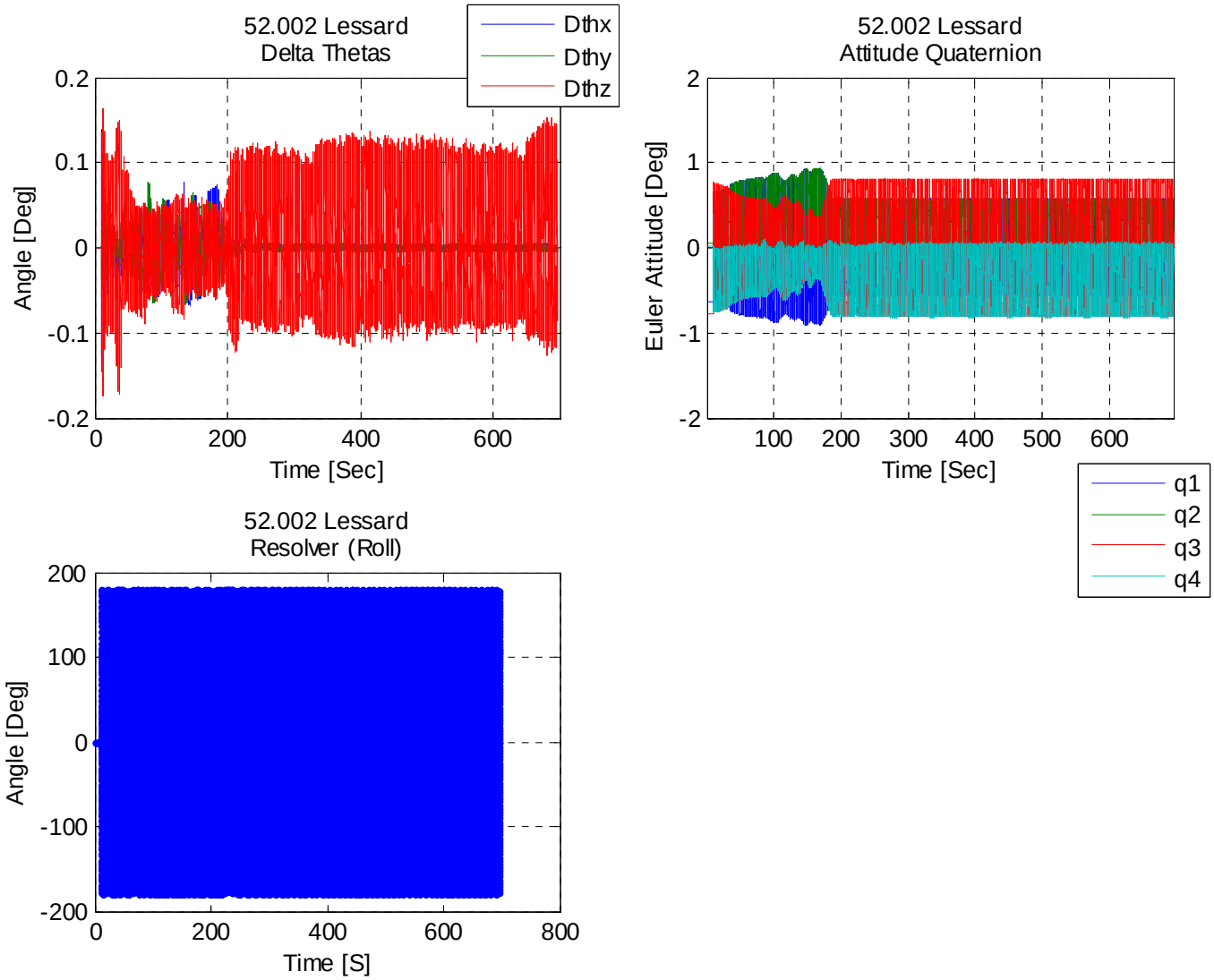

Figure 93. Main Payload: GLNMAC Delta Theta, Quaternion, and Roll Resolver

Figures 92 and 93 show the calculated omegas, delta thetas, delta velocities, delta omegas, quaternion and roll resolver from the GLNMAC. Upon analyzing all the raw flight data, it was determined that the data did not contain any corruption or anomalies. Since the recorded flight data was deemed to be of good quality, the attitude quaternion was converted to a DCM used to calculate the flight DCM for the attitude solution can be assumed to be valid and of good quality.